

Charge Transfer and Capacitive Properties of Polyaniline/ Polyamide Thin Films



UNIVERSITY *of the*
WESTERN CAPE

By

Dhielnawaaz Abrahams

A thesis submitted in partial fulfilment of the requirements for the degree of

Magister Scientiae in Nanoscience

Faculty of Science

University of the Western Cape

Cape Town, South Africa

Supervisor: Prof PGL Baker

March 2018

KEYWORDS

Capacitance

Conducting polymers

Cyclic voltammetry (CV)

Electrochemical impedance spectrometry (EIS)

Electrochemical supercapacitor

Electrochemistry

Electrolyte

Energy storage

Fourier transform infrared spectroscopy (FTIR)

Galvanostatic charge/discharge (GCD)

Polyamic acid (PAA)

Polyamic acid thin film (PAAF)

Polyaniline (PANI)

Polyaniline thin film (PANIF)

Polymer blend thin film (PBF)

Polymer blends

Pseudocapacitance

Scanning electron microscopy (SEM)

Supercapacitor

Thin film



ABSTRACT

Blending polymers together offers researchers the ability to create novel materials that have a combination of desired properties of the individual polymers for a variety of functions as well as improving specific properties. The behaviour of the resulting blended polymer or blend is determined by the interactions between the two polymers. The resultant synergy from blending an intrinsically conducting polymer like polyaniline (PANI), is that it possesses the electrical, electronic, magnetic and optical properties of a metal while retaining the poor mechanical properties, solubility and processibility commonly associated with a conventional polymer. Aromatic polyamic acid has outstanding thermal, mechanical, electrical, and solvent resistance properties that can overcome the poor mechanical properties and instability of the conventional conducting polymers, such as polyaniline.

PANI and PAA were synthesized independently and characterized using, Fourier-transform infrared (FTIR) and ultraviolet–visible (UV-Vis) spectroscopy to confirm chemical structure and functional groups. Cyclic voltammetry (CV) was used to identify the unique electrochemical behaviour of PAA and PANI respectively. Polyaniline/polyamic acid polymer blend thin film (PBF) was prepared via in-situ electrochemical polymerization and then characterized by CV, atomic force microscopy (AFM) and scanning electron microscope (SEM). The blended polymer thin films (PANI/PAA) were prepared electrochemically by polymerization of aniline and PAA (0.03 mg/ml ratio of 1:1) onto a GCE electrode using 15 cycles between -1000 mV and 1000 mV at 50 mV.s⁻¹.

Supercapacitors, also known as ultracapacitors or electrochemical capacitors, are devices based on the charge/discharge behaviour of highly porous material enabling to store energy as electrical charge. Supercapacitors have higher charge/discharge rate, longer life cycle and outstanding power density compared to batteries. Supercapacitors exhibit low energy density hindering their use in favourable applications.

The electrochemical performance of the individual polymers and the blend, with a view to establish them as supercapacitor materials, were characterized by galvanostatic charge/discharge (GCD), cyclic voltammetry (CV) and electrochemical impedance spectroscopy (EIS).

The SEM and AFM results confirmed the presence of a porous, rough nature for PBF. Maximum capacitance behaviour for PBF was observed at 0.5 V versus Ag/AgCl. Specific capacitance, life cycle and charge discharge of PBF was superior to that of the individual polymers. Higher capacitance values were measured for PBF as compared to PAA and PANI.

CV results showed that lithium perchlorate in propylene carbonate was the most appropriate electrolyte to use in investigating the specific capacitance values for the electrode materials. These specific capacitance values were calculated using GCD electrochemical techniques. The blended polymer film specific capacitance was calculated as $2,70 \times 10^{-09} \text{ F.g}^{-1}$ with a good charge discharge rate capability and cycling stability for a cycling test conducted at the current density of 1 A/g. Specific capacitance values for PAAF and PANIF at the current density of 1 A/g was 8×10^{-12} and $2,70 \times 10^{-10}$ respectively. A low energy density of $2,8 \times 10^{-10} \text{ Wh.kg}^{-1}$ at 1 A.g^{-1} was achieved with LiClO_4 in propylene carbonate at room temperature, as well as the highest power density of $1.7 \times 10^{-8} \text{ W/kg}$. These values suggest that the PBF supercapacitor is not suitable for peak-power applications. This could be attributed to the redox nature of both PAA and PANI, resulting in a redox material that shows low capacitive properties.

DECLARATION

I declare that “Charge transfer and capacitive properties of polyaniline/ polyamide thin films.” is my own work, that it has not been submitted before for any degree or assessment in any other university, and that all the sources I have used or quoted have been indicated and acknowledged by means of complete references.



Dhielnawaaz Abrahams

March 2018

ACKNOWLEDGEMENTS

I would thank and acknowledge following people and organisations for without their help, guidance and support I would not have been able to complete this thesis

- **Allah** Almighty to Him (S.W.T) all belongs all praise, glory, honour and adoration.
- To my parents, all that I am and all that I aspire to be I owe to you.
- To my supervisor Prof. P.G. L. Baker thank you very much for seeing my potential and guiding me all the way. All your advice, mentorship and understanding means the world to me. Thank you above all for teaching me character.
- Dr. Meryck Ward, Dr Lisebo Phelane and future doctor Mr Siyabulela Hamnca. Thank you for taking the time to impart knowledge.
- To all at SensorLab's research team and University of the Western Cape thank you very much.
- To my brothers and sisters thank you for all you do.
- To my little ones thank you for giving me reasons to smile every day.
- To my beloved MSA girls thank you for being my constant reminders, for a reminder is good for a believer.
- To my oldest true friend Crystal Hilderbrand there are no words to describe how much your support and advice means.
- To my friends and extended family for their love, support and care during the period of study.
- The Department of Science and Technology (DST), National Research Foundation (NRF), South African Human Asset Research Program (SANHARP), National Nanoscience Postgraduate Teaching and Training Program (NNPTTP), SensorLab and Chemistry Department for funding my studies

DEDICATION

To
Allah (S.W.T)
And
My Parents



UNIVERSITY *of the*
WESTERN CAPE

TABLE OF CONTENTS

KEY WORDS	i
ABSTRACT	ii
DECLARATION.....	iv
ACKNOWLEDGEMENTS	v
DEDICATION.....	vi
TABLE OF CONTENTS	vii
LIST OF FIGURES	ix
LIST OF TABLES	xii
LIST OF ABBREVIATIONS.....	xiii
Chapter 1	15
1.1 Introduction	15
1.1.2 Intrinsically conducting polymers (ICPs).....	16
1.1.3 Polymer blends.....	18
1.1.4 Polyaniline (PANI)	23
1.1.5 Polyamic acid (PAA).....	26
1.1.6 Characterization techniques of polymer blended materials.	27
1.2 Rationale and Motivation.....	27
1.3 Aims and Objective	29
1.3.1 Objectives of the study	29
1.4 Thesis Outline	30
Chapter 2	32
2.1 Introduction into Capacitance	32
2.2 Conducting Polymers as supercapacitor electrode materials.....	36
2.3 Conducting Polymers Blends as supercapacitor electrode materials	38
2.4 The importance of the electrolyte	39
Chapter 3	41
3.1 Microscopy Techniques.....	41
3.1.1 Scanning electron microscopy (SEM)	41
3.1.2 Atomic force microscopic (AFM)	42
3.2 Spectroscopic Techniques	43
3.2.1 Ultraviolet Visible Spectroscopy (UV-Vis):.....	43

3.2.2 Fourier Transform Infrared (FTIR) Spectroscopy	43
3.3 Electrochemical Techniques	45
3.3.1 Cyclic voltammetry (CV)	45
3.3.2 Galvanostatic charge/discharge (GCD)	49
3.3.3 Electrochemical Impedance (EIS)	51
Chapter 4	53
4.1 Materials.....	53
4.2 Method	53
4.3 Spectroscopic characterisation.....	55
4.3.1 FTIR of PAA	55
4.3.2 FTIR of PANI	57
4.3.3 FTIR of PAA/PANI Blend.....	58
4.3.4 Ultraviolet visible UV/vis of individual polymers and blend	59
4.4 Characterization of thin films.	60
4.4.1 Electrochemical characterization.....	60
4.4.1.1 Cyclic Voltammetry of thin film electrodes	61
4.5. Analysis by Supercapacitor Characterisation	76
4.5.1 Electrochemical Impedance Spectroscopy.....	76
4.5.1.1 Impedance analysis of PAA.....	77
4.5.1.2 Impedance analysis PANI.....	78
4.5.1.3 Impedance analysis PBF	78
4.5.2 Cyclic voltammetry of PAAF	81
4.5.3 Cyclic voltammetry of PANIF	83
4.5.3 Cyclic voltammetry of PBF	86
4.6 Galvanostatic Charge/Discharge (GCD)	89
4.7 Energy density and power density.....	92
Chapter 5	93
5.1 Surface characterization of electrode material	93
5.1.1 Scanning Electron Microscopy of PAA	93
5.1.2 Scanning Electron Microscopy of PANI.....	94
5.1.3 Scanning Electron Microscopy of PAA/PANI Blend.....	95
5.1.4 Atomic Force Microscopy	96
Chapter 6	99
References	101

LIST OF FIGURES

Figure 1.1: Conducting polymer structure showing the backbone as a result of sp ² hybridization.	16
Figure 1.2: Some widely known intrinsically conducting polymers.	17
Figure 1.3: Shows emeraldine base as well as the reduced and oxidised form of emeraldine base.	24
Figure 1.4: The chemical synthesis of polyaniline.	25
Figure 1.5: The chemical Synthesis of polyamide.	26
Figure 2.1: Plot of Ragone plot for various energy storage and conversion devices.	34
Figure 2.2: Various electrode materials utilized for superconductors.	36
Figure 3.1: Schematic depicting the working principle of an AFM microscope.	37
Figure 3.2: Schematic depicting the working principle of FTIR spectrometer.	44
Figure 3.3: A typical cyclic voltammogram for a reversible redox system.	46
Figure 3.4: Typical cyclic voltammogram of capacitive electrode materials.	48
Figure 3.5: Typical cyclic charge-discharge curve illustrating idea capacitor performance.	50
Figure 3.6: Typical Nyquist plot and its equivalent circuit.	51
Figure 4.1: Electrochemical synthesis of polymer blended thin film electrode (PBF), polyaniline thin film electrode (PANIF) and polyamic acid thin film electrode (PAAF).	54
Figure 4.2: FTIR spectrum of polyamic acid (PAA).	56
Figure 4.3: FTIR spectrum of polyaniline (PANI).	57
Figure 4.4: FTIR spectrum of PAA/PANI blend.	58
Figure 4.5: UV/Vis spectrum of PAA, PANI and PAA/PANI.	59
Figure 4.6: Electrochemical workstation configuration.	60
Figure 4.7: Electrodeposition of PAAF.	61
Figure 4.8: Cyclic voltammogram of PAAF in 1 M HCl at different scan rates (10-100	

Figure 4.9: Graph of anodic and cathodic peak current (I_p) vs. square root of scan rate ($\text{mV}\cdot\text{s}^{-1/2}$) for PAAF in 1 M HCl at different scan rates.	64
Figure 4.10: Electro-polymerization of PANIF.	67
Figure 4.11: Cyclic voltammogram of PAAF in 1 M HCl at different scan rates (10-100 $\text{mV}\cdot\text{s}^{-1}$).	68
Figure 4.12: Graph of anodic and cathodic peak current (I_p) vs. square root of scan rate ($\text{mV}\cdot\text{s}^{-1/2}$) for PANI in 1 M HCl solution at different scan rates for peaks.	70
Figure 4.13: Electrodeposition of PBF.	72
Figure 4.14: Cyclic voltammogram of PBF in 1 M HCl at different scan rates (10-100 $\text{mV}\cdot\text{s}^{-1}$).	73
Figure 4.15: Graph of anodic and cathodic peak current (I_p) vs. square root of scan rate ($\text{mV}\cdot\text{s}^{-1/2}$) for PAA in 1 M HCl solution at different scan rates for peaks.	75
Figure 4.16: Electrochemical impedance spectra (Nyquist plot) of PAA in 1 M HCl electrolyte.	77
Figure 4.17: Electrochemical impedance spectra (Nyquist plot) of PANIF in 1 M HCl electrolyte.	78
Figure 4.18: Electrochemical impedance spectra (Nyquist plot) of PBF in 1 M HCl electrode.	78
Figure 4.19: Plot of CPE versus voltage based on values for from Nyquist plots of PAAF, PANIF and PBF in 1 M HCl electrolyte at different potentials.	79
Figure 4.20: Plot of R_{ct} versus voltage based on values for from Nyquist plots of PAAF, PANIF and PBF in 1 M HCl electrolyte at different potentials.	80
Figure 4.21: Cyclic voltammogram of PAAF in 1 M LiClO_4 in PC at different scan rates (10-100 $\text{mV}\cdot\text{s}^{-1}$).	81
Figure 4.22: Cyclic voltammogram of PAAF in 1 M LiClO_4 in water at different scan rates (10-100 $\text{mV}\cdot\text{s}^{-1}$).	82
Figure 4.23: Cyclic voltammogram of PAAF in 1 M TT in PC at different scan rates (10-100 $\text{mV}\cdot\text{s}^{-1}$).	82
Figure 4.24: Cyclic voltammogram of PAAF in 0.004 M TT in PC at different scan rates (10-100 $\text{mV}\cdot\text{s}^{-1}$).	83
Figure 4.25: Cyclic voltammogram of PANIF in 1 M LiClO_4 in PC at different scan rates (10-100 $\text{mV}\cdot\text{s}^{-1}$).	84
Figure 4.26: Cyclic voltammogram of PANIF in 1 M LiClO_4 in water at different scan rates (10-100 $\text{mV}\cdot\text{s}^{-1}$).	84
Figure 4.27: Cyclic voltammogram of PANIF in 1 M TT in PC at different scan rates (10-100 $\text{mV}\cdot\text{s}^{-1}$).	85

Figure 4.28: Cyclic voltammogram of PANIF in 0.004 M TT in water at different scan rates (10-100 mV.s ⁻¹).	85
Figure 4.29: Cyclic voltammogram of PBF in 1 M LiClO ₄ in PC at different scan rates (10-100 mV.s ⁻¹).	86
Figure 4.30: Cyclic voltammogram of PBF in 1 M LiClO ₄ in water at different scan rates (10-100 mV.s ⁻¹).	86
Figure 4.31: Cyclic voltammogram of PBF in 1 M TT in PC at different scan rates (10-100 mV.s ⁻¹).	87
Figure 4.32: Cyclic voltammogram of PBF in 0.004 M TT in water at different scan rates (10-100 mV.s ⁻¹).	87
Figure 4.33: Galvanostatic plot of PAAF.	89
Figure 4.34: Galvanostatic plot of PANIF.	90
Figure 4.35: Galvanostatic plot of PBF.	90
Figure 4.36: Depiction of the capacitance values obtained by PAAF, PANIF and PBF.	91
Figure 5.1: SEM image of PAAF.	93
Figure 5.2: SEM image of PANIF.	94
Figure 5.3: SEM image of PBF.	95
Figure 5.4: AFM image of PAAF.	96
Figure 5.5: AFM image of PANIF.	97
Figure 5.6: AFM image of PBF.	97
Figure 6.1: Ragone plot of PBF supercapacitor.	100

LIST OF TABLES

Table 1.1: Polymer Blends synthesised in a variety of ways	20
Table 2.1: Comparing parameters of various energy storage devices	35
Table 2.2: EDLC and pseudo-capacitance compared	37
Table 2.3: Comparison of aqueous electrolyte and organic electrolyte	39
Table 4.1: Fourier transform Infrared peaks assignment for PAA	56
Table 4.2: Fourier transform Infrared peaks assignment for PANI	58
Table 4.3: The effect of scan rate on the anodic and cathodic peak currents and peak potentials of PAAF at different scan rates in 1 M HCl electrolyte	63
Table 4.4: Diffusion coefficients calculated for all PAAF peaks	65
Table 4.5: The effect of scan rate on anodic and cathodic peak current and peak potentials of PANI in CVs for different scan rates in 1 M HCl electrolyte	69
Table 4.6: Effect of scan rate on peak current and peak potentials for PANI	71
Table 4.7: The effect of scan rate on anodic and cathodic peak current and peak potentials of PANI in CVs for different scan rates in 1 M HCl electrolyte	74
Table 4.8: Effect of scan rate on peak current and peak potentials for PBF	76
Table 4.9: Capacitance of individual polymer and blend in different electrolytes	88

LIST OF ABBREVIATIONS

AFM: Atomic force microscopy

CV: Cyclic voltammetry

D_0 : Diffusion coefficient

EIS: Electrochemical impedance spectroscopy

E^0 : Formal potential

FTIR: Fourier transformer infrared

GCD: Galvanostatic charge/discharge

GCE: Glassy carbon electrode

HCl: Hydrochloric acid

LiClO_4 : Lithium perchlorate

PAA: Polyamic acid

PANI/PAA: Polyaniline/polyamic acid

PANI: Polyaniline

PI: Polyimide

R_a : Area roughness

SEM: Scanning electron microscopy

SPCE: Screen printed carbon electrode

UV: Ultra violet visible

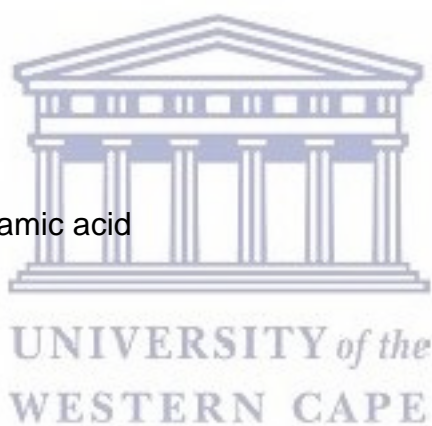
UV: Ultraviolet

Vis: Visible

A: Ampere

C: Capacitance

ICP: Intrinsically conducting polymers



Chapter 1

This chapter introduces the concept of conducting polymers and provides a background to polyaniline (PANI) and polyamic acid (PAA) as polymer materials. A review of blended polymers and techniques which are used to characterize them, are also presented.

1.1 Introduction

The word polymer was first coined by Berzelius as far back as 1883 (Percec, 2001). A century later the field of polymer science included biological, chemical and physical polymers (Carothers, 1931). The first synthetic polymer, phenol-formaldehyde was commercialized in 1909. More recently considerable research has been done in fabricating nanostructured materials (Berresheim, Müller and Müllen, 1999; Pan et al., 2010; Tran, Li and Kaner, 2009). Thus, today the field of synthetic and biological polymers stretch into various areas of biology, biochemistry, chemistry, electronics, materials, nanotechnology, medicine, energy etc. (Kumar and Sharma, 1998; Inzelt et al., 2000; Long et al., 2011; Luckachan and Pillai, 2011). The study of polymers has gained momentum due to the need and desire to fabricate and understand new kinds of plastics and fibres.

Being insulating materials in their natural state, polymers were originally considered and applied as insulators. In 1977 a new class of polymers possessing high electronic conductivity in the partially oxidized or reduced state was discovered. Scientists Alan J. Heeger, Alan G. MacDiarmid and Hideki Shirakawa found that the electronically conductive nature of polyacetylenes increased significantly upon its exposure to halogen vapours (Chiang et al., 1977). This discovery won the scientists the Nobel Prize in Chemistry in 2000 “for the discovery and development of electronically conductive polymers” (Shirakawa, 2001). Following the initial successful synthesis of conducting polyacetylene, electrically conducting polymers have generated tremendous interest.

1.1.2 Intrinsically conducting polymers (ICPs).

Intrinsically conducting polymers (ICPs) also known as conjugated polymers and more commonly known as “synthetic metals,” are polymers with highly-conjugated polymeric chains (Nguyen and Yoon, 2016: Nguyen and Yoon, 2016: Gvozdenovic et al., 2014). ICPs have low energy optical transition, low ionization potential and high electron affinity (Unsworth et al., 1992). The main structural characteristic of the conductive polymers is their π -conjugated systems that extend along a number of recurring monomers and eventually form the polymer backbone as depicted in Figure 1.1 (Roncali et al., 2002). This chain is as a result of the sp^2 hybridization of the C atoms, where a single s orbital and two p orbitals combine to form a three sp^2 hybrid orbitals. Along the direction of the sp^2 orbitals, the σ -bonds establish the backbone of the polymer leaving the p-orbitals to form the π conjugated system that allows electrons to be transported along the polymer backbone (Naarmann, 2002). The alternation of single and double bonded sp^2 hybridized atoms provide the polymer with its metallic semi-conducting nature. Bonds above and below the plane of the molecular backbone consist of weakly-bound electrons which enable charge transport between molecules. (Roncali et al., 2002; Malliaras et al., 2005)

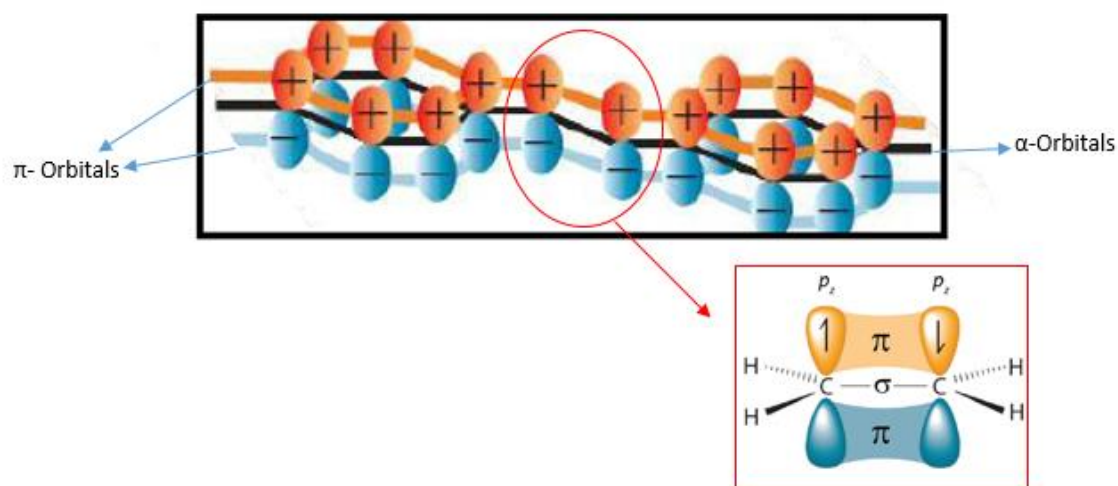


Figure 1.1: Conducting polymer structure showing the backbone as a result of sp^2 hybridization.

This occurrence allows organic polymers to possess the electrical, electronic, magnetic and optical properties of a metal while retaining the mechanical properties, solubility, processability, etc., commonly associated with a conventional polymer (Chiang et al., 1977). These polymers become conductive upon partial oxidation or reduction, a process commonly referred to as doping (Bhadra, Singha and Khastgir, 2006; Unsworth et al., 1992). It has been demonstrated that the electrical properties of conductive polymers can be reversibly changed over the full range from an insulator to a metallic conductor (Malliaras et al., 2005 ; Nalwa, 2008).

A variety of ICPs as well as their derivatives have been synthesized, industrialised and investigated (e.g., polyacetylene (PA), polyaniline (PANI), poly(para-phenylene) (PPP), polypyrrole (PPy), polyfuran (PF), polythiophene (PTh), poly(3,4-ethylenedioxythiophene) (PEDOT)) (Figure 1.2) (Park et al., 2005).

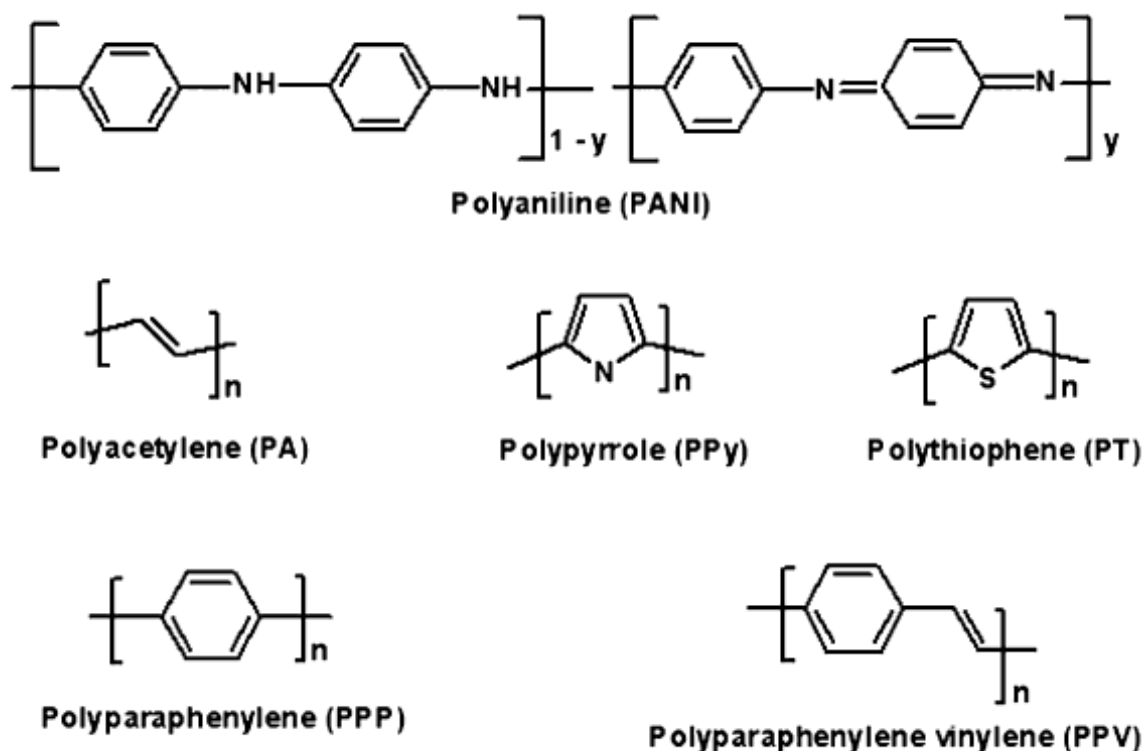


Figure 1.2: Some widely known intrinsically conducting polymers.

Good electrical and optical properties of these ICPs make them excellent candidates for multidisciplinary applications such as, electronics, thermoelectronics, electrochemistry, electromagnetism, electromechanics, electro-luminescence, electro-rheological, chemistry, membranes, and sensors (Huang, Chen and Wen, 2006: Bossi et al., 2000: Gorey et al., 2014: Rao, Subrahmanya and Sathyanarayana, 2003: Angelopoulos, 2001: Unsworth et al., 1992). However, poor mechanical properties and instability limit some industry applications. The main problem associated with the effective utilization of all ICPs including PANI is inherent in their lower level of conductivity compared to metal, and their infusibility and poor solubility in almost all available solvents (Cho et al., 2004: Rao, Subrahmanya and Sathyanarayana, 2003). The solubility of some ICPs can be improved through doping with a suitable dopant or modifying the starting monomer (Bhadra, Singha and Khastgir, 2006: Bhadra, Singha and Khastgir, 2008). Therefore, there is ample scope for modifying the conductivity and processability of these polymers through the selection of a suitable dopant and suitable level of doping and also by controlling its structure during synthesis (Bhadra et al., 2008). Another avenue for the successful utilization of the polymers is through blending it with a commercially available polymer that has good processability and mechanical properties.

1.1.3 Polymer blends

Polymer blends are defined as a mixture of at least two polymers or copolymers, in which the constituent polymers are above 2 weight percent. The behaviour of the resulting blended polymer or blend is thus determined by the Interactions between the two polymers. Blending polymers together offers researchers the possibility to create novel materials that has a combination of desired properties of the individual polymers, for a variety of functions as well as improving specific properties (Vikki et al., 1996).

Blending methods have been developed with the knowledge that difficulties in polymer blend processability are related to aromatic structure, interchain hydrogen bonds, as well as the effective charge delocalization in its structure (Vikki et al., 1996). These

blending methods can be categorized into chemical and electrochemical methods. Blending methods are more desirable for large-scale production and processability. While electrochemical polymerization on a large scale is not practical, but rather finds usefulness in small geometry systems. (Sezer, Ustamehmetoğlu and Saraç, 1999) There are several synthetic routes for the preparation of polymer blends by chemical method a few are given here below:

- Solution blending

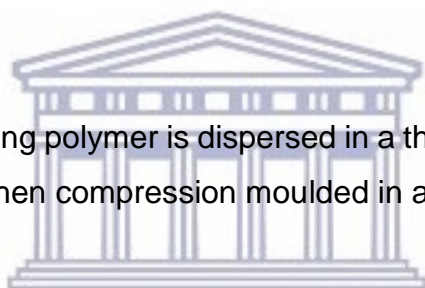
The individual polymers are all dissolved in a common solvent and there upon processed into thin films.

- Dry blending

These blends are produced by blending the powders of polymers.

- Melt processing

In this process, the conducting polymer is dispersed in a thermoplastic polymer matrix by mechanical mixing and then compression moulded in a hot press.



Electrochemical synthesis routes (potentiostatic polymerization, galvanostatic polymerization, cyclic voltammetry) for producing blended materials have several advantages over chemical routes. The electrochemical synthesis of polymer blends are carried out in an inert atmosphere. In the potentiostatic electropolymerization process, the voltage is maintained constant, whereas in the galvanostatic method the polymerization occurs at a constant current (Sezer, Ustamehmetoğlu and Saraç, 1999).

These advantages of electrochemical synthesis routes include:

- i) The blend/polymer material is produced in the form of a freestanding or adsorbed thin film.
- ii) The film produced can be in the nano meter range. Whereas powders or very thick films are typically produced with chemical polymerization.

- iii) The electrical properties of the film can be easily modified by utilising various electrolysis conditions. Thus the synthesis is easier and better to control.
- iv) The electrochemical synthesis route is considered as a “clean” method.
- v) It allows for better ways for the quantitative assessment of the polymer performance to be evaluated by electrochemistry.
- vi) The entrapment of molecules in the conducting polymers is possible.
- vii) Offers the ability for instantaneous polymerization and film formation to occur.

(Babu et al., 2009; Skotheim and Reynolds, 2007; Sezer, Ustamehmetoğlu and Saraç, 1999).

However, when using electrochemical synthesis methods it is important to note that the size of the blended film will depend on the size of the electrode. Further, an appropriate matrix polymer electrolyte system for the penetration of the ionic species into the polymer matrix should be investigated. Additionally, the applied potential, deposition time, deposition temperature, water content, electrolyte, electrode system, electrodes deposition technique should be investigated as it will in turn influence the material and the application of the thin film.

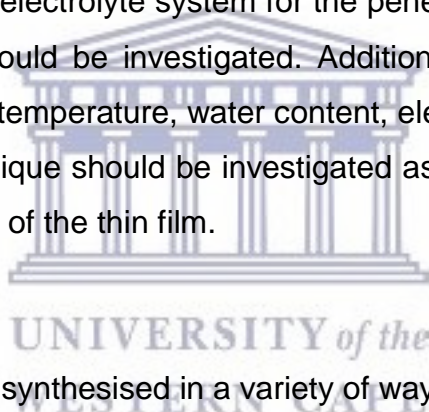


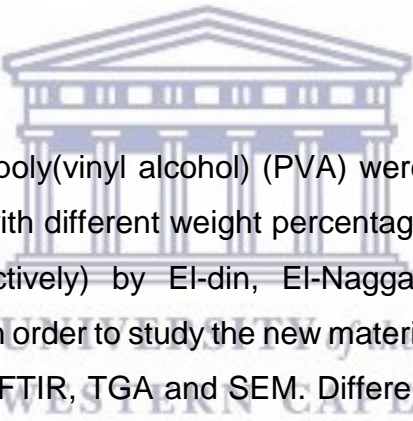
Table 1.1: Polymer Blends synthesised in a variety of ways

Common synthesis methods for polymer blends	Polymer used for blend	Reference
In situ synthesis	Nylon-6 polyacrylamide	(Park et al., 2018)
In situ, coagulation, dry blending	PMMA, polystyrene methyl methacrylate–butadiene–styrene copolymer	(Terlemezyan, Ivanova and Tacheva, 1993)
Melt processing	PVC, polyethylene	(Shacklette, Han and Luly, 1993)

	terephthalate, nylon-12	
Chemical in situ polymerization	polyaniline–nylon-6	(Park et al., 1992)
Chemical in situ polymerization	poly(acrylamide)–polyaniline	(Bhat and Joshi, 1993)
Solution blending	Polyaniline–PVC	(Thangarathinavelu et al., 1994)
Melt processing	Polyaniline–polyvinyl chloride	(Shacklette, Han and Luly, 1993)
Potentiostatic polymerization	polyaniline–polycarbonate	(Dogan et al., 1993)
Cyclic voltammetry	Polyaniline–nitrilic rubber	(Tassi,. and DePaoli et al., 1990)

One ICP that has received widespread attention in recent years is that of PANI. The nature of PANI as a ICP has allowed the polymer, its blends as well as its derivatives to be used in various applications such as capacitors, microelectronics, electric devices, sensors and many more (Molapo et al., 2012; Lu et al., 1986). In a recent study PANI/PVC blended films were prepared in n-methyl-2-pyrrolidone (NMP) using a solution blending technique. The blend was achieved by using various weight percentages of PANI (2, 5, 8, 11, 14, 17 and 20 weight percentage respectively). The blended material showed good flexibility compared to the individual polymers. The authors observed that the films had a division threshold occurring at 16 percentage weight of PANI. Various techniques were employed in order to characterize the composite such as fourier transform infrared (FTIR), thermogravimetric analysis (TGA) and scanning electron microscopy (SEM) and differential thermal analysis (DTA).The FTIR spectra revealed that the interaction between PVC and PANI is through very strong hydrogen bond interactions. Additionally it was reported that the mixing of PANI in PVC had caused an increase of thermal stability as well as rigidity of composite PANI/PVC (Lamour, 2014).

Aromatic polyimides hold outstanding thermal, mechanical, electrical, and solvent resistance properties and have been widely used in the electronic industry, aerospace, automobiles, wire insulating, and high performance parts (Li et al., 2004). Many of these properties are not inherent to ICPs. Selampinar et al, 2007 performed a study producing a blend of PPy and polyimide using an electrochemical synthesis technique. FTIR, SEM and TGA was employed in order to characterize the blended material as well as individual materials. The FTIR spectra allowed the authors to distinguish individual polymers from each other and the blended film. By the thermal analysis technique, TGA authors could confirm the improved thermal stability of the blended materials as compared to the individual polymer materials. Thus the resulting blended material resulted in a material having superior thermal properties (Selampinar et al, 2007).



Polyacrylamide (PAM) and poly(vinyl alcohol) (PVA) were blended together using a solution-casting technique with different weight percentages (70:30, 50:50 and 30:70 weight percentages respectively) by El-din, El-Naggar and Ali, 2003. Various techniques were employed in order to study the new materials properties these include ultra violet visible (UV-vis), FTIR, TGA and SEM. Different mechanical properties of blends were also studied. Significant changes were observed in FTIR, UV-vis, TGA and SEM. The combined results of all techniques showed a change not only in the thermal stability of the blended material but also the mechanical properties as compared to the initial polymer materials. Again the FTIR spectra obtained indicated the presence of hydrogen bonding between individual polymers in the blend. The specific hydrogen bonding occurred between $-\text{CONH}_2$ groups in PAM and the $-\text{OH}$ group in PVA. Additionally it also confirmed the hydrophilic nature of the blended materials. The authors could conclude that the blend films with a weight percentage above 50:50 ratio would exhibit a higher thermal stability as well as an improved mechanical property as compared to the individual polymers. UV-vis was used to investigate the various optical properties. While TGA analysis was done in order to

investigate the weight loss that occurred as the temperature of blends increased or decreased (El-din, El-Naggar and Ali, 2003).

Polymer films have also been used in energy conservation as well as energy storage and production systems. The research of Mohamoud, et al, 2014 showed that polymer blends of PANI composites and PVA produced by a combination of in situ electropolymerization and nanogravimetric techniques and showed significant improvements of the redox behaviour and electrochemical capacitance. The blended material showed a 40% increase in capacitance property than the individual PANI material. These improvements were attributed to the presence of multiple hydrogen bonds that result in the increase of chain-chain interactions. The materials structure was studied using FTIR and X-ray diffraction (XRD). TGA and Differential thermal analysis (DTA) techniques were employed to investigate the thermal behaviour of material. While electrochemical techniques (cyclic voltammetry and galvanostatic methods) were used to obtain the specific capacitance properties of the materials (Mohamoud, et al, 2014).

The emergence of nanoscience and nanotechnology tools has made it possible to produce polymer blended nano films. These films are 10-100 nm in thickness and offer the additional advantage of very high surface area in the films produced. Other forms of polymer nanostructures can also be produced with very high surface area and associated reactivity (Pan et al., 2010; Berresheim, Müller and Müllen, 1999; Tran, Li and Kaner, 2009; Long et al., 2011; Luckachan and Pillai, 2011).

1.1.4 Polyaniline (PANI)

PANI is easy to synthesise, it is a low cost monomer with easily tuneable properties and has better stability compared to other ICPs (Sarop et al., 2003; Genies et al., 1990).

Various techniques have been employed to produce and develop a variety of different nanostructured PANI Materials such as electrodeposition, electro polymerization,

seeding, and interfacial polymerization to name but a few (Nguyen and Yoon, 2016)

The electrochemical method of polymerization is preferred because of its capability to produce thin nanostructured films and better-ordered polymers. The best films are reported to be produced using a three electrode cell system, i.e. working electrode, counter electrode and reference electrode respectively (Molapo et al., 2012)

PANI displays three oxidation states which are identified and categorised by the ratio of imine nitrogens: amine nitrogens. Leucoemeraldine is known for the fully reduced state of PANI, having a clear/white colour. While the fully oxidized state is known as pernigraniline possessing a blue/violet colour. The emeraldine form is related to a partially oxidized or reduced state and has a deep green or blue colour (Molapo et al., 2012; Bhadra et al., 2009)

The chemical structure of the emeraldine base form of polyaniline can be denoted as $[(-XX-NH-XX-NH-) (-XX-NyZZyN-)]_n$. Where XX denotes a $-C_6H_4-$ ring in the benzenoid form and ZZ denotes a $-C_6H_4-$ ring in the quinoid form. The emeraldine base form can be fully reduced to the leucoemeraldine, $(-XX-NH-XX-NH-)_n$, and fully oxidized to the pernigraniline $(-B-NyZZyN-)_n$ forms. Thus it can be said that the base form of polyaniline consists of alternating reduced and oxidized repeated units. The presence of both the reduced and oxidised form, as shown in Figure 1.3 is referred to as the emeraldine base. (Molapo et al., 2012; Bhadra et al., 2009)

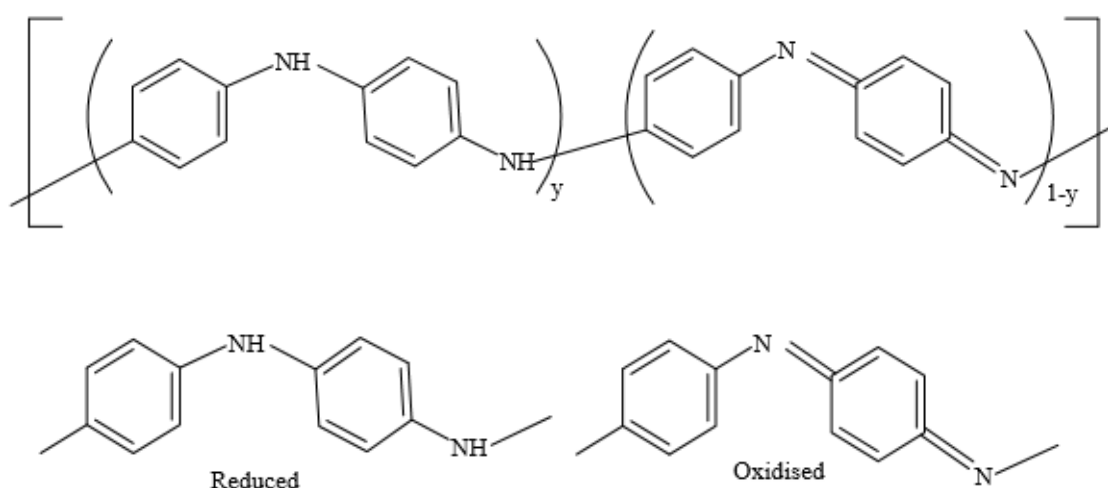


Figure 1.3: Shows emeraldine base as well as the reduced and oxidised form of emeraldine base (Molapo et al., 2012).

In addition to its desirable properties it is the only conducting polymer whose electrical properties can be controlled by charge-transfer doping and/or protonation, as a result of its reversible electrochemical response during anodic oxidation and cathodic reduction. Making it ideal for the development of secondary electrode in rechargeable batteries and electrochromic display devices (Molapo et al., 2012). However, two major limitations of conducting polyaniline are its poor processibility by conventional methods and its poor mechanical properties. These limitations can be overcome by preparing conducting polyaniline blends and composites which have the mechanical properties of the insulating host matrix and the electrical properties of the conducting polyaniline guest. When the host is a polymer, the resulting system is termed a polyaniline blend (or composite), but when the host is a non-polymer material (e.g. metal oxides, silica), it is invariably referred to as a composite (Nenoff 2006).

Common methods used in synthesising polyaniline are electrochemical and chemical oxidative polymerisation methods. The chemical oxidative polymerisation method of synthesis, involves the presence of an oxidising agent in an acidic medium.

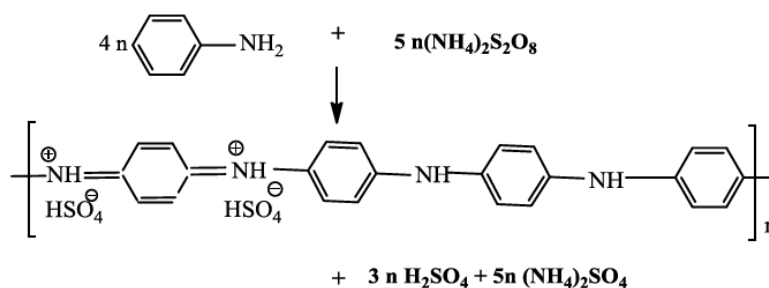


Figure 1.4: The chemical synthesis of polyaniline.

The electrochemical method of preparing polyaniline is most widely and reliably used owing to its ability to direct the experimental condition for suitable purposes.

Electrochemical polymerization of aniline has been carried out in different polymer matrixes such as polyurethane (PU), polycarbonate (PC), poly(methylmethacrylate (PMMA), poly-*p*-phenylene terephthalamide (PPT) (Anand, Palaniappan and Sathyanarayana, 1998) .

1.1.5 Polyamic acid (PAA)

Polyamide is a unique polymer structure with excellent solvent resistance, thermal, electrical and physical properties. As a result it has found use in applications in membranes for gas separation, microelectronics, photonics industry, aerospace, automobiles, wire insulating, and high performance parts and optics devices due to their unique properties as polymers (Stephans, Myles and Thomas, 2000: Mathakari et al., 2009: Liberman, Malba and Bernhardt, 1996). The synthesis of polyamide can be seen below in Figure 1.5.

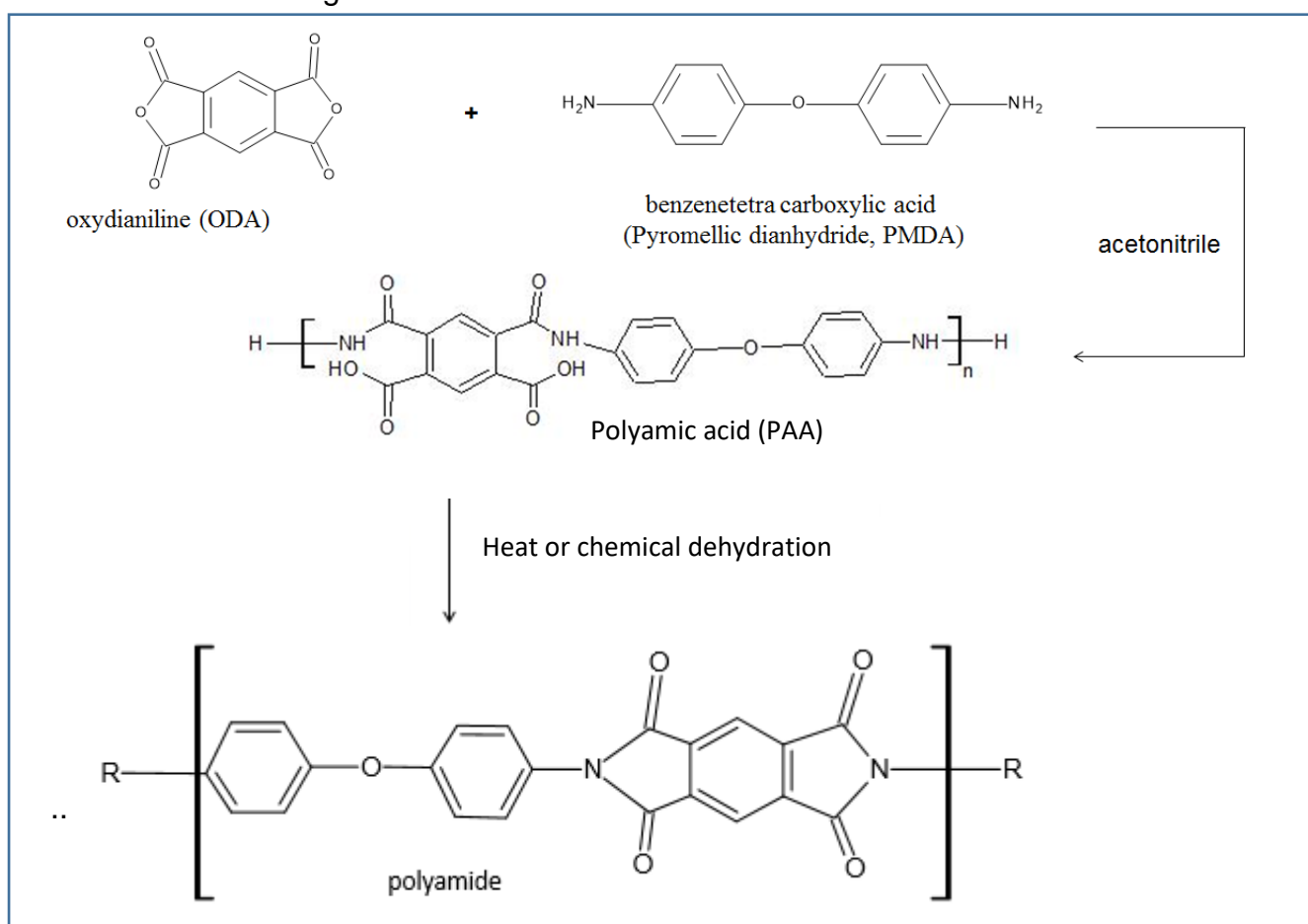


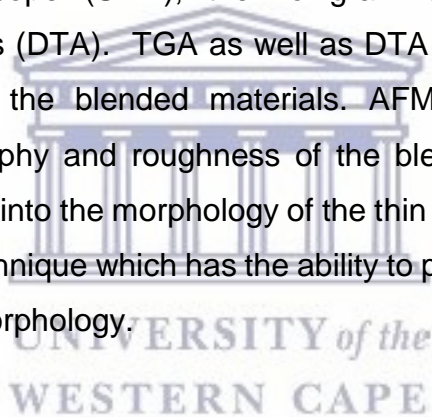
Figure 1.5: The chemical Synthesis of polyamide.

Polyamic acid is the precursor to polyamide polymer. Polyamic acids have amides and carboxylic acid functional groups in the backbone of the polymer. The carboxylic acid behaviour of its backbone allows polyamic acid the ability to create novel polyfunctional materials in the nanoscale (Sadik et al., 2010). Additionally the

polyfunctional nature of the carboxylic group allows the precursor, polyamic acid to have a more superior complexing power when compared to that of polyamide. Research done by Padavan and wan et al., 2010 and Andreescu et al., 2005 have given researches the confidence that polyamic acid possesses the possibility for improving existing nanomaterials and aid in the development of novel nanomaterials that can be used in a variety of devices in a host of different fields

1.1.6 Characterization techniques of polymer blended materials.

Different techniques are used to investigate the properties of polymer blends and polymer blended thin films. Among these techniques the most common are atomic force microscopy (AFM), high resolution transmission electron microscopy (HRTEM), scanning electron microscope (SEM), thermo gravimetric analysis (TGA) and Differential thermal analysis (DTA). TGA as well as DTA are used in order to study the thermal behaviour of the blended materials. AFM is suitable for attaining information on the topography and roughness of the blended material. HRTEM is utilised to gain more insight into the morphology of the thin film particles, as compared to AFM. While SEM is a technique which has the ability to provide detailed information of the polymer materials morphology.



1.2 Rationale and Motivation

The single most evident issue facing humanity in the next 50 years is that of energy. Energy is seen as an essential necessity to the well-being of humans as it is closely linked to quality of life. In recent years there has been an ever increasing demand for energy globally. This demand is as a result of increasing globalisation, industrialisation and population growth. The world's energy is mainly supplied by non-renewable energy sources. Fossil fuel, one such source; has become popular during the last 100 years as they possess useful characteristics. However, in recent year's concerns over global warming, depleting fossil fuels and increasing fossil fuel costs, have resulted in the interest and development of alternative, cheap and reliable energy

storage/generating/conversion devices. One such device capable of storing electricity is a capacitor. (Viswanathan, 2006: Wang, Zhang and Zhang, 2012: Armand and Tarascon, 2008: Park et al., 2010; Wu et al., 2013)

Today organic semiconductors/conductors, prove more appealing than their inorganic semiconductors/conductors counterparts. This is largely due to their flexible nature, low manufacture cost, and processibility simplicity, in addition chemical modifications can be used as a means to tune their optical and electronic properties. These superior properties therefore make them outstanding candidates as advanced materials in the field of photonics and electronics (Shinar and Shinar, 2009: Nalwa, 2008).

Supercapacitors are seen as the next big thing in energy storage, as they can be charged and discharged a million times, in a matter of seconds. A supercapacitor, also known as an electrochemical capacitor is a device that operates on the charge discharge of a high surface area material, like polymers. It possesses a thin electrolytic dielectrics to obtain capacitances that is far superior in magnitude than conventional capacitors (Wang, Zhang and Zhang, 2012). Considered an advanced version of capacitors, supercapacitors have a unique ability to combine the energy storage capabilities of batteries with the power storage capabilities of conventional capacitors. Filling the gap between batteries and conventional capacitors (Kötz and Carlen, 2000). Conducting polymers attracted much attention as electrode materials because of their high electrical conductivity which reduces the internal resistance and high pseudocapacitance. This work will focus on the development of a polyaniline/polyamic acid blend as a material for supercapacitors.

1.3 Aims and Objective

The aim of this study is to investigate polyaniline/polyamide polymer blend for an effective charge transfer mechanism and the subsequent improved efficiency and capacitance.

1.3.1 Objectives of the study

- Aim 1
Synthesise and characterise PANI and PAA single polymers and polymer blend.
Objective 1: Synthesis PAA and characterise by electrochemical technique (CV) and spectroscopic techniques (Uv-vis, FTIR).
Objective 2: Synthesis PANI and characterise by electrochemical technique (CV) and spectroscopic techniques (Uv-vis, FTIR).
Objective 3: Synthesis PBF and characterise by electrochemical technique (CV) and spectroscopic techniques (Uv-vis, FTIR).
- Aim 2
Evaluate the PAA and PANI individual polymers and polymer blends in terms of energy storage capacity.
Objective 1: Evaluation of specific capacitance by CV and galvanostatic charge/discharge (GCD).
Objective 2: Evaluation of specific capacitance and resistance by electrochemical impedance spectroscopy (EIS)
Objective 3: Evaluation of Morphology by SEM and AFM.
- Aim 3
Evaluation of the potential contribution of PBF.
Objective 1: Comparison of results obtained for specific capacitance, solubility, etc. for PBF in the context of other blended polymer systems reported in literature.
Objective 2: Evaluation of PBF in the context of the classical Ragone plot.

1.4 Thesis Outline

This thesis is presented in six chapters. The layout of which can be seen below.

Chapter 1:

This chapter introduces the concept of conducting polymers and provides a background into polyaniline (PANI) and polyamic acid (PAA) as polymer materials. Additionally it presents a review of blended polymers and techniques used to characterize them. Furthermore, the motivation for the project as well as its aims and objectives are stated.

Chapter 2:

Supercapacitor devices that utilise conducting polymers will bridge the gap between carbon-based supercapacitors and batteries in order to form units of intermediate specific energy. This chapter provides a detailed literature review on polymer supercapacitor electrode materials.

Chapter 3:

This chapter addresses the operating principles of various analytical techniques and instrumentation used to characterize individual polymer materials as well as the blended material.

Chapter 4:

This chapter presents the characterization of the conducting polymers and conducting blend illustrating the morphological, structural, spectroscopic, electrochemical properties. The evaluation of the electrochemical performances in terms of capacitance properties of the individual polymers and the blend were characterized by galvanostatic charge/discharge (GCD), cyclic voltammetry (CV) and electrochemical impedance spectroscopy (EIS)

Chapter 5:

This chapter presents the characterization of the conducting polymers and conducting blend illustrating the morphological and structural properties.

Chapter 6:

Concludes by comparing the results obtained for specific capacitance for individual polymers as well as the polymer blended in the context of other blended polymer systems reported in literature. Evaluation of polymer blend in the context of the classical Ragone plot.



Chapter 2

It is proposed that supercapacitor devices that utilise conducting polymers will bridge the gap between carbon-based supercapacitors and batteries in order to form units of intermediate specific energy. This chapter provides a detailed literature review on polymer supercapacitors.

2.1 Introduction into Capacitance

As a result of our ever increasing dependency on energy, energy storage devices have become a primary research focus area. With a view to develop to more efficient energy storage devices (Viswanathan, 2006). An ideal energy storage device should be able to store and deliver large amounts of energy i.e. it must possess a high energy density. Additionally it should also be able to provide pulses of high energy in a short amount of time measured as a high power density (Wu et al., 2013: Armand and Tarascon, 2008: Park et al., 2010)

Conventional capacitors store energy in the form of electrical charge. A capacitor device consists of two conducting materials separated by a dielectric layer. Capacitors have been used as energy storage devices for nearly a century, however, their low capacitance have limited them to low power applications, typically as components in analogue circuits. Recent developments in manufacturing methods as well as the advances in the fields of science and technology leading to the emergence of nanoscience has allowed the production of materials with high surface-area and electrodes of low resistance that have the ability to store amounts of energy in the form of electric charge. Growing understanding of the actual charge transfer processes that takes place in the electric double-layer, enable scientists to propose new solutions to high-power electrochemical capacitors (Wang, Zhang and Zhang, 2012: Kang et al., 2012).

Supercapacitors also known as an ultracapacitors or electrochemical capacitors, show a higher power density compared to batteries and solar cells and also higher energy density compared to conventional capacitors because of unique charge storage mechanisms. Besides bridging the gap between capacitors and batteries, supercapacitors also possess a number of desirable qualities that make them an attractive energy storage option (Kötz and Carlen, 2000).

Supercapacitors provide a mode of electrical charge and energy storage, complementary to that of batteries, based on charging and discharging the interfaces of high specific-area materials such as porous carbon or porous metal oxides. They can store electric charge and deliver corresponding energy at high densities in a highly reversible way, as does a regular capacitor, and hence can be operated at specific power densities (watts/kg) substantially higher than can most batteries. (Chalk and Miller, 2006; Kashem and Ledwich, 2007)

Supercapacitor performance is based on the charge build-up from an electrolyte through electrostatic attraction as a result of polarized electrodes. The systems capacitance is directly proportional to the electrode surface area. Electrostatic attraction of ions in the electrode/electrolyte interface, occurs in micropores proportional to the available surface area, while mesopores offer efficient charge circulation routes (Pandolfo and Hollenkamp, 2006; Kim et al., 2008; Fuertes et al., 2005)

The Ragone plot (Figure 2.1) depicts the power densities of various energy storage devices as a function of their energy densities. Conventional capacitors have a high power density and a low energy density while batteries have a low power density and a high energy density. Supercapacitors occupy the region between conventional capacitors and batteries (Kötz and Carlen, 2000). Despite greater capacitances than conventional capacitors, supercapacitors have yet to match the energy densities of mid to high-end batteries and fuel cells. In supercapacitors the charge/discharge conduct and performance of a supercapacitor are determined by the mode it stores energy.

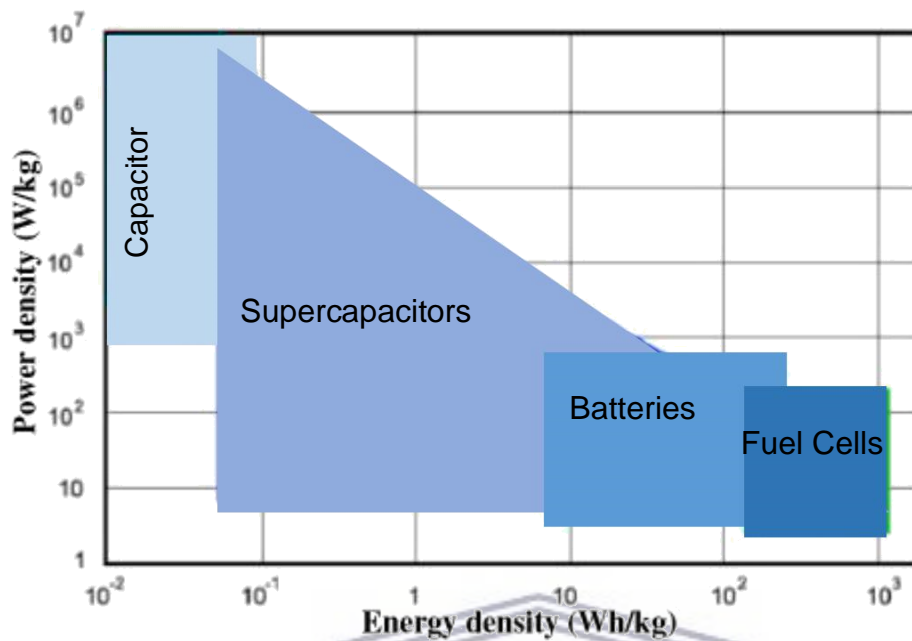
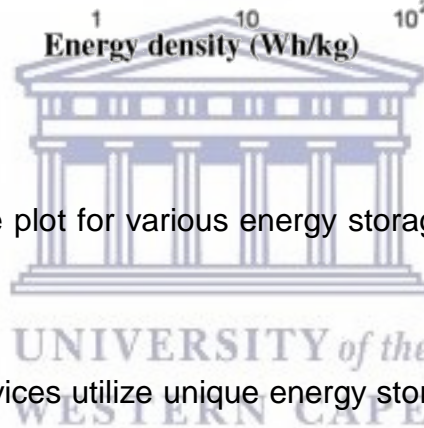


Figure 2.1. Plot of Ragone plot for various energy storage and conversion devices. (Kötz and Carlen, 2000)



Various energy storage devices utilize unique energy storage mechanisms. The way energy is stored influences the charge/discharge behaviour and performance of the device. In conventional capacitors, energy is stored as a result of energy produced electrostatically as positive and negative charges on two parallel plates. Whereas in batteries, the energy is produced from the net chemical reaction between an electrode and electrolyte. Alternatively in fuel cells, the energy storage is based on the oxidation reaction that occurs at the catalytic electrodes (Conway, 1999; Pandolfo and Hollenkamp, 2006; Brodd, 2018). Table 2.1 below compares different parameters across the four mentioned storage devices.

Parameters	Capacitors	Batteries	Fuel cells	Supercapacitors
<u>Electrical characteristics</u>	Has capacitive behaviour: Not any chemical changes High degree of reversibility	No capacitive behaviour: chemical reactions occur. Can be reversible.	No capacitive behaviour: chemical reactions occur. Not reversible	Has capacitive behaviour: Not any chemical changes High degree of reversibility
<u>Charge/discharge time</u>	1 ps-1 ms	1-10 hours	-	1 ms-1 s
<u>Cycle life</u>	Excellent >1 million	Good 150-2,000	-	Excellent >1 million
<u>Energy density</u>	Relatively low 0.01-0.3 Wh/kg	Moderate 30-265 Wh/kg	High 500-2,000 Wh/kg	Relatively low 0.5-20 Wh/kg
<u>Power density</u>	Good >5,000 W/kg	Moderate to Good 100-3,000 W/kg	Low to Moderate 1-1,000 W/kg	Good to Excellent 5,000-10,000 W/kg
<u>Operating voltage range</u>	Low to High 6-800 V	Low 1.2-4.2 V	Low 0.6-0.7 V	Low 1.0-4.5 V
<u>Operating temperature range</u>	-20 to +100 °C	-20 to +65 °C	+50 to +1000 °C	-40 to +85 °C

In case of electrochemical supercapacitor, storage is achieved as the result of Faradic electrosorption or redox reaction at the electrodes (Conway, 1999). On this basis of charge storage mechanisms, the supercapacitors can be presented in two types:

- (i) Electrochemical double-layer capacitors (ECDL): The capacitance develops from the charge separation at the electrode and electrolyte interface.

- (ii) Pseudocapacitors: Utilizes the charge transfer pseudo-capacitance arising from reversible Faradaic reaction occurring at the electrode surface. Made possible by the electrosorption, reduction-oxidation reactions, as well as the intercalation processes.

Pseudo-capacitors exhibit somewhat lower power density than EDCLs because Faradaic processes are normally slower than non-Faradaic processes. (Conway, 1999; Burke et al., 2000).

2.2 Conducting Polymers as supercapacitor electrode materials

The electrode material is seen as an important aspect in the capacitive behaviour of the supercapacitor. Desirable electrode materials include porous carbon, transition metal oxides and conducting polymers. Carbon is the most widely used electrode material, but considerable research is being conducted into metal-oxides and conducting polymers. The correct choice of material is fundamental to the optimal performance of the supercapacitor.

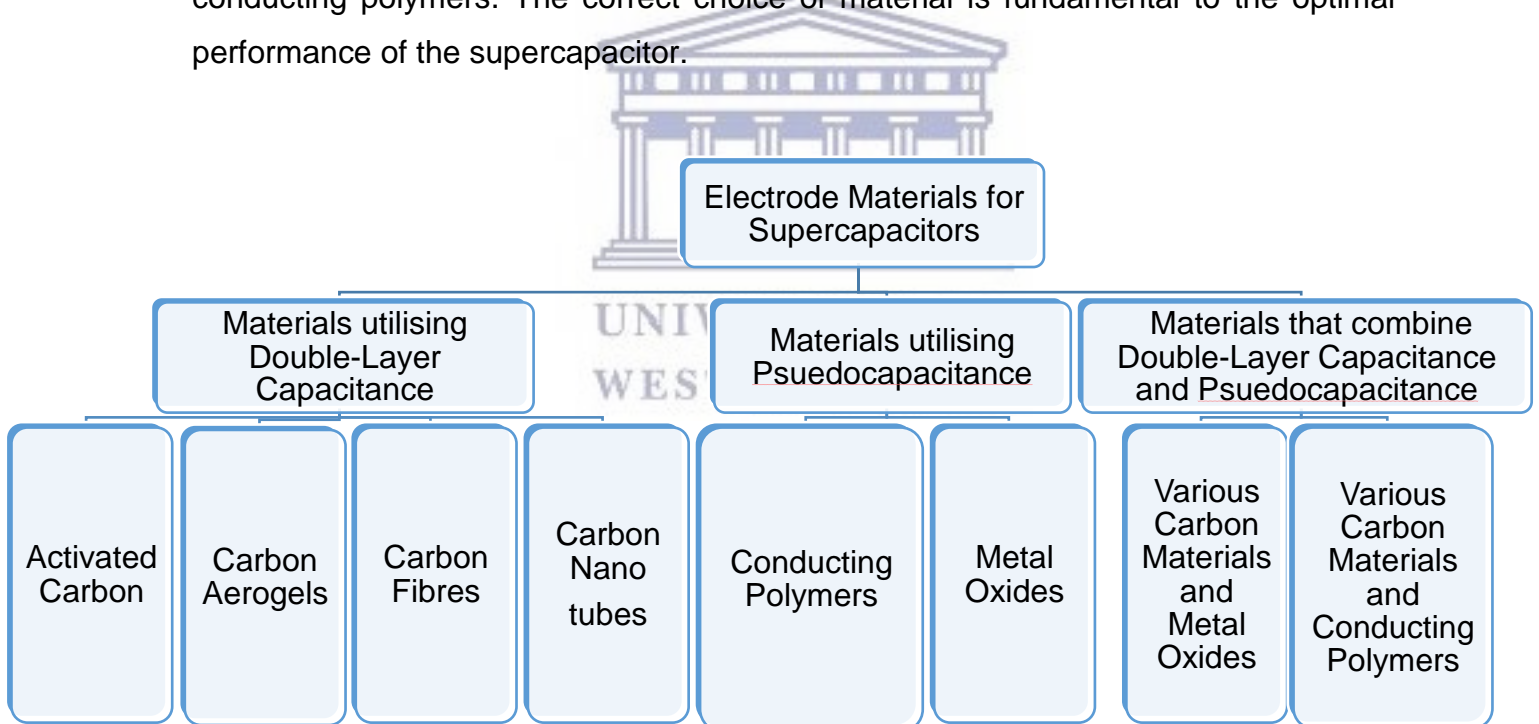


Figure 2.2: Various electrode materials utilized for superconductors (Peng et al., 2008).

Conducting polymers store and release charge through redox processes. When oxidation occurs, ions are transferred from the solution to the polymer backbone.

When reduction occurs the ions are released from the polymer back into the solution. Charging in conducting polymer films therefore takes place throughout the bulk volume of the film, and not just on the surface as is the case with carbon. This offers the opportunity of achieving higher levels of specific capacitance. Thus the energy storage is as a result of the fast and reversible reactions occurring on the electrode surface (Conway, 1999).

The important processes that are responsible for the pseudo-capacitance are:

- (i) Surface adsorption of ions from the electrolyte,
- (ii) Redox reactions involving ions from the electrolyte and
- (iii) Doping and undoping of active conducting polymers on electrode (Burke et al., 2000).

Surface area plays a vital role in (i) and (ii) mentioned above, high surface area with micro-pores promotes the ion access to the electrode material (Burke et al., 2000)

Table 2.2: EDLC and pseudo-capacitance compared (Conway et al., 2003)

Double-layer capacitance	Pseudo-capacitance
Involves non-Faradaic process.	Involves Faradaic process.
Highly reversible charging/discharging.	Moderately reversible however has intrinsic electrode kinetic rate limitation determined by the potential dependent Faradaic leakage resistance (R_f).
Possesses restricted voltage range.	Possesses restricted voltage range
Exhibits mirror-image voltammogram.	Exhibits mirror-image voltammogram.

Polyaniline has an excellent pseudocapacitance property as the electrode in supercapacitors. However, due to the single pseudo-capacitance effect, these supercapacitors cannot obtain a sufficient high specific capacitance and energy density for use in supercapacitors (Yu et al., 2016).

2.3 Conducting Polymers Blends as supercapacitor electrode materials

Nimali et al., 2005 investigated a new supercapacitor electrode material by blending polyacrylonitrile (PAN) and polymethyl methacrylate (PMMA). The polymer blends were synthesised via electrospinning methods. SEM analysis showed that the pore sizes in the blend could be tuned by varying the amount of PMMA loading in the blend compositions. The optimum blend composition of PANI:PMMA (95%:5%), showed the highest surface area and lower charge transfer resistance among the blend compositions studied. Electrochemical methods were used to obtain capacitance values for PANI:PMMA (95%:5%) incorporated carbon nano fibres showed the highest capacitance of 140 F.g^{-1} was achieved and evaluated by cyclic voltammetry techniques. The energy densities of 67 Wh.kg^{-1} at 3.5 V and 101 Wh.kg^{-1} at 4 V and also showed good cycling stability with 85% capacitance retention after 1000 cycles by galvanostatic charge/discharge.

In recent years a number of studies concerning the dielectric properties of inorganic polymer composites, such as Lead zirconate titanate (PZT)/ polyvinylidene fluoride (PVDF) have been reported. These compound material in particular is described as having high dielectric properties (Bayer et al., 2008; Shimizu et al., 2006; Bayer et al., 2005). Extensive amount of research concerning complex materials comprised of PVDF is seen to be favourable as extensive amount of research concerning complex materials comprised of PVDF (Kao et al., 2004; Zhang et al., 2002).

In a study by Li et al., 2008 a poly-(vinylidene fluoride) (PVDF) and polyamide (PA11) blended polymer capacitor have been developed. The blend has high dielectric constant. PA11 is said to show acceptable piezoelectric behaviour after appropriate electroprocessing (Scheinbeim et al., 2003; Xue et al., 2000; Newnham et al., 1986). The blends showed a high dielectric constants that exceed that of the individual polymers used. Analysis by SEM indicated this behaviour may originate from interfacial polymer-polymer interactions occurring between individual polymers within the blended material. DSC and XRD results showed that blending PA11 with PVDF affected the crystalline behaviour of the individual polymers granting the blend superior

mechanical properties. Researchers noticed that PA11/PVDF blends exhibited a slightly high dielectric loss.

2.4 The importance of the electrolyte

An electrolyte is defined as “A liquid that conducts electricity as a result of the presence of positive or negative ions“. Electrolyte optimization is a critical step to improve performance of supercapacitors. Since the resistance of the electrolyte is able to limit the power density, while its ion concentration and operating voltage has the ability to limit the energy density. Thus capacitance of a supercapacitor is influenced by the choice of electrolyte. The ability to store charge is dependent on the accessibility of the ions to the porous surface-area. The ideal pore size distribution in the electrode depends upon the size of the ions in the electrolyte. Thus the material of the electrode needs to be considered when choosing an electrolyte (Frackowiak et al., 2005).

There are currently two main types of electrolyte being used in supercapacitors, namely organic and aqueous electrolytes. Organic electrolytes are the most commonly used in commercial devices, due to their higher dissociation voltage. This allows cells to attain voltages of 2 – 2.5 V, however the resistivity of organic electrolytes is relatively high, thereby limiting cell power. Aqueous electrolytes, electrolyse using water and have a lower breakdown voltage, typically 1 V, but have better conductivity and are relatively more cost effective compared to organic electrolyse (Frackowiak et al., 2005). Further comparisons between organic and aqueous electrolytes are shown below in Table 2.2.

Table 2.3: Comparison of aqueous electrolyte and organic electrolyte (Frackowiak et al., 2005)

Aqueous Electrolytes	Organic Electrolytes
Unit cell voltage is limited to typically 1 V which reduces the energy density.	Unit cell voltage is above 2 V which resulting in high energy density.
Has low specific resistance. Can obtain high power density.	Specific resistance higher than that of aqueous electrolyte Low power density.
Less expensive.	Relatively more expensive.

Tetraethylammonium tetrafluoroborate (TEABF₄) in propylene carbonate (PC) or acetonitrile (AN) are the most common organic electrolytes used and KOH and H₂SO₄ are common aqueous electrolytes used. Recently ionic liquid electrolytes have found favour as they can operate at increased electrochemical windows and have improved thermal stability. The performance with an aqueous electrolyte will yield a higher specific capacitance than of other types of electrolyte. Additionally, waste organic solvents may cause environmental pollution, aqueous solutions used as electrolyte is more preferable. However, material type and morphology will influence the electrolyte used.

A desired electrolyte would be one of a high dielectric constant. There is also the requirement of an electrolyte that can enhance the conductivity and migration of current. Thus it is important that the ion sizes of the electrolyte are not larger than the pore sizes of the material.

The electrode material and accompanying electrolyte are key issues to consider when investigating supercapacitor properties. Considering global social, economic and environmental issues researchers need to develop supercapacitor with high specific capacitance, good energy density, long life cycle, light weight, low toxicity, low cost, flexible, having good thermal and mechanical properties. ICPs have been regarded as promising pseudo-capacitive supercapacitor. The high specific capacitance due to the multi-redox reactions of PANI shows potential for supercapacitor applications.

Pseudocapacitors store charge via Faradic process which involves the transfer of charge between electrode and electrolyte. A pseudo-capacitor typically stores a greater amount of capacitance per gram than an EDLC, as the bulk of the material reacts. PANI materials are active and operate well under certain conditions. It becomes important to use them in the suitable electrolyte solutions.

Chapter 3:

This chapter addresses the operating principles of various analytical techniques and instrument used to characterized the individual polymer materials as well as the blended material.

3.1 Microscopy Techniques

3.1.1 Scanning electron microscopy (SEM)

Scanning electron microscope (SEM) is widely considered as one of the most powerful techniques for characterizing the surface morphology of various materials. It has the ability to produce very high resolution images of samples in the bulk and nano size range. The working principle of SEM is based on the production of various signals from secondary electrons (SE), back-scattered electrons (BSE), X-rays, specimen current, cathodoluminescence (CL), and transmitted electrons. It produces very high resolution images that can show details up to 1nm. The image is produced by scanning with a high energy focused beam of electrons in a raster scan pattern. The electrons from the beam then interact with electrons in the sample and measurable signals are produced. These signals are used to generate a high resolution image of the sample and provides information about the sample's surface morphology, topography, composition, electrical conductivity etc. (Savage and Diallo, 2005; Kim et al., 2002; Aroon et al., 2010).

In this study SEM analysis was conducted on a Hitachi S3000N Scanning Electron Microscope and Zeiss Auriga, High resolution (fegsem) field emission gun scanning electron microscope. An acceleration voltage of 5.0 kV was employed at various magnifications. Scanning electron microscopy (SEM) was used to study the morphology of polyaniline, polyamic acid and the polyaniline/polyamic acid blend after electropolymerization.

3.1.2 Atomic force microscopic (AFM)

Atomic force microscopy (AFM) also known as scanning force microscopy (SFM) has been used since the initial stages of imaging nanoscale materials. It produces topography information of analysed samples on a nanometre scale resolution measurement along with other properties. A very high-resolution scanning probe, called a cantilevers employed, producing resolution on the order of fractions of a nanometer. The force between a cantilever and the sample is measured and this force is then used to generate a topographical image of the samples (Kim et al., 2002; De et al., 2012).

The Nanosurf easyScan 2 is an atomic force microscope system that will be used to attain topographical and roughness information on the polyaniline, polyamic acids and polyaniline/polyamic acids thin films

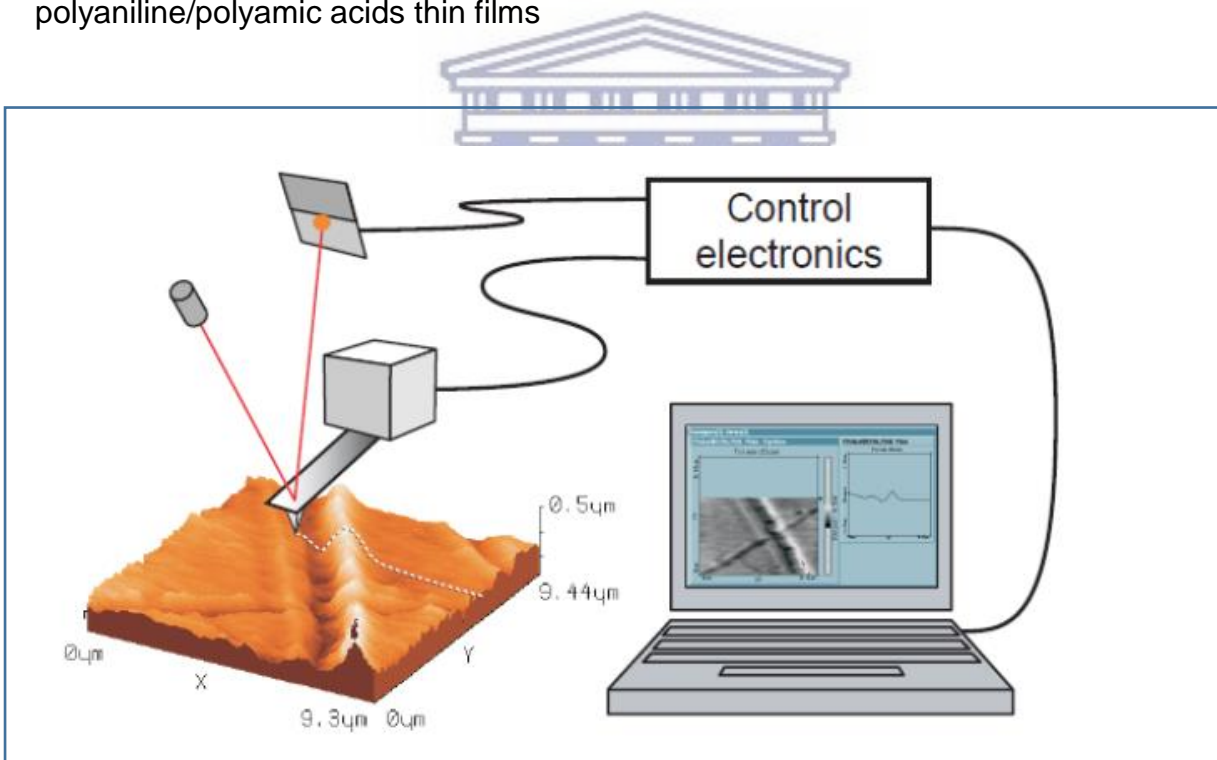


Figure 3.1: Schematic depicting the working principle of an AFM microscope.

3.2 Spectroscopic Techniques

3.2.1 Ultraviolet Visible Spectroscopy (UV-Vis):

Ultraviolet Visible Spectroscopy (UV-Vis) is a type of molecular spectroscopy where the interactions of UV-visible light waves and matter are studied. The absorbance of light by a sample is considered, because light is a form of energy and absorption of light by matter causes the energy of molecules/atoms to increase. UV-Vis operates on the principle of using Ultraviolet (UV) and visible radiation to study the changes in electronic energy levels within the molecule. These changes in the energy levels are as a result of the transfer of electrons from π - or non-bonding orbitals. The technique offers useful information about π -electron systems, conjugated unsaturations, aromatic compounds and conjugated non-bonding electron systems. (Pena-Pereira, Costas-Mora, Romero, Lavilla, & Bendicho, 2011).

For UV-Vis analysis the NICOLET evolution 100 Uv-vis instrument was used to determine the amount of light absorbed by the individual polymer material and polymer blended material as well as to determine the energy bands of the materials. The polymers as well as the blend was dissolved in 1 M HCl and placed in a 4 cm³ quartz cuvettes. The UV-Vis absorption spectra were recorded in the region of 200- 1200 nm.

3.2.2 Fourier Transform Infrared (FTIR) Spectroscopy

Fourier Transmittance Infrared (FTIR) is a method of infrared spectroscopy employed to identify and analyse molecules and atoms within the structure of materials. It provides researchers with qualitative and semi quantitative information. Infrared radiation reacts with sample molecules to cause band vibrations that are characteristic of the functional groups. IR radiation may be absorbed by the sample or pass through (transmitted). A spectrum is produced from molecular absorption and transmission energies.

This spectrum made up of absorption peaks is a molecular fingerprint of the sample. The absorption peaks correspond to frequencies of vibrations between the bonds of the atoms and molecules that make up the material. Molecules differ from each other in terms of chemical composition and structure. Hence, it is possible to obtain positive identification of materials (Chen, Zou, Mastalerz, Hu, Gasaway, & Tao, 2015).

FTIR characterization was performed on a PerkinElmer Spectrum 100, FT-. In infrared spectroscopy. IR spectrometer was used to study the structure and functional groups of chemically synthesized polyaniline (PANI) and polyamic acid (PAA) and the polymer blended material.

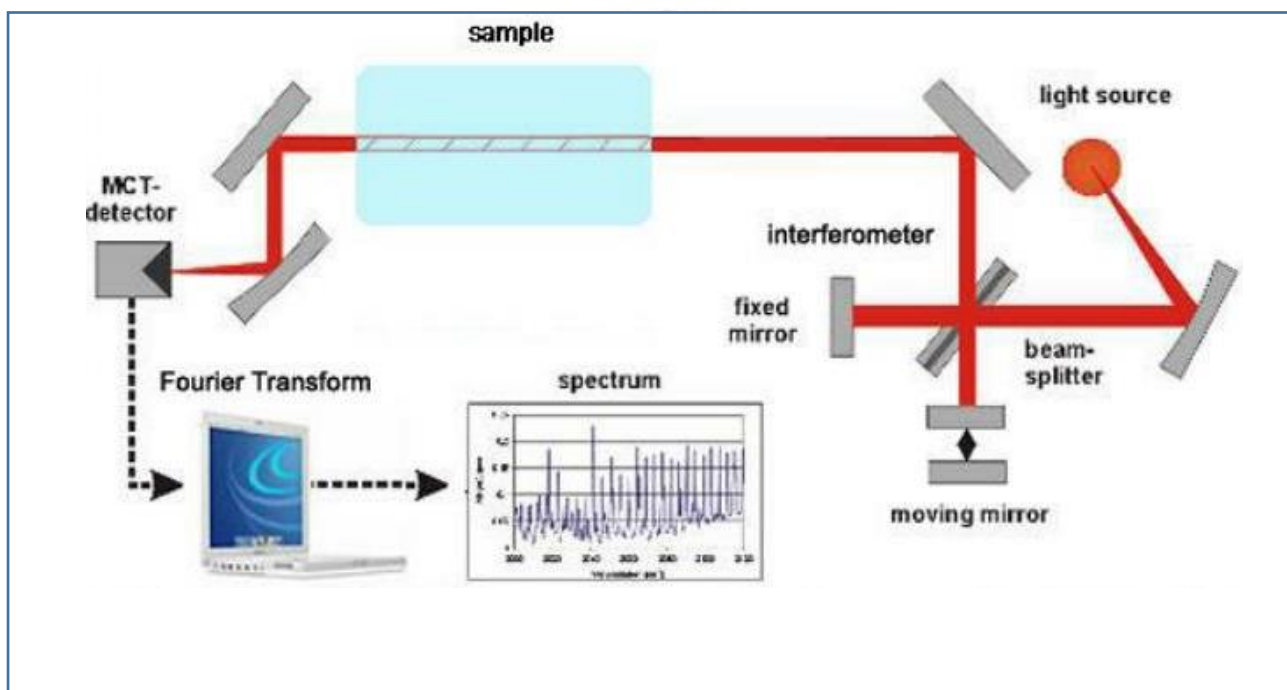


Figure 3.2: Schematic depicting the working principle of FTIR spectrometer.

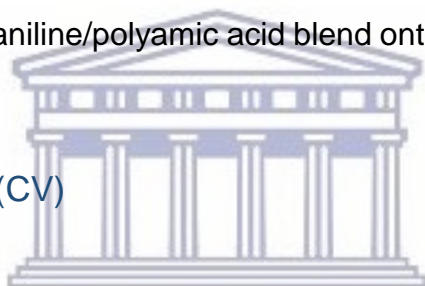
3.3 Electrochemical Techniques

Electrochemical methods allows researchers to blend polymer material and produce them in the form of a freestanding thin film in the nano meter range. Voltammetric techniques have been performed with the use of a PalmSens PTrace 4.4 electrochemical work station using a conventional three-electrode cell. The cell set up includes a glassy carbon working electrode (WE), Ag/AgCl reference electrode (RE) and Pt wire used as a counter electrode (CE)

Electrochemical analyses is divided into two main categories, namely:

- i) Potentiometry: Measures the potential that originates between two electrodes.
- ii) Amperometry: Measures the current that flows between two electrodes.

The working electrodes were prepared by electrodepositing polyamic acid (PAA), polyaniline (PANI) and polyaniline/polyamic acid blend onto glassy carbon electrodes.



3.3.1 Cyclic voltammetry (CV)

Cyclic voltammetry (CV) is widely used to investigate the redox behaviour and to determine the potential window of electrodes or devices. It has been used extensively for the evaluation of the redox properties of conductive and semi-conductive materials (Nicholson, 1965). The principle of CV is based on the measurement of the resulting current when applying a linear potential to an electrode between two potential limits. The rate of change of potential with time is referred to as the scan rate. This is accomplished with a three electrode arrangement whereby the potential relative to some reference electrode is scanned at a working electrode while the resulting current flowing through a counter (or auxiliary) electrode is monitored in a quiescent solution (Reid et al., 2001; Dufresne et al., 2013; Bil'dyukevich et al., 2009; Scally, Davison and Zhang, 2006). A supporting electrolyte is used during the experiment to prevent the migration of charged reactants and products (Evans, O'Connell, Petersen, & Kelly, 1983).

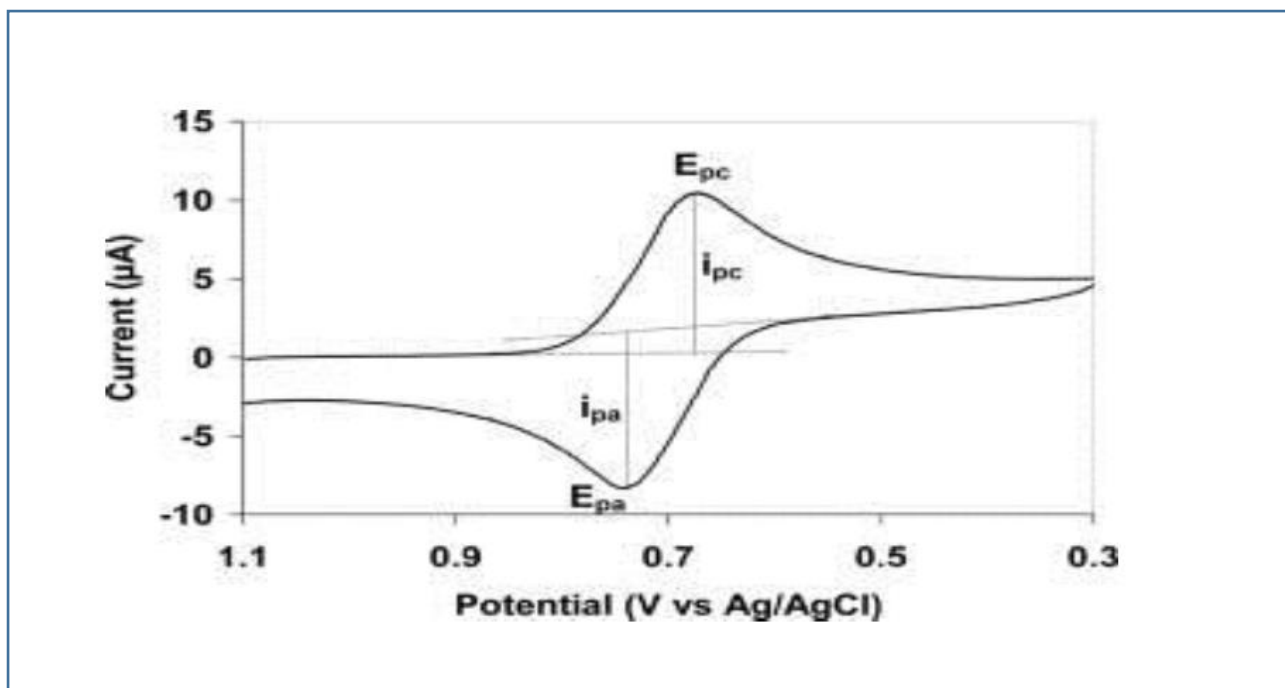


Figure 3.3: A typical cyclic voltammogram for a reversible redox system.

The cathodic and anodic peak (peak potential (E_{pc} , E_{pa}), or peak current (I_{pc} , I_{pa})) provides important information about the sample under investigation. Electrochemical reversibility, irreversibility or quasi-reversibility as well as the electron movement, mass transfer and diffusion coefficient of the system may be obtained (Kang et al., 2007).

The peak current for a reversible system is given by the Randles-Sevcik equation

$$I_p = 2.69 \times 10^5 n^3/2 A D_0^{1/2} C_0 \nu^{1/2}$$

Where:

I_p is the forward peak current (A);

n is the number of electrons exchanged per molecule of the anodic species;

A is the area of the electrode (cm^2);

D_0 the diffusion coefficient ($\text{cm}^2 \cdot \text{s}^{-1}$);

C_0 concentration ($\text{mol} \cdot \text{cm}^{-3}$) and

ν , the scan rate ($\text{V} \cdot \text{s}^{-1}$).

The peak-to-peak separation (ΔE_p) in an electrochemically reversible process is given by the separation between the anodic and cathodic peak potentials

$$\Delta E_p = E_{pa} - E_{pc} = \frac{59}{n}$$

The formal potential (E^0) is represented by the following equation and is obtained from the average values of the peak potentials:

$$E^0 = \frac{E_{pa} + E_{pc}}{2}$$

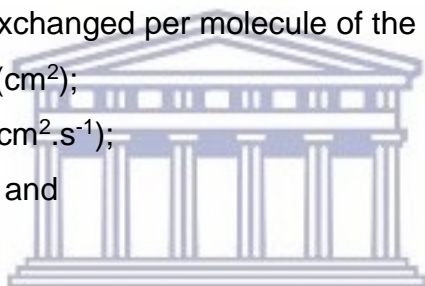
The rate of the electron transfer is lower than that of the mass transport for an electrochemically irreversible process. The peak potentials depend on the scan rate and as a result it gradually shift from the formal potential with increase in scan rate (Peiro, 2003).

The peak current for an irreversible process is given by

$$I_p = 2.69 \times 10^5 \alpha^{1/2} n^{3/2} A D_0^{1/2} C_0 \nu^{1/2}$$

Where:

- I_p is the forward peak current in amperes (A);
- α is the transfer coefficient;
- n the number of electrons exchanged per molecule of the anodic species;
- A the area of the electrode (cm^2);
- D_0 the diffusion coefficient ($\text{cm}^2 \cdot \text{s}^{-1}$);
- C_0 concentration ($\text{mol} \cdot \text{cm}^{-3}$) and
- ν the scan rate ($\text{V} \cdot \text{s}^{-1}$).



UNIVERSITY of the
WESTERN CAPE

A quasi-reversible process occurs when the rate of the electron transfer is in the same order of magnitude as the mass transport. For a quasi-reversible system, the electron transfer processes behaves reversibly at lower scan rates and irreversibly at higher scan rates. (Peiro, 2003).

For supercapacitors CV can additionally be used to:

- i) Attain stability information of the electrode material.
- ii) Aid in choosing the appropriate/ most desired electrolyte for the electrode material being studied.
- iii) Establish the electrolyte concentration.
- iv) Evaluate the capacitance of an electrode material.

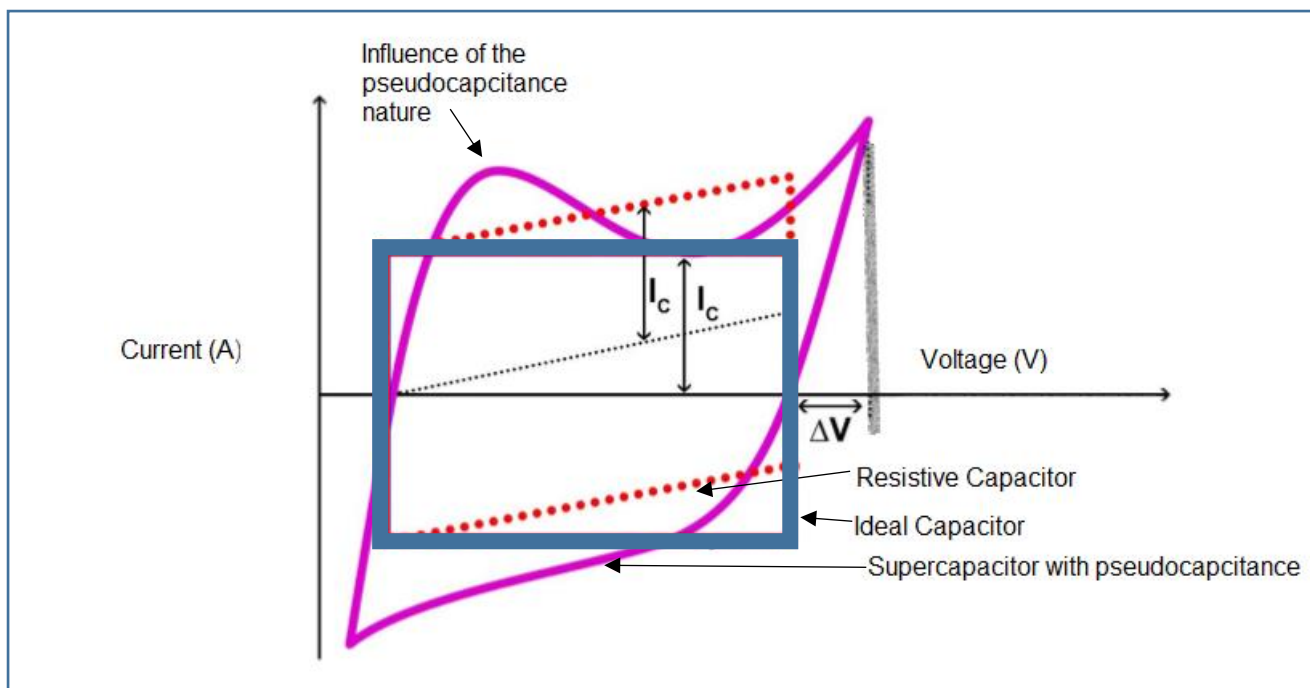


Figure 3.4: Typical cyclic voltammogram of capacitive electrode materials.

The capacitance can be calculated from CV using the following equation.

$$C_s = \frac{\int I dV}{vm\Delta V}$$

Where:

C_s is the specific capacitance ($F g^{-1}$);

I is the current (A);

V is the potential (V);

v is the potential scan rate ($V.s^{-1}$);

ΔV is the potential window (V) and

m is the mass of the electroactive material on the electrode (g). (Frackowiak, E., & Beguin, F et al., 2001)

In this study CV was used for understanding redox reactions of PANI, PAA and PANI/PAA to obtain information about the chemical reactions that occur. CV provided an information about the unique electrochemical behaviour of PANI, PAA and

PANI/PAA and electron kinetic differences between the materials. CV evaluation of individual polymers as well as the blend were carried out in 5 ml of 1 M HCl electrolyte solution, scanning was done from -1000 mV to 1000 mV at various scan rates (10 mV.s⁻¹ – 100 mV.s⁻¹ in 10 mV.s⁻¹ increments).

CV was further used to evaluate the capacitance nature of individual polymers as well as the blend. Experiments were carried out in a 5 ml electrolyte solutions. Four different electrolyte solutions were used, namely lithium perchlorate (LiClO₄) in water, tetrabutylammonium tetrafluoroborate ((CH₃CH₂CH₂CH₂)₄N(BF₄)) in water, LiClO₄ in propylene carbonate (PC) , and (CH₃CH₂CH₂CH₂)₄N(BF₄) in PC, respectively, scanning was done from -1000 mV to 1000 mV at various scan rates (10 mV.s⁻¹ – 100 mV.s⁻¹ in 10 mV.s⁻¹ increments).

3.3.2 Galvanostatic charge/discharge (GCD)

Galvanostatic charge/discharge (GCD) is widely used to calculate the capacitance and cycling stability of electrode materials. The galvanostatic charge/discharge technique is seen as a more accurate technique to evaluate the specific capacitance of materials as compared to CV techniques. The technique operates by employing positive and negative constant currents across the working electrode in order to charge and discharge the electrode. It operates on the principle of measuring the resulting voltage when applying a constant current to an electrode over time. This data is then represented as a triangular-like curve. A typical GCD curve is shown in figure 3.5, showing voltage versus the function of the time. The specific capacitance is determined by the equation below:

$$C = \frac{4I\Delta t}{m\Delta V}$$

Where:

I is the current (A);

Δt is the discharge time (s);

m is the mass of electrode material (m) and

U is the potential window (V).

The technique provides us with information on the materials performance under practice operating conditions. It is widely accepted as a reliable method to determine the capacitance and energy density of supercapacitors. A galvanostatic curve has 4 areas of interest.

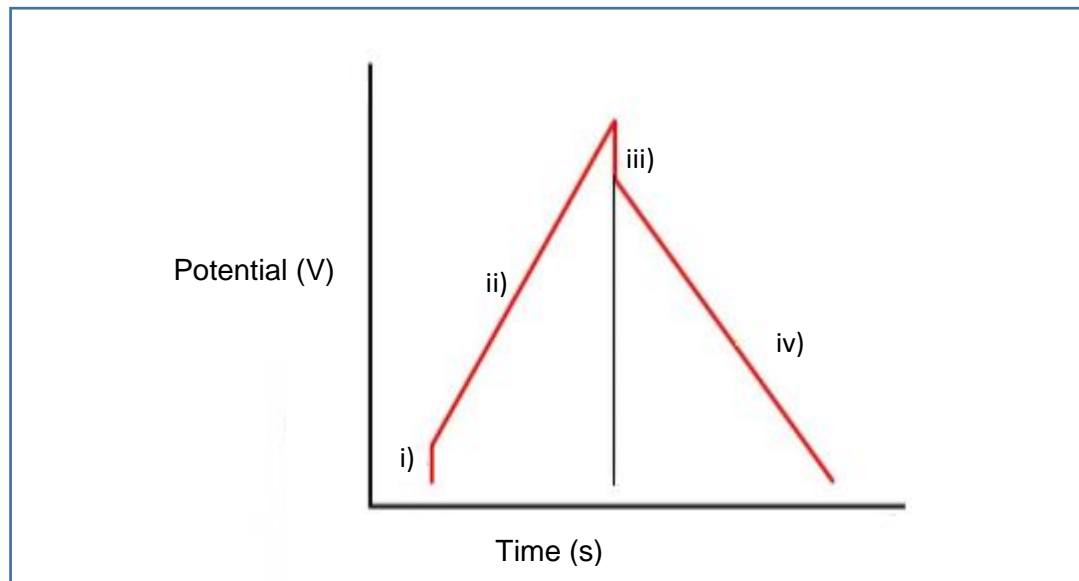


Figure 3.5: Typical cyclic charge-discharge curve illustrating idea capacitor performance.

- (i) The initial process.
- (ii) Charging behaviour of the system.
- (iii) Ohmic Potential drop (represents the negative resistive ohmic loss associated with the resistance of the cell).
- (iv) Discharging behaviour of the system.

This technique provided information on PANI, PAA and PANI/PAA performance under practice operating conditions. The charge/discharge behaviour of PANI, PAA and PANI/PAA blend will be evaluated to determine the specific capacitance and energy density of the supercapacitor electrode materials.

3.3.3 Electrochemical Impedance (EIS)

Electrochemical impedance spectrometry (EIS) allows us to obtain information about the equivalent series resistance (ESR), charge transfer resistance and diffusion impedance of the material. It allows us to separate Faradaic charge transfer from capacitance charge transfer and used to attain information on the different system components of the system (Macdonald, 2006).

The technique differs from CV as a sinusoidal voltage signal is imposed at a range of frequencies and the resulting current is measured. The data is represented as a sinusoidal output signal. The output is an indication of the magnitude of the impedance owed to the electrochemical system under investigation and the time lag on the sinusoidal output signal. Impedance is a measure of the ability of a circuit to resist the flow of an alternating current. The data collected from impedance evaluation can be viewed as a Nyquist plot of real versus imaginary impedance (Macdonald, 2006). (Fasmin & Srinivasan, 2017).

The plot has two distinct sections: a semicircle section and a linear portion. The semicircle section at higher frequencies corresponds to the electron transfer process, while the linear portion corresponds to the lower frequencies where the diffusion process of the electrochemical system is measured. The electron transfer resistance (R_{ct}) equates to the semicircle diameter and gives information about the systems conductivity (Wang, Moser, & Gratzel, 2005).

Data obtained can be interpreted in terms of electrical equivalent circuits (EEC's). The equivalent circuit maps the electrochemical cell in terms of electrical components such as ideal resistors and capacitors (Jorcin, Orazem, Peberé, & Tribollet, 2006).

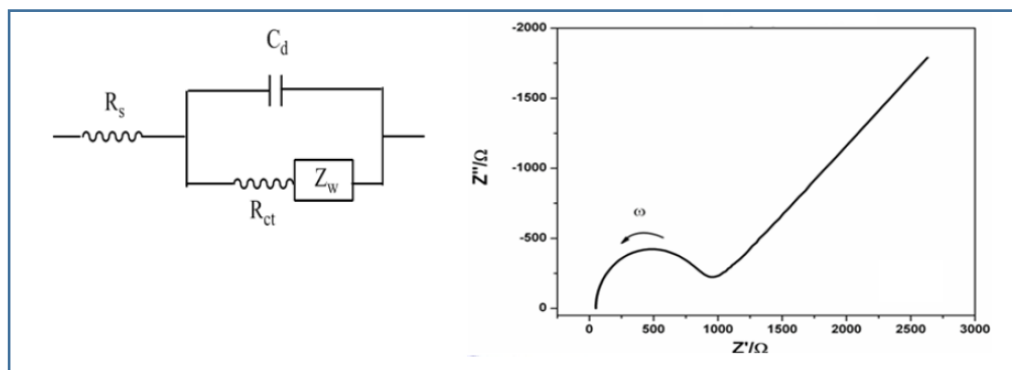


Figure 3.6: Typical Nyquist plot and its equivalent circuit.

The Nyquist plot (represented by real part of the impedance Z' vs. imaginary part Z'') represents the charge transfer kinetics of the modified electrodes in which R_s is the ohmic (internal or solution) resistance, also known as the solution resistance (R_s) between the working electrode and the reference electrode. Constant phase element (CPE) is the capacitance phase element at the electrolyte interface and W (Warburg impedance) represent the mass transfer element associated with diffusion, and it depends on the frequency of the potential perturbation. The charge transfer resistance (R_{ct}) is the resistance to electron transfer at the electrode/electrolyte interface.

EIS was used to evaluate the resistance and capacitance of PAA, PANI and PANI/PAA and respectively.

Instrumental techniques discussed above have been used to obtain a variety of information of the desired properties needed to investigate a good supercapacitor electrode material.



Chapter 4

This chapter presents the synthesis and preparation of the individual polymer materials as well as the blended material. Furthermore, it discusses the characterization of the individual polymer materials as well as the blended material; this includes microscopic, spectroscopic and electrochemical characterization.

4.1 Materials

The reagents 4,4-oxydianiline (97%) (ODA), 1,2,4,5-benzenetetracarboxylic acid (96%), pyromellitic dianhydride (PMDA), hydrochloric acid (32%) (HCl), acetonitrile (99.8%)(ACN), ammonium persulfate (98%) (APS), ferric chloride (98%) ((NH₄)₂S₂O₈), tetrabutylammonium tetrafluoroborate ((CH₃CH₂CH₂CH₂)₄N(BF₄)) (99%), propylene Carbonate (98%) (PC), lithium Perchlorate (99.99%) (LiClO₄), were all obtained from Sigma-Aldrich, South Africa. All chemicals were of analytical grade and were used without further purification. Deionized (ultra-pure) water with a resistivity of 18.2 MΩ/cm, purified by a Milli-QTM system (Millipore) was used as reagent water in the preparation of all solutions.

4.2 Method

Electrolytes.

Hydrochloric acid was prepared by dilution of 32% HCl to a fixed concentration of 1M. Lithium perchlorate was prepared by dilution of 99.99% LiClO₄ to a fixed concentration of 1 M (in distilled water).

Tetrabutylammonium tetrafluoroborate was prepared by dilution 99% ((CH₃CH₂CH₂CH₂)₄N(BF₄)) to a fixed concentration of 0.04 M

Tetrabutylammonium tetrafluoroborate was prepared by dilution 99% ((CH₃CH₂CH₂CH₂)₄N(BF₄)) to a fixed concentration of 1 M (in PC).

Lithium perchlorate was prepared by dilution 99.99% LiClO₄ to a fixed concentration of 1 M (in PC).

Polyamic acid

Polyamic acid was prepared by mixing 2.0021 g of ODA (0.01 M) and 157 ml of ACN. This stock solution was stirred constantly to obtain a homogeneous solution. A further 50 ml of ACN containing 2.1812 g of PMDA (0.01 M) was added in a drop wise manner at 8 minute intervals, over a period of 60 minutes. Upon completion the mixture was left to stir at room temperature for 24 hours. The resulting yellowish precipitate was filtered through a membrane under suction and dried at room temperature. The amount of PAA obtained was 3.45 g, corresponding to 83% yield.

Polyaniline

Polyaniline was chemically synthesised by dissolving 1 ml of aniline in 10 ml HCl/100 ml distilled water. The solution was stirred for 30 minutes at 50 °C whereafter 2.40 g $(\text{NH}_4)_2\text{S}_2\text{O}_8$, and 1.88 g of FeCl_3 , was added respectively to the solution. The resulting mixture was stirred for another 3 hours at 50 °C. The resulting green precipitate was filtered through a membrane under suction and finally dried at room temperature. The content of the reaction was placed in the oven at 50 °C overnight to evaporate the solvents and the remaining content was washed with ethanol and dried at 50 °C

Polymer Thin Film

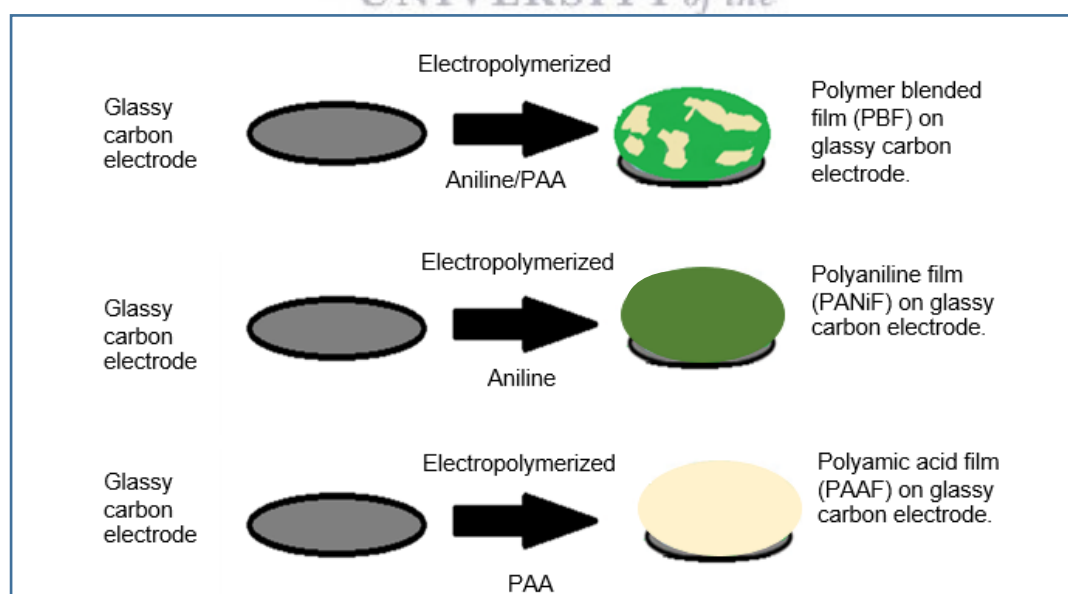
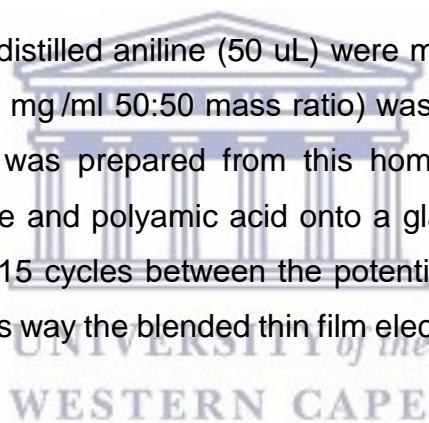


Figure 4.1: Electrochemical synthesis of polymer blended thin film electrode (PBF), polyaniline thin film electrode (PANiF) and polyamic acid thin film electrode (PAAF).

PAA thin film was produced by dissolving 50 ug of PAA in 3 ml of 1 M HCl. The resulting solution (0.03 g/ml solution) was sonicated for 60 min. There upon the polymer was electrochemically polymerized onto a glassy carbon electrode in a three electrode system for 15 cycles between the potential range of -1000 mV and 1000 mV at 50 mV.s⁻¹. In this way the PAA thin film electrode (PAAF) was produced.

PANI thin film was produced by was dissolving 50 uL of distilled aniline in 3 ml of 1 M HCl. The resulting solution (0.03 g/ml solution) was sonicated for 60 min. There upon the polymer was electrochemically polymerized onto glassy carbon electrode in a three electrode system for 15 cycles between the potential range of -1000 mV and 1000 mV at 50 mV.s⁻¹. In this way the PANI thin film electrode (PANIF) was produced.

Polyamic acid (50 ug) and distilled aniline (50 uL) were mixed with 3 ml of 1 M HCl. The resulting solution (0.03 mg/ml 50:50 mass ratio) was sonicated for 60 min. The blended polymer thin film was prepared from this homogeneous solution by the polymerization of polyaniline and polyamic acid onto a glassy carbon electrode in a three electrode system for 15 cycles between the potential range of -1000 mV and 1000 mV at 50 mV.s⁻¹. In this way the blended thin film electrode (PBF) was produced.



4.3 Spectroscopic characterisation

4.3.1 FTIR of PAA

The PAA powder was pressed into a potassium bromide (KBr) pellet for FTIR analysis. The FTIR spectra obtained was recorded over the range of 4000 cm⁻¹ to 500 cm⁻¹ and shown in Figure 4.2 below. The identifying FTIR absorption bands were observed at comparable values to literature reports. (Andreescu et al, 2005; Noah et al, 2012).

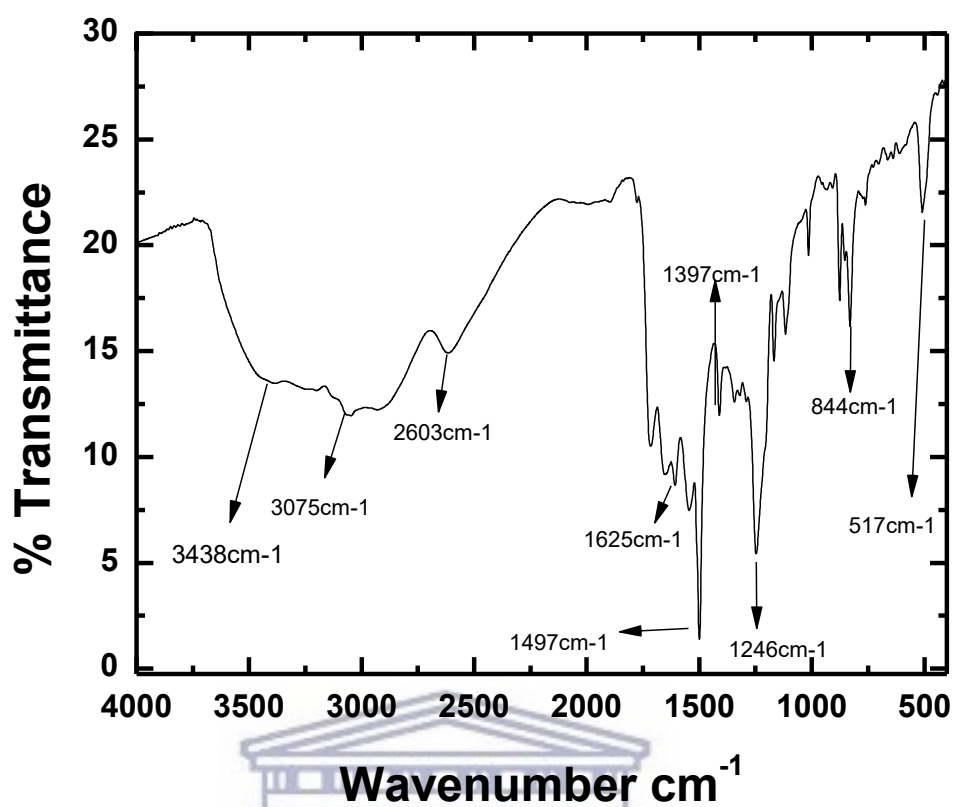


Figure 4.2: FTIR spectrum of polyamic acid (PAA).

The absorption bands as observed in the FTIR spectrum for PAA are indicated below:

Table 4.1: Fourier transform Infrared peaks assignment for PAA

Assignment	Frequency (cm ⁻¹)
amide group	517
ether group	1246
amide group	1397
amide group	1625
carboxylic acid	2603
NH	3075

4.3.2 FTIR of PANI

The FTIR spectrum of pure PANI exhibits the characteristic bands in the 500 cm^{-1} - 4000 cm^{-1} range. The peak at 1552 cm^{-1} can be attributed to the C=N and C=C stretching modes for the quinoid rings. The peaks at 1496 cm^{-1} which correspond to the stretching vibration of the absent benzoic rings in PANI. The absence of the stretching vibration of benzoic group in PANI confirms the existence of fully oxidized PANI. The band at 1288 cm^{-1} belongs to the C–N stretching of a secondary aromatic amine strengthened by protonation of PANI, The band at 1143 cm^{-1} is considered to be a measure of the degree of electron delocalization in PANI chains and thus is a characteristic peak related to PANI conductivity. The identifying FTIR absorption bands were observed at comparable values to literature reports (Polyaniline: The Infrared Spectroscopy of Conducting Polymer Nanotubes (IUPAC Technical Report, 2011: Zhu, Peng and Jiang, 2013)

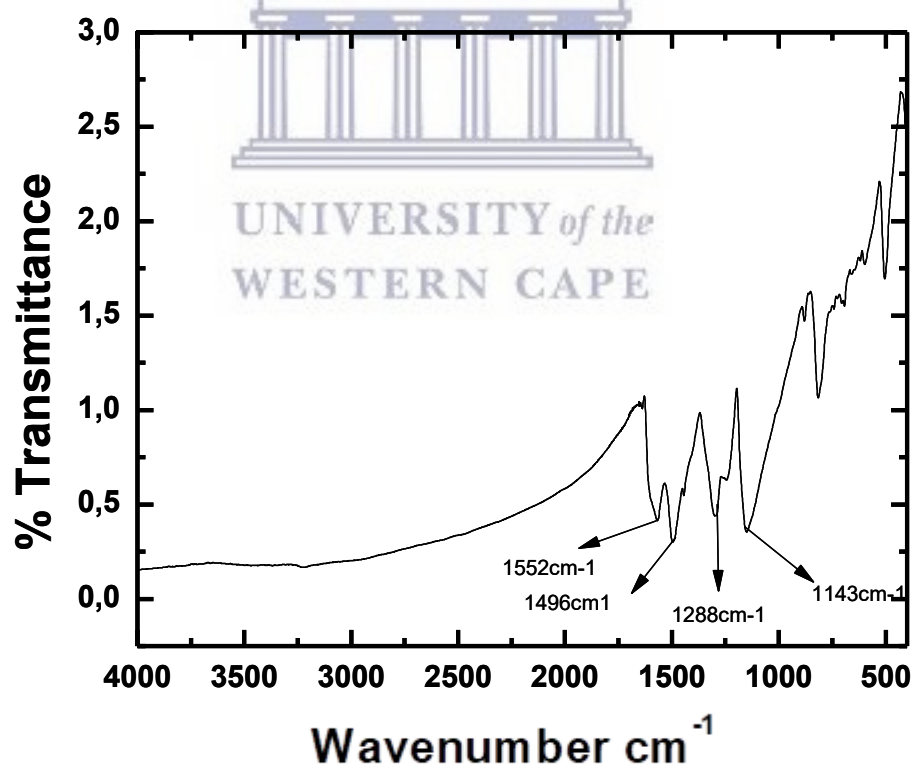


Figure 4.3: FTIR spectrum of polyaniline (PANI).

The absorption bands as observed in the FTIR spectrum for PANI are indicated below:

Table 4.2: Fourier transform Infrared peaks assignment for PANI

Assignment	Frequency (cm ⁻¹)
amide group	1143
C–N	1288
ether group	1496
C=N and C=C	1552

4.3.3 FTIR of PAA/PANI Blend

Equal amounts of polyamic acid and polyaniline where each prepared individually by chemical synthesis. The resulting powders where mixed together (ratio 1:1) in a mortar and pestle. The mixed powder was pressed into a KBr pellet, for FTIR analysis. The FTIR structure of PAA/PANI pellet (Figure 4.4) show strong characteristics of PAA indicating the physical dominance of the polymer as the host material.

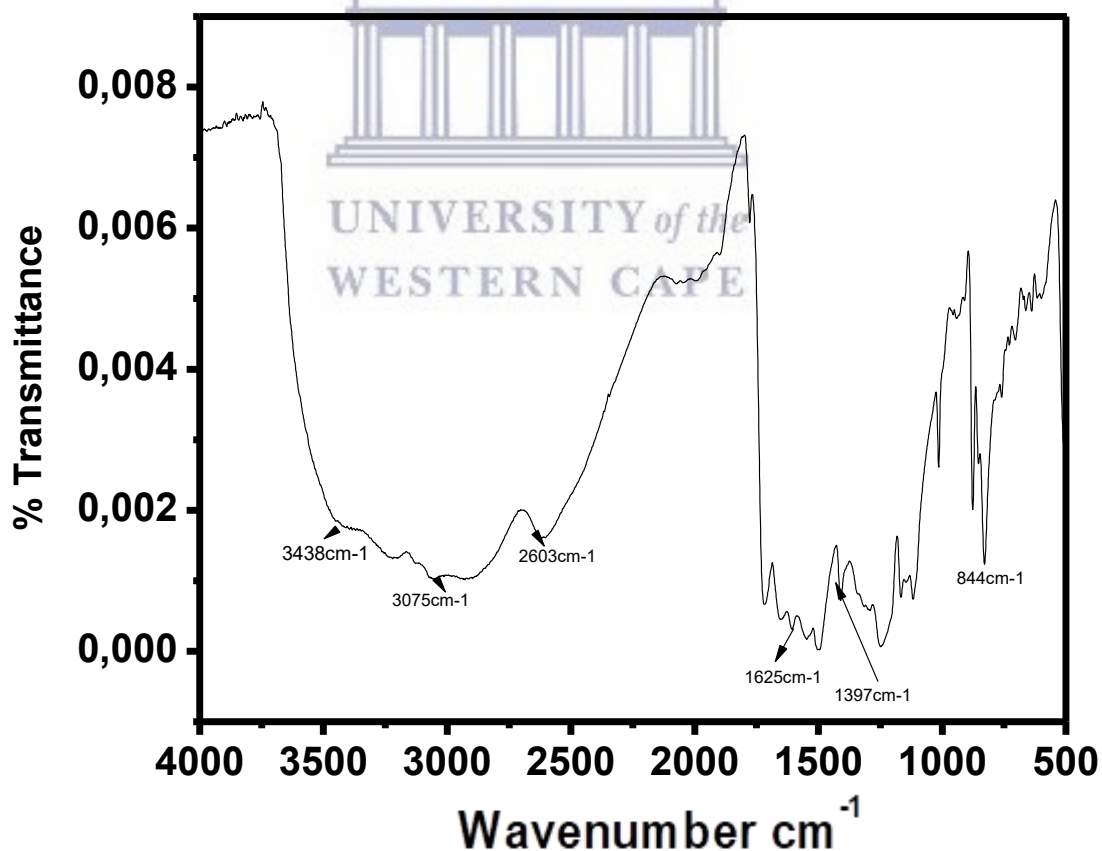


Figure 4.4: FTIR spectrum of PAA/PANI blend.

4.3.2 Ultraviolet visible UV/vis of individual polymers and blend

UV/vis analysis was done by making up a 3 ml 1 M HCl solution of 10 μ L PANI, PAA and PAA/PANI respectively. The absorbance of the materials were recorded by placing 1 ml of the resulting solution in a cuvette and performing the analysis. The absorbance spectra figure 4.5 was measured in the range 200 -1200 nm. PANI has the highest wavelength while PAA has the highest absorbance.

The UV-Vis spectra of PANI shows three peaks at 357 nm, 453 nm and a broad peak at 518-880 nm, which are characteristic of emeraldine salt. The peak at 357 nm was assigned to $\pi - \pi^*$ of benzoic rings, 453 nm was assigned to $n - \pi^*$ due to polaron band, and 518-880 nm was due to $\pi - n$ which is as a result of excitons and doping level. PAA showed two peaks to $\pi - \pi^*$ and $\pi - \pi^*$. The identifying FTIR absorption bands were observed at comparable values to literature reports. (Huang and MacDiarmid, 1993; Nekrasov, Ivanov and Vannikov, 2000).

The UV-Vis spectra of PANI/PAA, Figure 4.5 show strong characteristics of PAA indicating the physical dominance of the polymer as the host material in the polymer blend. PANI decrease absorbance in the PANI/PAA blend.

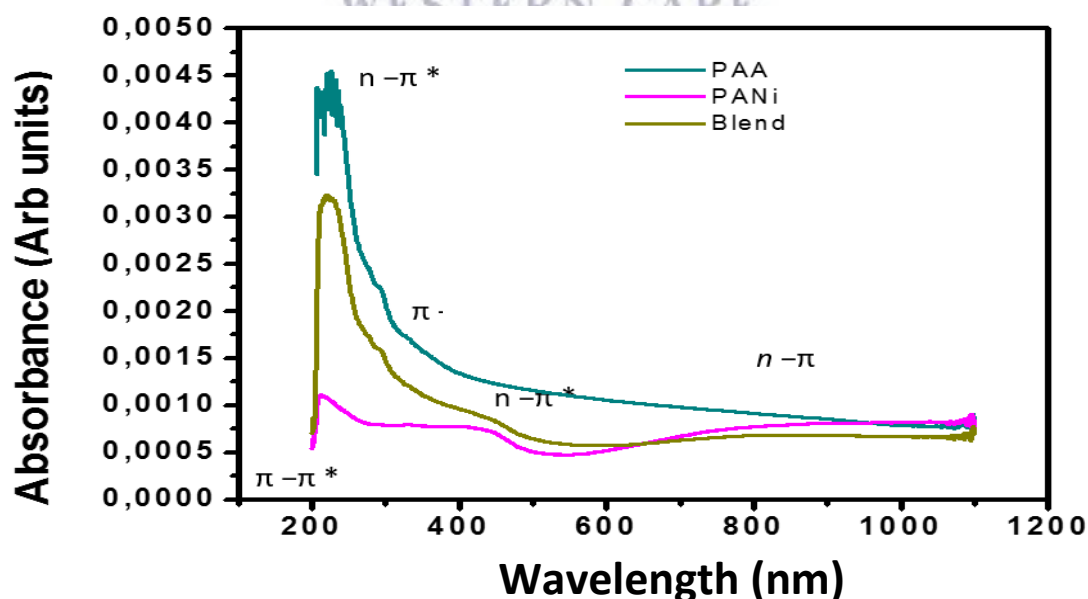


Figure 4.5: UV/Vis spectrum of PAA, PANI and PAA/PANI.

4.4 Characterization of thin films.

4.4.1 Electrochemical characterization

Cyclic voltammetry (CV) experiments were carried using PalmSens 3.0 electrochemical workstation (Bioanalytical Systems, USA.). Often the three-electrode configuration is utilized in measuring the electrochemical behaviour of electrode materials (figure 4.6). This includes a working electrode (WE) where the polymer material was deposited, reference electrode (RE) which was Ag/AgCl and a platinum wire counter electrode (CE) submerged in 5 ml of 1 M HCl electrolyte.

All experimental solutions were purged with high purity Argon gas and blanketed with Argon atmosphere during measurements. The experiments were carried out at controlled room temperature (25 °C).

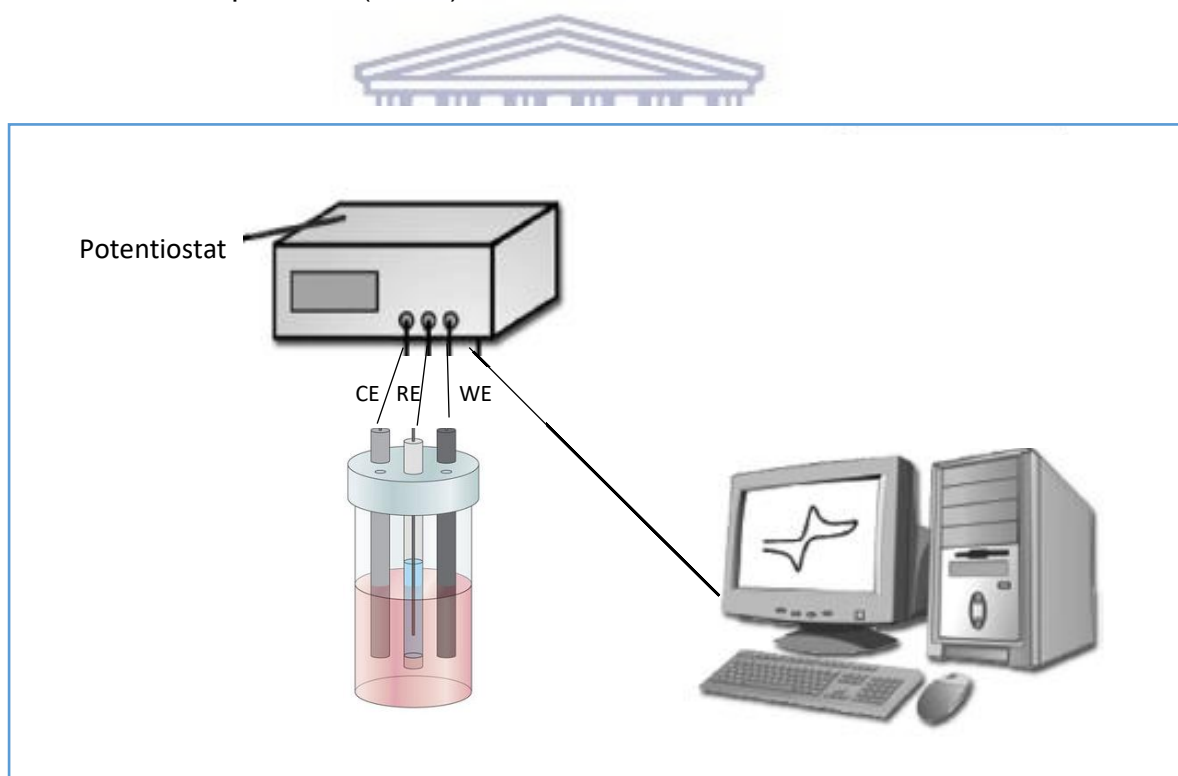


Figure 4.6: Electrochemical workstation configuration.

4.4.1.1 Cyclic Voltammetry of thin film electrodes

The PAAF, PANIF and BPF were prepared by in-situ electrodeposition onto three different glassy carbon electrodes (GCE) respectively. Uniform films were obtained after 15 cycles in the potential window of -1000 mV and 1000 mV at 50 $\text{mV}\cdot\text{s}^{-1}$ (Figure 4.7, 4.10 and 4.13). The PAAF, PANIF and BPF electrodes were further characterized by CV at different scan rates in 1 M HCl. The kinetics of the electron transfer processes involved were studied by varying the scan rate ($\text{mV}\cdot\text{s}^{-1}$) and observing the effect on the peak currents and peak potentials for all thin film electrodes.

In the electrosynthesis of PAAF the system was scanned across a potential range of -1000 mV -1000 mV. An oxidative localised charge is produced at the electrode interface which attracts the dissolved PAA in solution and results in an adsorbed polymer thin film of PAA. This adsorption is observed as a rise in current which typically peaks after 5 cycles indicating that the PAA is deposited on the electrode. The additional 10 cycles allows a layer of sufficient thickness for the duration of the experiment to be formed on the GCE (Figure 4.7).

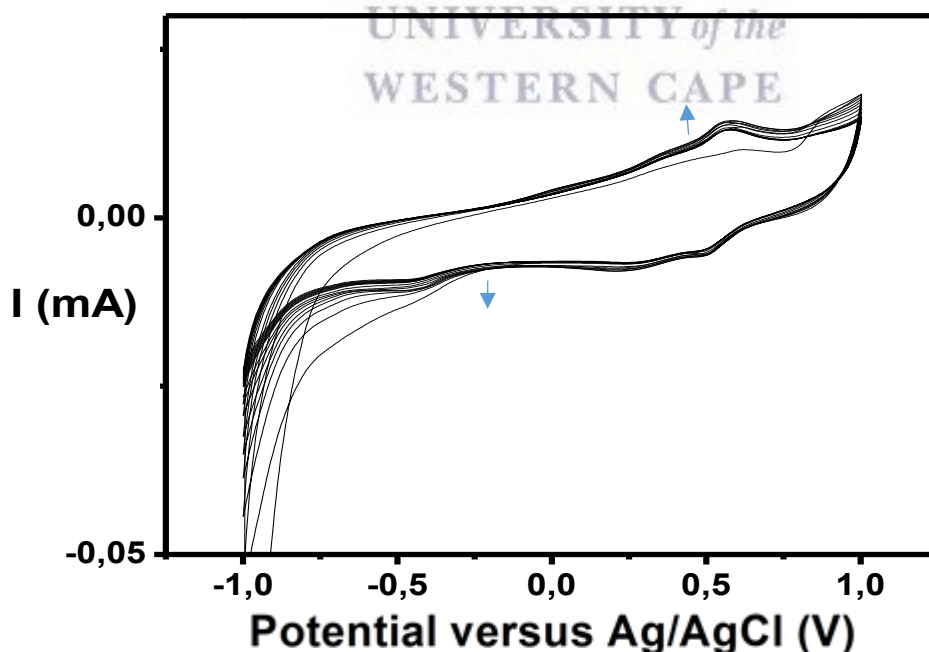


Figure 4.7: Electrodeposition of PAAF.

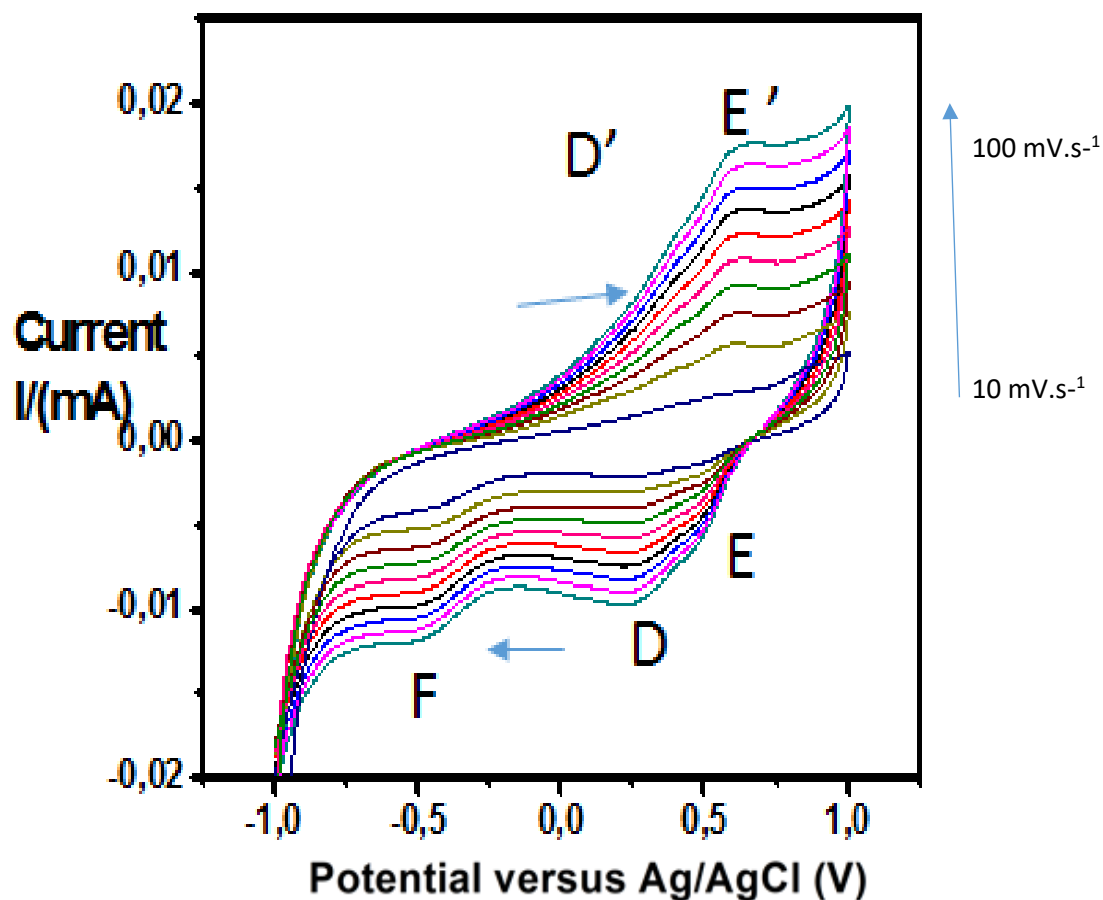


Figure 4.8: Cyclic voltammogram of PAAF in 1 M HCl at different scan rates (10-100 $\text{mV}\cdot\text{s}^{-1}$).

The cyclic voltammogram for PAAF is in agreement with reported studies (Andreescu et al, 2005; Hess et al, 2014; Zamfir et al., 2016) with two anodic peaks due to the NH and OH functional groups in the polyamic structure (E and D) and two cathodic peaks (E' and D'). The current peaks of PAAF increased with the increasing scan rate.

Table 4.3: The effect of scan rate on the anodic and cathodic peak currents and peak potentials of PAAF at different scan rates in 1 M HCl electrolyte.

Scan rate v mV/s	Peak potential separation	Peak potential separation	I_{pa1}/I_{pc1} (peak E/E')	I_{pa2}/I_{pc2} (peak D/D')			
	ΔE^{o_1} (peak E-E')	ΔE^{o_2} (peak D-D')					
	10,00	0,40			-0,06	-1,31	-1,45
	20,00	0,45			-0,05	-1,60	-1,70
30,00	0,43	-0,06	-1,89	-1,98			
40,00	0,42	-0,07	-1,95	-2,14			
50,00	0,42	-0,04	-1,84	-1,99			
60,00	0,42	-0,07	-1,83	-2,05			
70,00	0,43	-0,06	-1,83	-2,09			
80,00	0,43	-0,05	-1,82	-2,18			
90,00	0,41	-0,05	-1,78	-2,03			
100,00	0,42	-0,06	-1,78	-2,13			

UNIVERSITY of the
WESTERN CAPE

PAAF displayed two redox couples E/E' and D/D' with peak current ratios I_{pa1}/I_{pc1} and I_{pa2}/I_{pc2} respectively. The peak current ratios all ranged from 1.31 to 2.13 which indicated a two electron process for the system. The redox couple E_{pa1}/E_{pc1} was found to be irreversible at formal potential $E^{o_1} = 0,42$ V (vs Ag/AgCl) based on peak separation ($\Delta E^{o_1} = 0.4$ V) whereas the second redox couple at $\Delta E^{o_2} = -0,057$ V, showed quasi irreversible behaviour. The peak currents for PAAF redox peaks, increased with the increase of scan rates, indicating diffusion controlled electron mobility within the polymer backbone.

The peak currents were plotted as a function of the square root of scan rate in order to evaluate the diffusion behaviour of PAAF as shown in figure 4.9. A straight line with high correlation coefficient was obtained which confirmed the diffusion controlled behaviour at the interface according to the Randles-Sevcik equation.

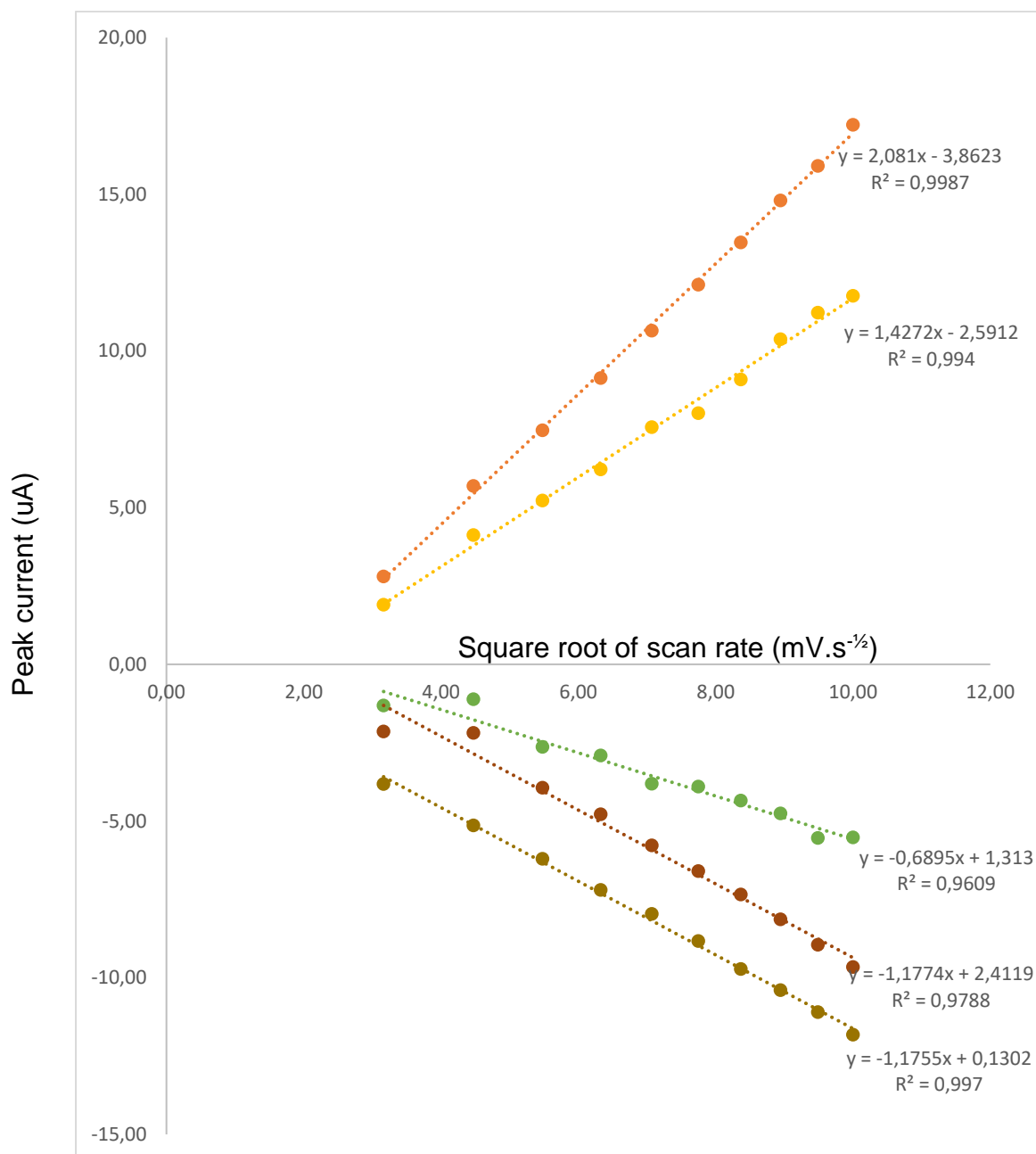


Figure 4.9: Graph of anodic and cathodic peak current (I_p) vs. square root of scan rate ($mV.s^{-1/2}$) for PAAF in 1 M HCl at different scan rates.

The rate of electron transport (D_0) within the polymer layer was evaluated from the slope of the straight line plots for an irreversible system, the Randles Sevcik equation is given as:

$$I_p = 2.69 \times 10^5 \alpha^{1/2} n^{3/2} A D_0^{1/2} C_0 \nu^{1/2}$$

The electron transport diffusion coefficient, D_0 , was found to

Table 4.4: Diffusion coefficients calculated for all PAAF peaks.

<u>PAA</u>	
<u>Peak</u>	<u>D_0 (cm².s⁻¹)</u>
E'	1.44x10 ⁻⁰⁸
D'	7,87x10 ⁻⁰⁸
D	3,80x10 ⁻⁰⁸
E	6,50x10 ⁻⁰⁸
F	6,49x10 ⁻⁰⁸

UNIVERSITY of the

The calculated diffusion coefficient obtained for PAAF is lower compared to previously reported diffusion coefficients of PAAF (Andreescu et al., 2005; Hess et al., 2014). This can be attributed to PAAF having formed a thicker layer. Thicker PAA film, can act as insulators, reducing the electroactive surface of the working electrode and can reduce the diffusion coefficient (Zamfir et al., 2016).

The electron transport diffusion coefficient, D_0 , was found to be slightly smaller for oxidation (1.44x10⁻⁰⁸ cm².s⁻¹) compared to reduction (6.50x10⁻⁰⁸ cm².s⁻¹) with the formal potential for the redox couple E'/E determined as 424 mV (vs Ag/AgCl).

The electron transport diffusion coefficient, D_0 , was found to be slightly larger for oxidation (7,87x10⁻⁰⁸ cm².s⁻¹) compared to reduction (3,80x10⁻⁰⁸ cm².s⁻¹) with the formal potential for the redox couple D'/D determined as 1304 mV (vs Ag/AgCl).

The surface concentration PAAF on the surface of the GCE can be determined by using the Brown Anson approximation below.

$$I_{p,a} = \frac{n^2 F^2 A \Gamma}{4RT} v$$

Where:

$I_{p,a}$ is the peak current (A)

n is the number of electrons (2)

F is Faradays constant (96485 C.mol⁻¹)

A is the geometric area of the electrode surface (0.03 cm²)

R is the gas constant in J mol⁻¹ K⁻¹ (8.314 J.mol⁻¹K⁻¹)

T is presented by the absolute temperature (298.15 K)

v is the scan rate in (V.s⁻¹)

Γ represents the surface concentration coverage/density (mol.cm⁻²).

Therefore Γ for PAAF is calculated to be 6.54×10⁻⁹ mol.cm⁻².

The electropolymerisation of distilled aniline in an acidic medium was carried out for 15 cycles at 50 mV.s⁻¹ in a 3 electrode system. The electrosynthesis system was scanned across the potential range -1000 mV -1000 mV. The CV behaviour of the PANI film (PANIF) grown on a glassy carbon electrode is shown in figure 4.10. Polymerisation reaction was initiated by the formation of resonance-stabilised aniline radical cations from the protonated aniline monomer. The cyclic voltammogram revealed that the polymerisation current increases as the number of voltammetric cycles increases, confirming the conductive nature of the polymer. The PANIF thickness increased with successive potential cycles. A homogenous film was produced after the 15 successive voltammetric cycles.

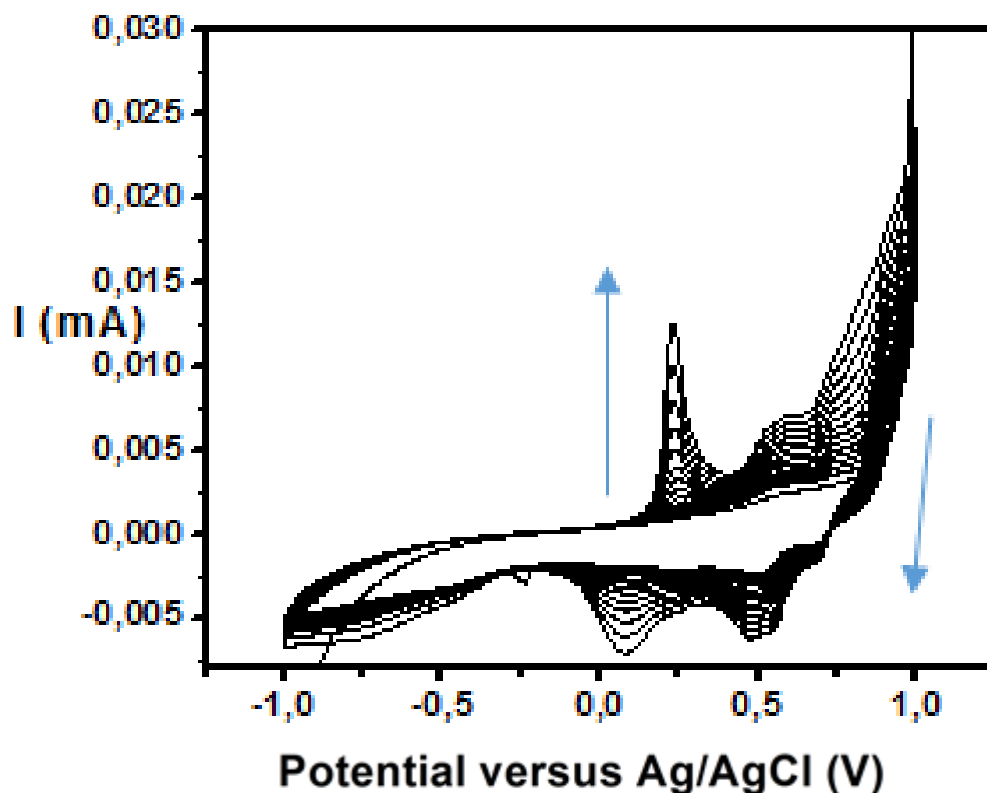


Figure 4.10: Electro-polymerization of PANIF.

The scan rate dependency of PANIF showed 3 redox couples. The first redox peak corresponds to pernigraniline radical cation/pernigraniline (A/A'). Peaks B/B' are emeraldine radical cation/emeraldine and the final redox peak is the leucoemeraldine/leucoemeraldine radical cation (C/C'). The three anodic and cathodic redox peaks in the CVs are characteristically typical of the electrosynthesis of polyaniline (Wang, Li and Xia, 2006; Tóth et al., 2013).

The redox peaks A/A' and C/C' indicate the conversion of leucoemeraldine to emeraldine and emeraldine to pernigraniline, respectively. The middle redox peak B/B' could be referred to as the dimers or benzoquinone/hydroquinone couple of the polymeric chains but with a lesser amount of intensity (Wang et al., 2006). Three anodic and cathodic corresponding peaks can be observed with increase in the peak currents as the potential scan increases. The three redox peaks have been assigned accordingly. Figure 4.11: Cyclic voltammogram of PANIF in 1 M HCl at different scan rates (10-100 $\text{mV}\cdot\text{s}^{-1}$).

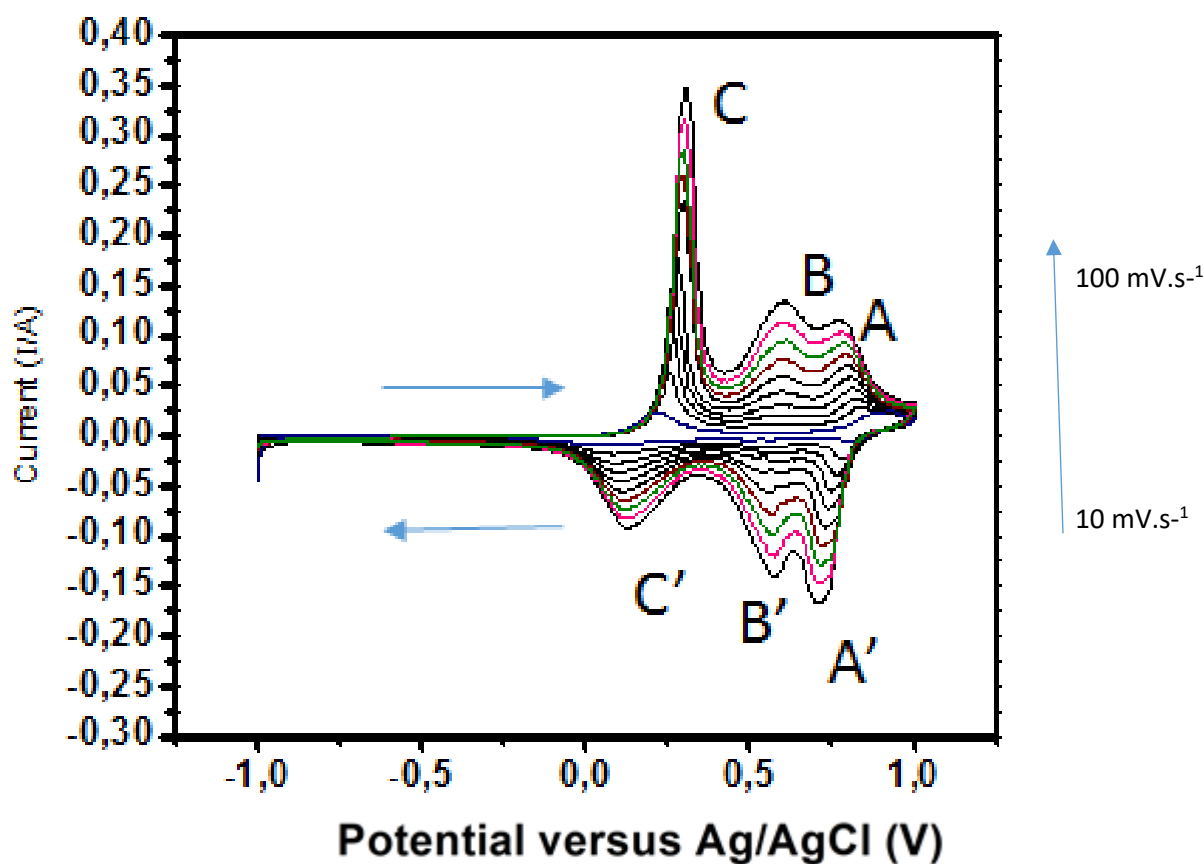


Figure 4.11: Cyclic voltammogram of PAAF in 1M HCl at different scan rates (10-100 $\text{mV}\cdot\text{s}^{-1}$).

UNIVERSITY of the
WESTERN CAPE

PANIF displayed three redox couples A/A', B/B' and C/C' with peak current ratios I_{pa1}/I_{pc1} , I_{pa2}/I_{pc2} and I_{pa3}/I_{pc3} respectively. The ΔE_p ($E_{p,a} - E_{p,c}$) values calculated for each of the scan rates, exhibit ΔE_p value less than 65 mV. This indicates the fast and reversible electrochemistry nature of PANIF. The peak currents for PANIF redox peaks, increased with the increase of scan rates, indicating diffusion controlled electron mobility within the polymer backbone.

Table 4.5: The effect of scan rate on anodic and cathodic peak current and peak potentials of PANI in CVs for different scan rates in 1 M HCl electrolyte.

Scan rate v mV/s	Peak potential separation ΔE°_1 (peak A-A')	Peak potential separation ΔE°_2 (peak B-B')	Peak potential separation ΔE°_3 (peak C-C')	I_{pa1}/I_{pc1} (peak A/A')	I_{pa2}/I_{pc2} (peak B/B')	I_{pa3}/I_{pc3} (peak C/C')
10,00	0,05		0,14	3,13		2,66
20,00	0,05	0,56	0,16	1,22	1,11	3,71
30,00	0,08	0,57	0,17	0,97	1,09	3,91
40,00	0,05	0,58	0,18	0,85	1,15	3,92
50,00	0,06	0,57	0,19	0,80	1,22	3,96
60,00	0,06	0,58	0,21	0,76	1,03	4,26
70,00	0,06	0,58	0,21	0,73	0,68	4,02
80,00	0,06	0,59	0,21	0,72	0,95	3,84
90,00	0,07	0,58	0,21	0,68	0,96	3,82
100,0	0,08	0,59	0,21	0,68	0,95	3,77

The Randles Sevcik equation was used to determine the rate of electron transport (D_0) within the polymer layer using the equation.

The peak currents were plotted as a function of the square root the of scan rate in order to evaluate the diffusion behaviour of PANIF as shown in figure 4.9. A straight line with high correlation coefficient was obtained which confirmed the diffusion controlled behaviour at the interface according to the Randles-Sevcik equation.

$$i_p = (2.69 \times 10^5) n^{3/2} A C D_0^{1/2} v^{1/2}$$

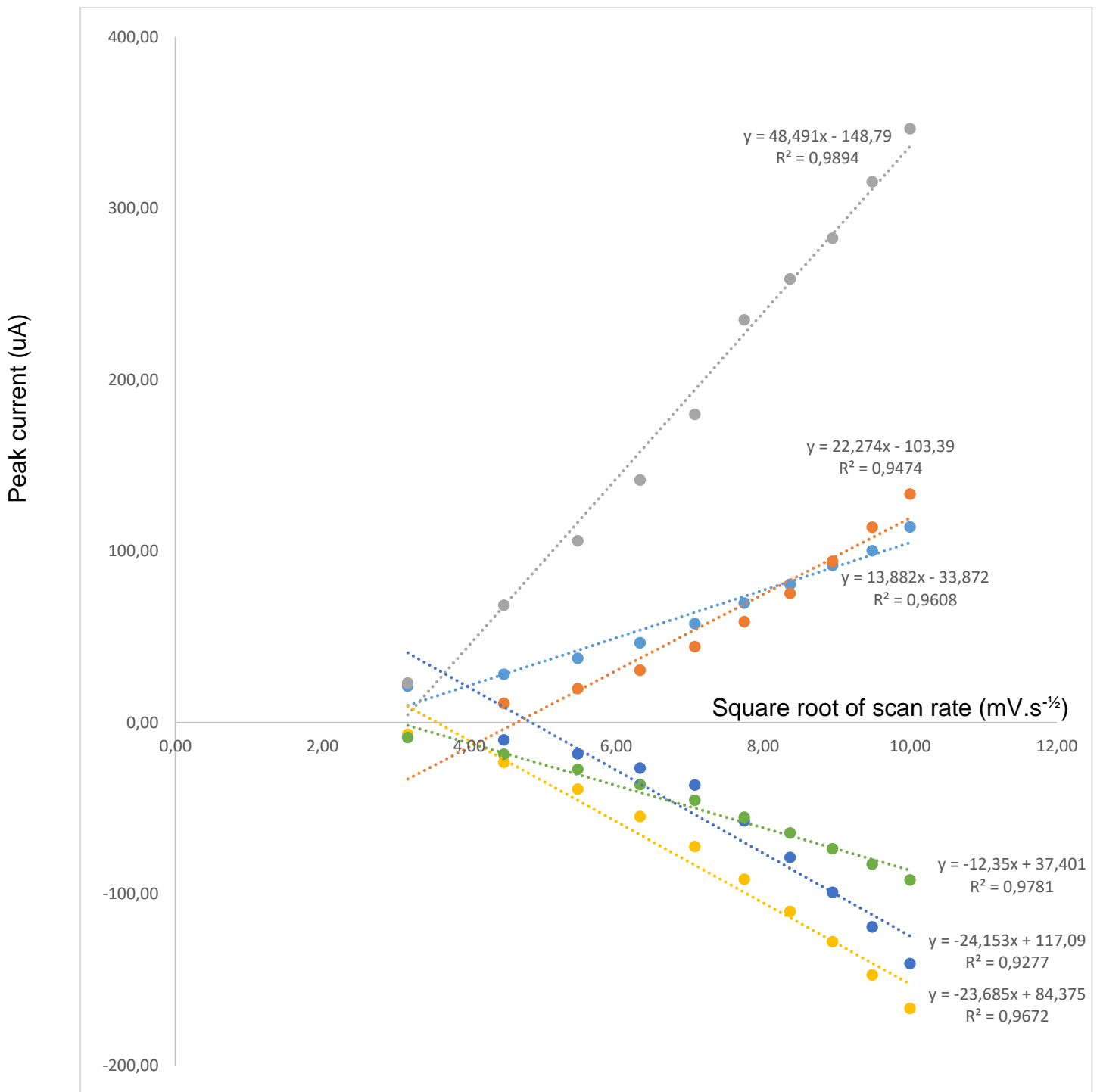


Figure 4.12: Graph of anodic and cathodic peak current (I_p) vs. square root of scan rate ($\text{mV}\cdot\text{s}^{-1/2}$) for PANI in 1 M HCl solution at different scan rates for peaks.

The electron transport diffusion coefficient, D_0 , was found to be.

Table 4.6: Effect of scan rate on peak current and peak potentials for PANI

PANI	
Peak	D_0 ($\text{cm}^2.\text{s}^{-1}$)
A	7.30×10^{-06}
B	1.17×10^{-06}
C	2.55×10^{-06}
A'	1.27×10^{-06}
B'	9.65×10^{-07}
C'	1.25×10^{-06}

The calculation of diffusion coefficients from oxidation currents (7.30×10^{-06} , 7.30×10^{-06} and $2.55 \times 10^{-06} \text{ cm}^2.\text{s}^{-1}$) was observed to be higher than diffusion coefficients from reduction currents (1.27×10^{-06} , 9.65×10^{-07} and $1.25 \times 10^{-06} \text{ cm}^2.\text{s}^{-1}$), indicating that the kinetics of the system favour the oxidised state. This is as a result of the electrochemical synthesis refers to the oxidation of the aniline and growth of the polymer chain (PANI) onto the electrode. D_0 is the electron charge transport coefficient also in regards to polymer materials it is the rate of electron charge propagation along the polymer chain. An increased value was obtained in this study as to compared to $8.68 \times 10^{-9} \text{ cm}^2.\text{s}^{-1}$ reported by Mathebe et al., 2004 indicating much a faster electron charge transfer.

The surface concentration PANIF on the surface of the GCE can be determined by using the Brown Anson approximation below.

$$I_{p,a} = \frac{n^2 F^2 A \Gamma}{4RT} V$$

Γ was calculated to be $1.92 \times 10^{-8} \text{ mol}.\text{cm}^{-2}$.

Polyamic acid (50 μg) and distilled aniline (50 μL g) were mixed with 3 ml of 1 M HCl. The resulting solution (0.03 mg/ml 1:1 ratio) was sonicated for 60 min. 50 μl of the mixture was placed into an electrochemical cell along with 3 ml 1 M HCl. The blended polymer thin film was prepared from this homogeneous solution by the interfacial polymerization of polyaniline and polyamic acid onto glassy carbon electrode in a three electrode system for 15 cycles between the potential range of -1000 mV and 1000 mV at 50 $\text{mV}\cdot\text{s}^{-1}$.

The cyclic voltammogram revealed that the polymerisation current increases as the number of voltammetric cycles increases, confirming conductive nature of the polymer. The PANI/PAA polymer blended thin film (PBF) thickness increased with successive potential cycles. A homogenous film was produced after the 15 successive voltammetric cycles.

For the electrodeposition of PBF the electrochemical response was seen to be similar to that of PANIF, except for the oxidation of the monomer occurred at slightly lower potential and at decreased peak currents. This response could be attributed to the fact that the same oxidative localised charge that oxidized the monomer attracts the PAA in solution that results in PAA being trapped in the polymer. The regions where PAA has thicker particle layers can be cause of the lower values seen.

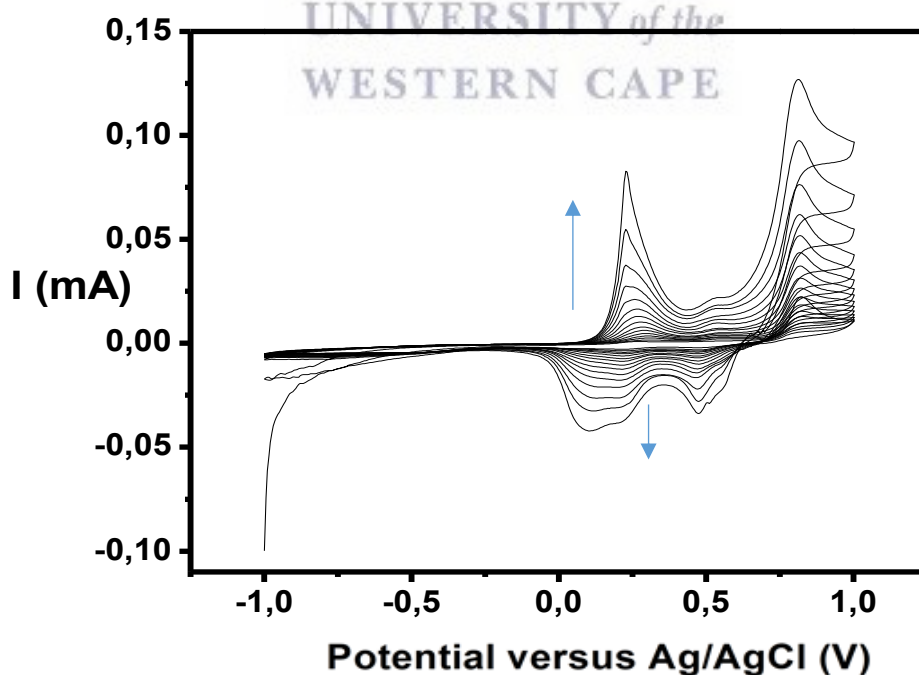


Figure 4.13: Electrodeposition of PBF.

To date, not much has been reported PBF electrochemistry. However the cyclic voltammogram showed a redox peak resulting from electron delocalization and the growth of PANIF on the electrode as the scan rates increased. The redox peak corresponds to pernigraniline radical cation/pernigraniline (A/A') .Peaks B/B' are emeraldine radical cation/emeraldine and the final redox peak is the leucoemeraldine/leucoemeraldine radical cation (C/C'). The presence of the anodic peak D from PAA can also be observed for OH functional group. The peak currents for PBF redox peaks, increased with the increase of scan rates, indicating diffusion controlled electron mobility within the PBF. All peaks associated with PAAF in the range -1000 mV to 0 mV have been suppressed and are not seen in the voltammogram figure 4.14 below.

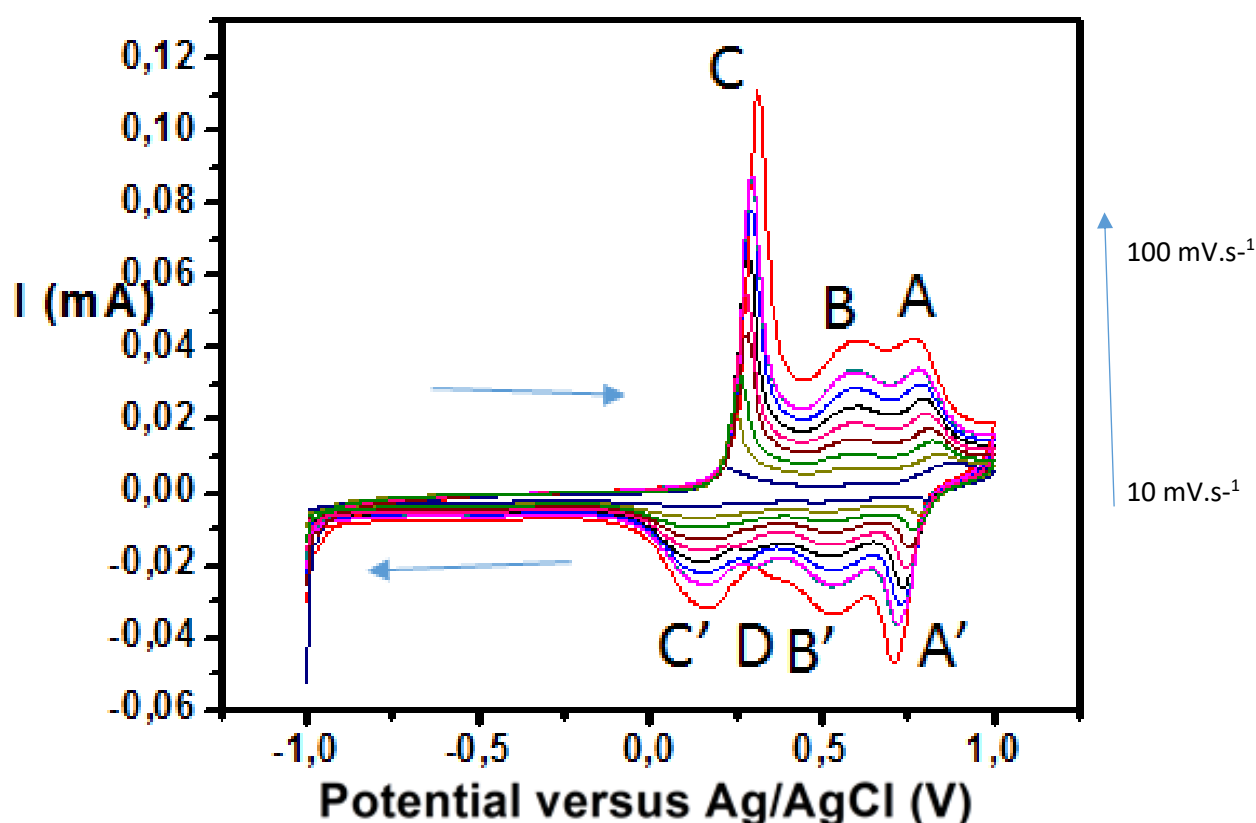


Figure 4.14: Cyclic voltammogram of PBF in 1 M HCl at different scan rates (10-100 $\text{mV}\cdot\text{s}^{-1}$).

Table below provides the electrochemical parameters calculated from scan rate dependent CV data. The peak potential separation values obtained for PBF redox peak B-B' is lower than that of PANIF. The peak is present at 500 mV-650 mV.

Table 4.7: The effect of scan rate on anodic and cathodic peak current and peak potentials of PANI in CVs for different scan rates in 1 M HCl electrolyte.

Scan rate v mV/s	Peak potential separation ΔE_o (peak B-B')	Peak potential separation ΔE_o (peak C-C')	Peak potential separation ΔE_o (peak A-A')	I_{pc}/I_{pa} (peak B/B')	I_{pc}/I_{pa} (peak C/C')	I_{pc}/I_{pa} (peak A/A')
10,00	0,52	0,79	3,68	-0,99	-2,18	-4,35
20,00	0,54	0,19	3,62	-0,16	-3,26	-1,95
30,00	0,55	0,19	3,59	-1,40	-3,43	-1,42
40,00	0,52	0,22	3,55	-1,38	-3,90	-1,20
50,00	0,54	0,21	3,55	-1,34	-3,51	-1,09
60,00	0,55	0,22	3,54	-1,38	-3,49	-1,01
70,00	0,56	0,22	3,53	-1,36	-3,60	-0,99
80,00	0,55	0,23	3,50	-1,32	-3,50	-0,95
90,00	0,55	0,07	3,50	-1,32	-3,48	-0,94
100,00	0,56	0,24	3,48	-1,26	-3,55	-0,91

The peak currents for PBF redox peaks, increased with the increase of scan rates, indicating diffusion controlled electron mobility within the polymer backbone. The Randles Sevcik equation was used to determine the rate of electron transport (D_o) within the polymer layer.

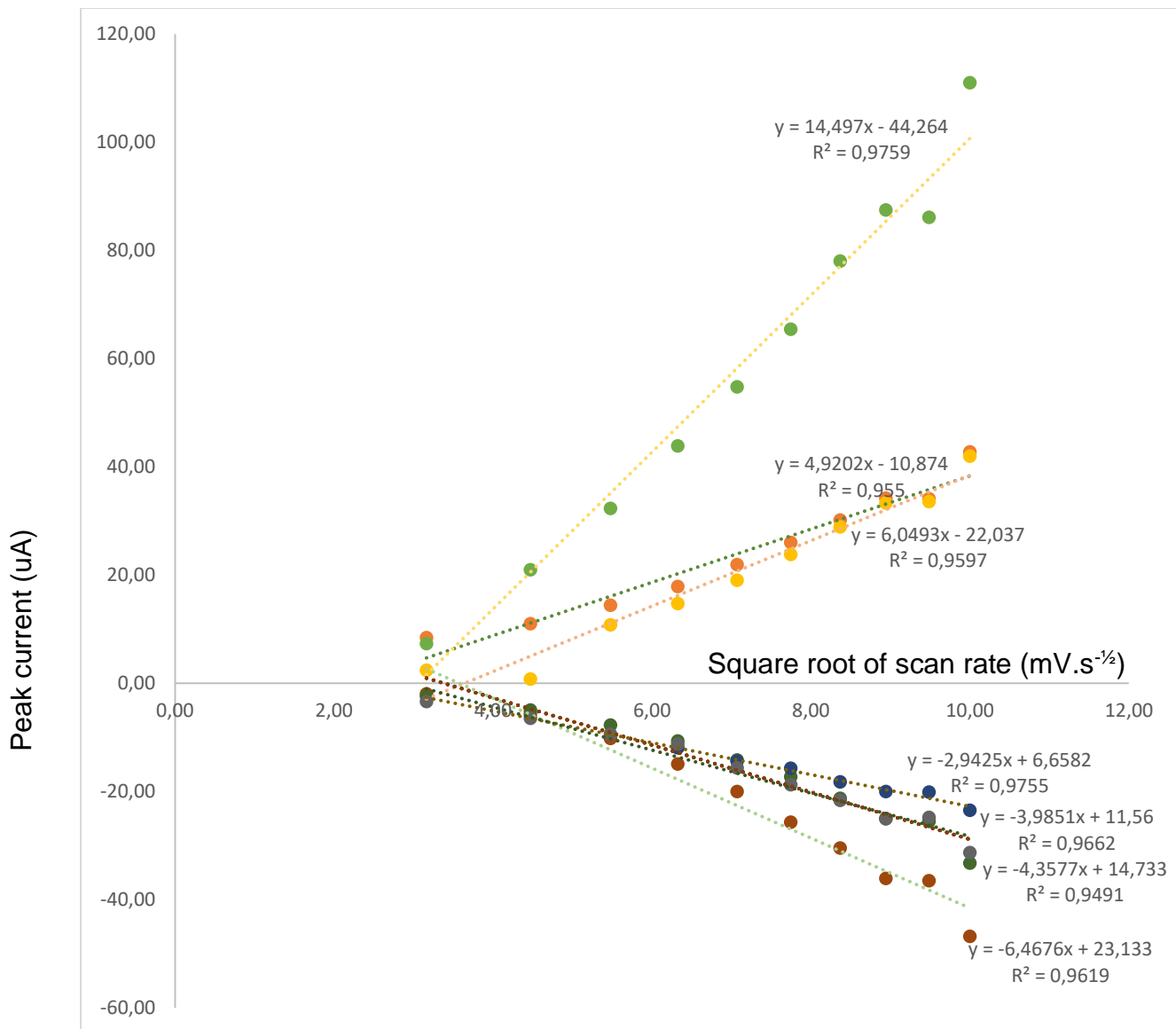


Figure 4.15: Graph of anodic and cathodic peak current (I_p) vs. square root of scan rate ($\text{mV}\cdot\text{s}^{-1/2}$) for PAA in 1 M HCl solution at different scan rates for peaks.

$$I_p = 2.69 \times 10^5 \alpha^{1/2} n^{3/2} A D_0^{1/2} C_0 \nu^{1/2}$$

The electron transport diffusion coefficient, D_0 , was found to be:

Table 4.8: Effect of scan rate on peak current and peak potentials for PBF

<u>Blend</u>	
<u>Peak</u>	<u>D_o ($cm^2.s^{-1}$)</u>
A'	$3,56 \times 10^{-07}$
C	$8,00 \times 10^{-07}$
A	$2,72 \times 10^{-07}$
B	$3,34 \times 10^{-07}$
D	$1,63 \times 10^{-07}$
B'	$2,40 \times 10^{-07}$
C'	$2,20 \times 10^{-07}$

The calculation of diffusion coefficients from oxidation currents was observed to be higher than diffusion coefficients from reduction currents, indicating that the kinetics of the system favour the oxidised state as was observed in PANI.

The diffusion of charged species at the PAAF interface was found to be slower as compared to the diffusion coefficients of PANIF and PBF. However PBF was seen to be slower than PANIF.

By the equation

$$I_{p,a} = \frac{n^2 F^2 A \Gamma}{4RT} V$$

Γ was calculated to be 7.29×10^{-9} mol.cm⁻².

4.5. Analysis by Supercapacitor Characterisation

4.5.1 Electrochemical Impedance Spectroscopy

In impedance analysis the charge transfer and mass transport mechanism of the system occurring at the electrolyte/electrode interface and in active electrode materials are measured. The summation of ohmic resistance of the electrolyte and/or electrode and a charge transfer resistance gives the total series resistance of the system.

The electronic properties of individual polymers as well as the blend were studied by EIS, and the data was modelled as a simple electrical equivalent circuit model, accounting for solution resistance (R_s), Charge transfer resistance (R_{ct}) as well as interfacial capacitance, modelled as a constant phase element (CPE).

The circuit was composed of solution resistance (R_s), constant phase element (CPE) which describes the double layer capacitance properties, the electron transfer resistance (R_{ct}) as well as the warburg impedance (W) which represent the mass transfer element and is associated with diffusion.

The measurement was performed in 1 M HCl aqueous solution within a frequency range of 100 kHz to 0.1 Hz and an alternating perturbation voltage of 10 mV.

4.5.1.1 Impedance analysis of PAA

The impedance data for the PAAF was collected in a stepwise manner at 100 mV increments between 0 and 1000 mV (vs Ag/AgCl). The qualitative assessment of the Nyquist plot obtained confirmed that the most effective redox behaviour, could be observed at 500 mV (Figure 4.26).

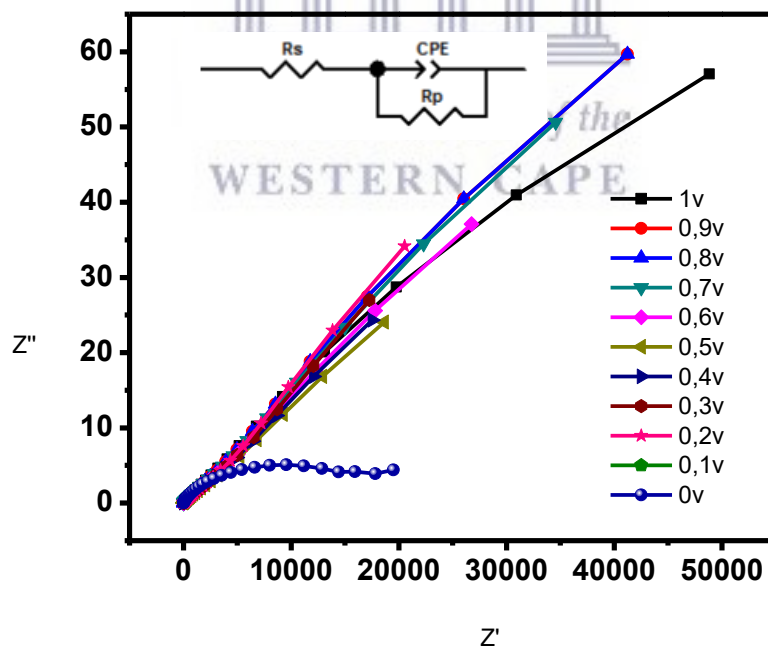


Figure 4.16: Electrochemical impedance spectra (Nyquist plot) of PAA in 1 M HCl electrolyte.

4.5.1.2 Impedance analysis PANI

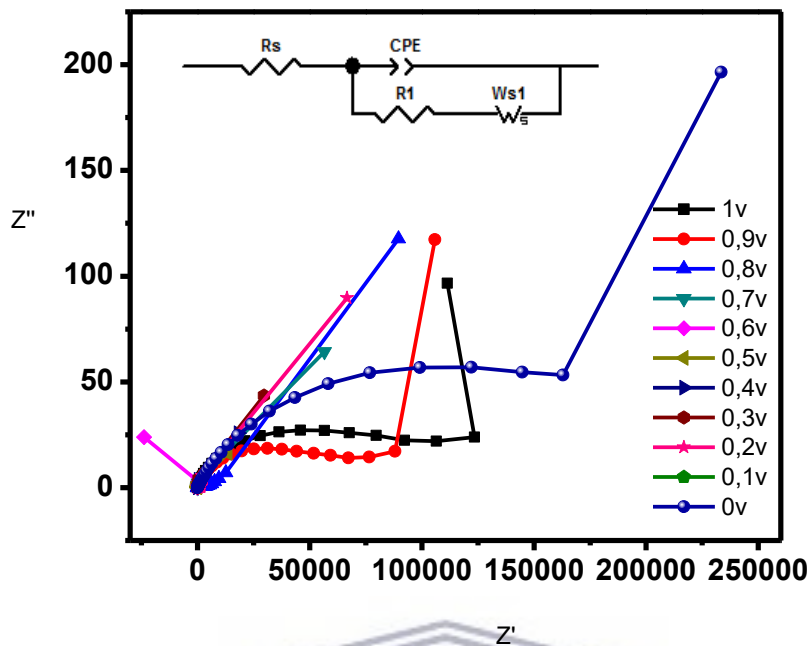


Figure 4.17: Electrochemical impedance spectra (Nyquist plot) of PANIF in 1 M HCl electrolyte.

4.5.1.3 Impedance analysis PBF

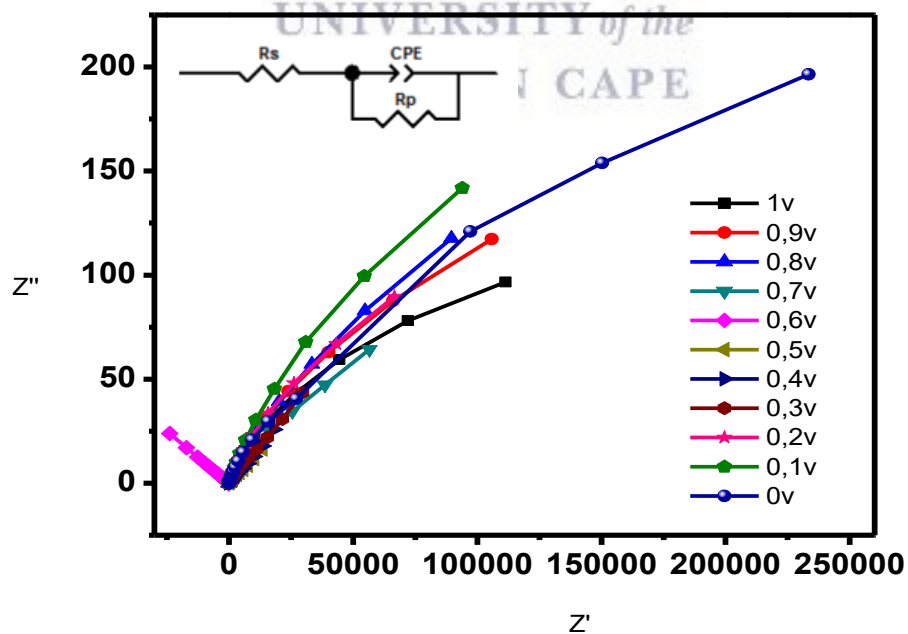


Figure 4.18: Electrochemical impedance spectra (Nyquist plot) of PBF in 1 M HCl electrode.

The CPE is the capacitance phase element for the semiconductor || electrolyte interface. According to figure 4.19 below the PBF is highest at 0.5 V. Additionally at this voltage the CPE is higher for the PBF as compared to the individual polymers. It can also be seen that the CPE of values PBF follow that PAAF. Thus the CPE of the blended material is influenced by PAAF.

The capacitance for the impedance data was obtained using the following equation (Jorcin et al., 2006)

$$CPE = (1/Z_{CPE} \cdot j \cdot \omega)^{-\alpha}$$

Where;

α = fractional exponent values between 0 to 1 (0.85)

j = imaginary number = $\sqrt{-1}$

ω = angular frequency $\omega = 2\pi f$

Z_{CPE} = Real Impedance

CPE = Capacitance

The capacitance value for PBF is seen to be 4.85 F.

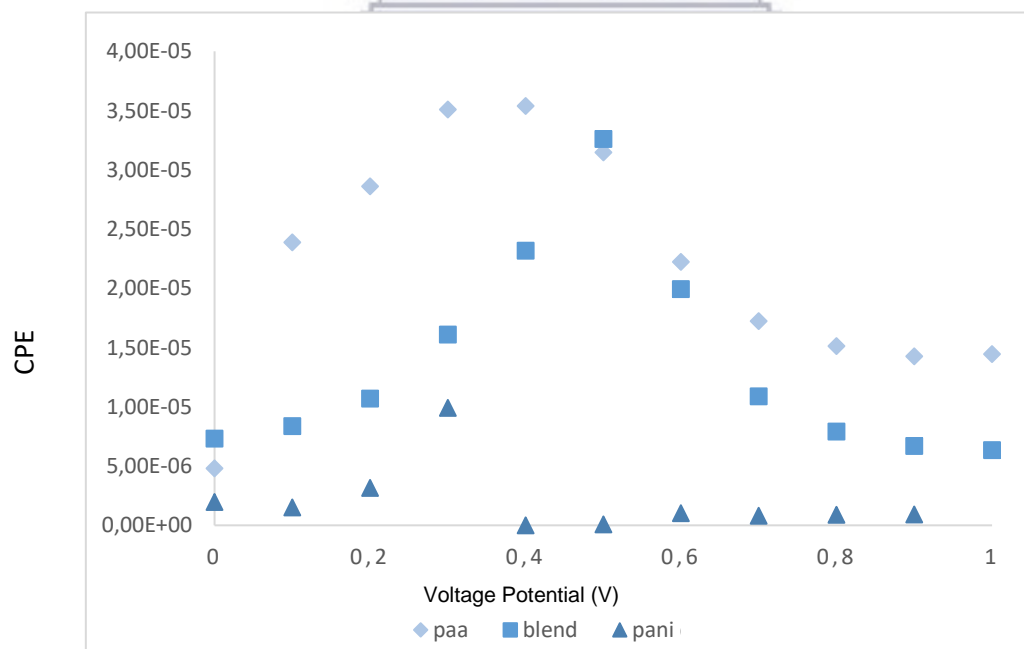


Figure 4.19: Plot of CPE versus voltage based on values from the Nyquist plots of PAAF, PANIF and PBF in 1 M HCl electrolyte at different potentials.

The charge transfer resistance PBF is seen to be larger than the charge transfer resistance for the individual polymer blends, this greater value for the charge transfer resistance indicates that the charge transfer speed was slower. However at the potential value 0.5 V the R_{ct} value obtained is seen to be its lowest and lower than that of individual polymers. The charge having less charge transfer resistance indicating that it is a better charge conducting material than individual polymers. Thus the polymer material operates best as a redox system at the voltage value of 0.5 V.

R_{ct} values were seen to be 24465 Ω , 15129 Ω , 21300 Ω for PAAF, PBF and PANIF respectively.

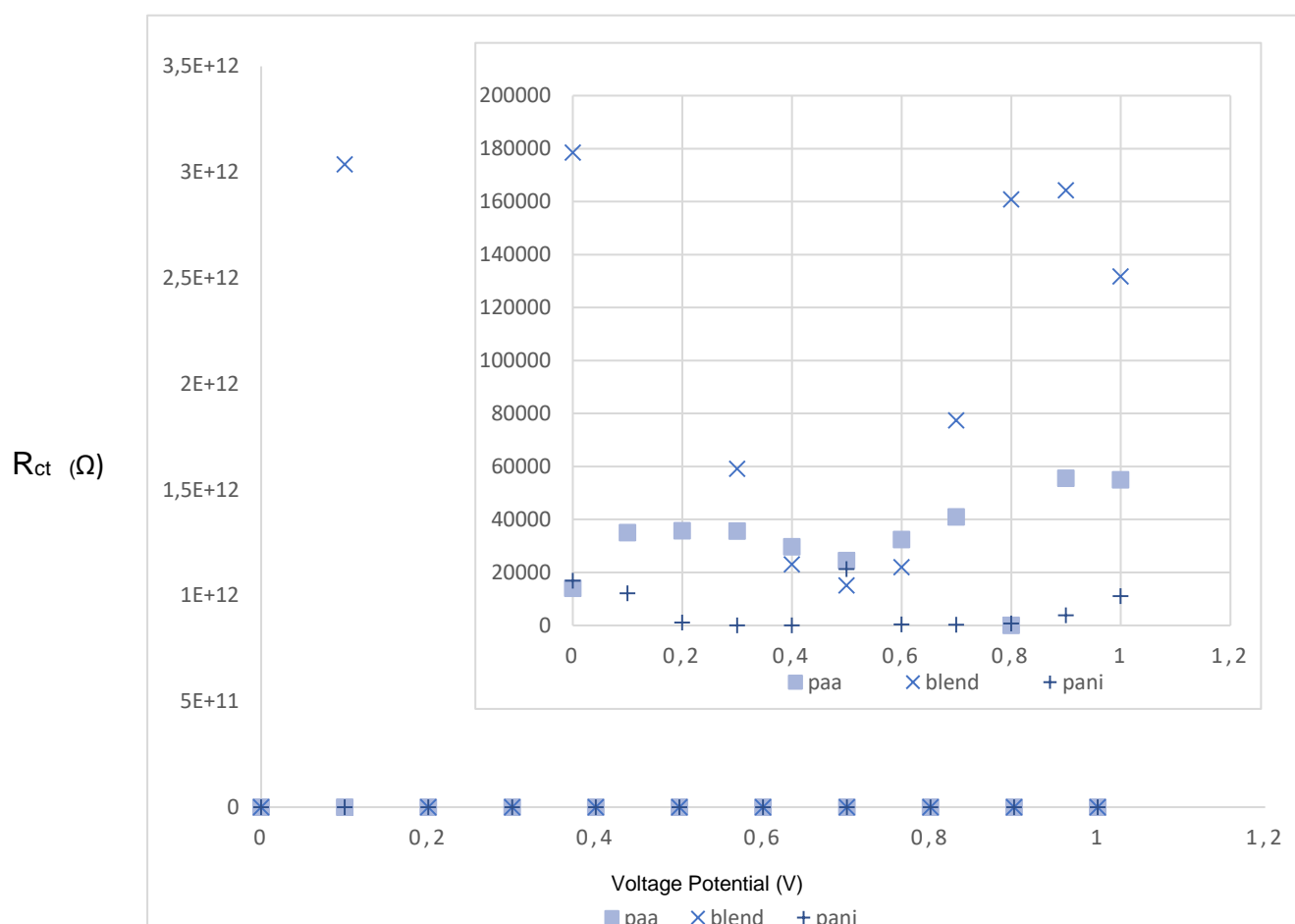


Figure 4.20: Plot of R_{ct} versus voltage based on values from Nyquist plots of PAAF, PANIF and PBF in 1 M HCl electrolyte at different potentials.

Cyclic voltammetry (CV) experiments were carried using PalmSens 3.0 electrochemical workstation (Bioanalytical Systems, USA.). The PAAF, PANIF and

PBF modified electrode were further characterized using CV at different scan rates in four different electrolytes 1 M lithium perchlorate (LP) in propylene carbonate (PC), 0.004 M tetrabutylammonium tetrafluoroborate (TT) in water, 1 M TT in PC and 1 M lithium perchlorate in water respectively.) In order to evaluate the specific capacitance of the electrode materials as well as select the most suitable electrolyte. The voltammogram can be seen below.

4.5.2 Cyclic voltammetry of PAAF

The PAAF shows very little capacitance nature as can be seen by the voltammograms below as redox peaks are present in the in the voltammogram. With the increase in the scan rate the area of the curve can be seen to increase resulting in higher specific capacitance values for higher scan rates. Tetrabutylammonium tetrafluoroborate electrolytes can be seen to be undesired for PAAF as the area under is very small as compared to LiClO₄ based electrolytes. PAAF in electrolyte LiClO₄ in water, figure 4.23 shows more pseudocapacitive behaviour as compared to LiClO₄ in PC that shows more capacitive behaviour owing to the voltammograms being more rectangular in shape. This is affirmed with by the specific capacitance value for the system being the greatest at $1,07 \times 10^{-7} \text{ F.g}^{-1}$.

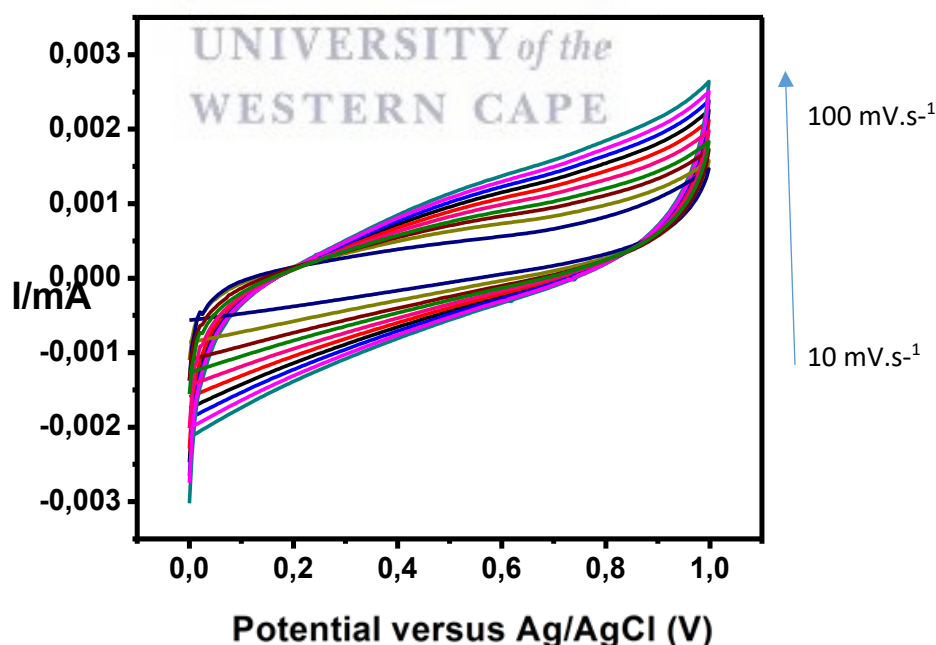


Figure 4.21: Cyclic voltammogram of PAAF in 1 M LiClO₄ in PC at different scan rates (10-100 mV.s⁻¹).

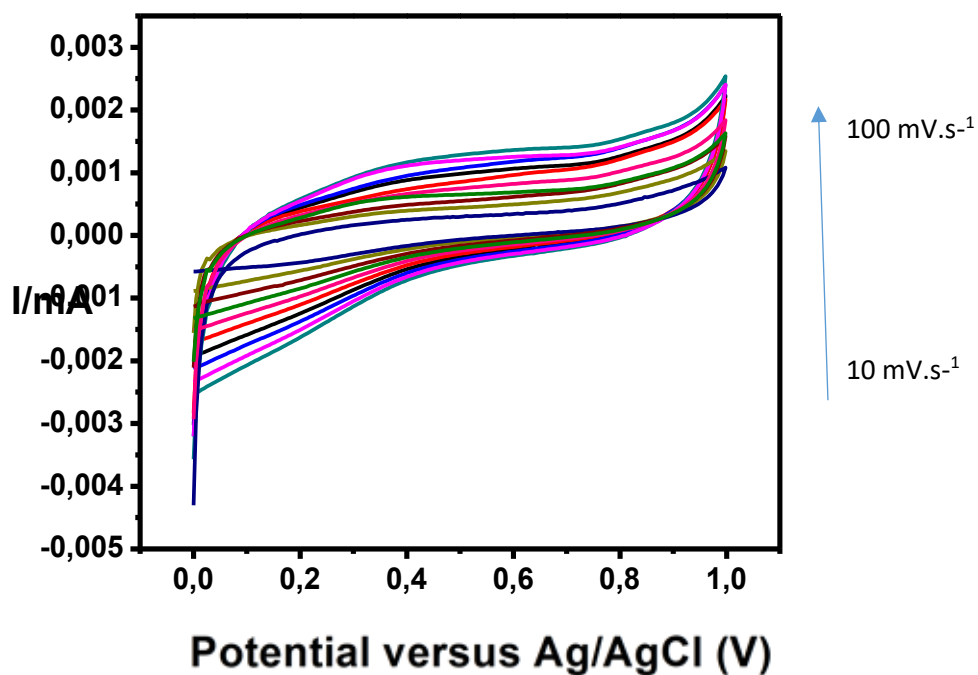


Figure 4.22: Cyclic voltammogram of PAAF in 1 M LiClO₄ in water at different scan rates (10-100 mV.s⁻¹).

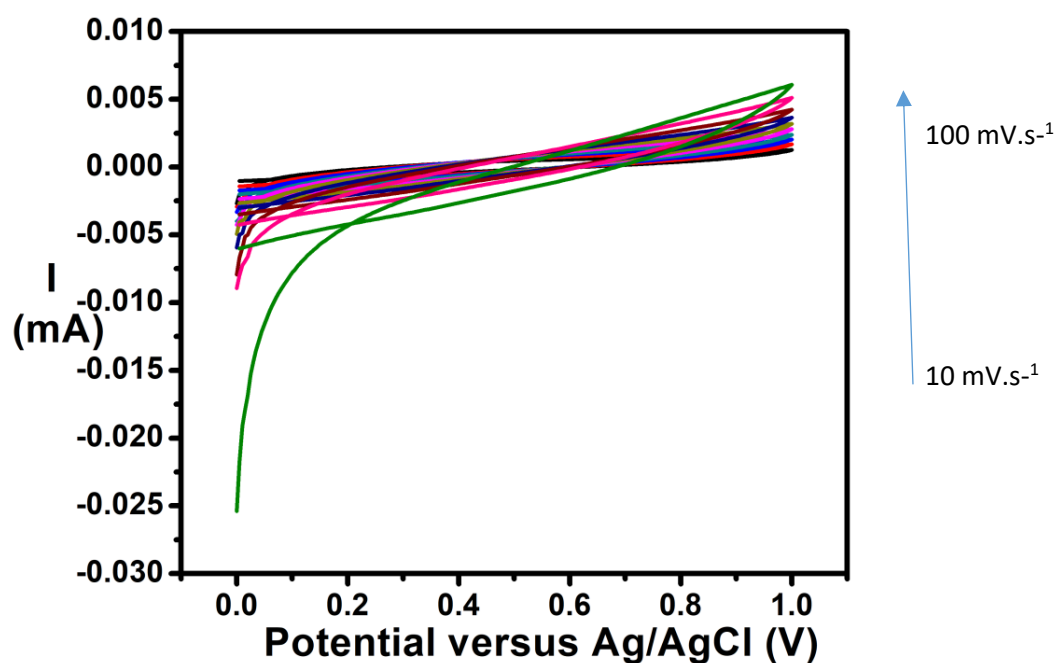


Figure 4.23: Cyclic voltammogram of PAAF in 1 M TT in PC at different scan rates (10-100 mV.s⁻¹).

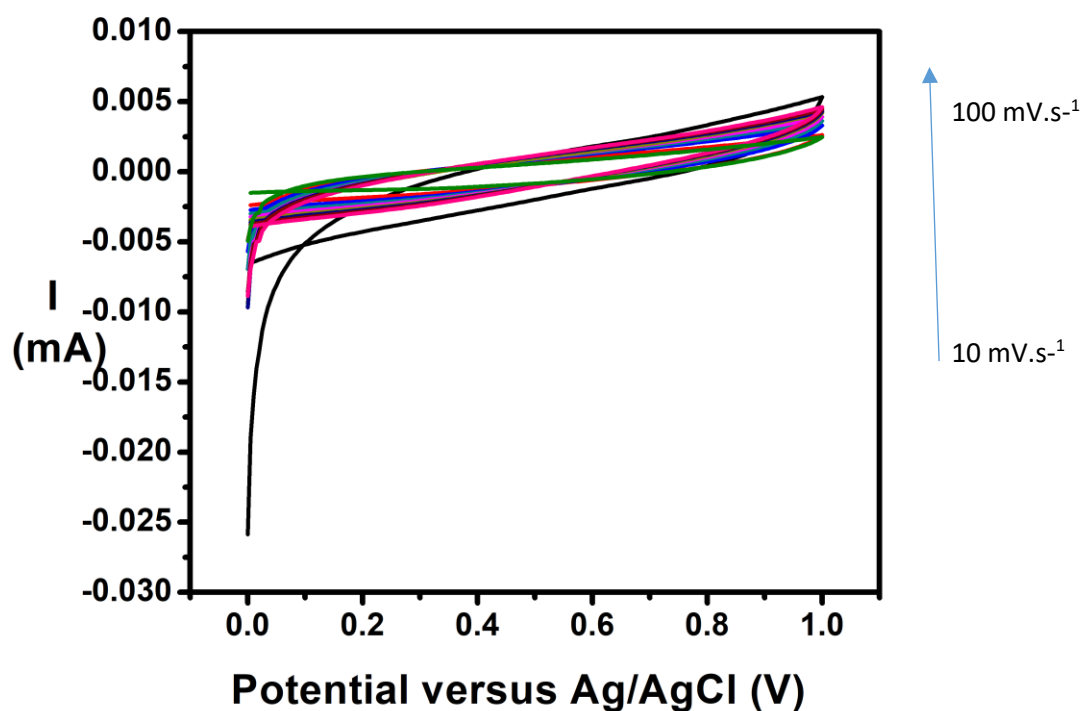
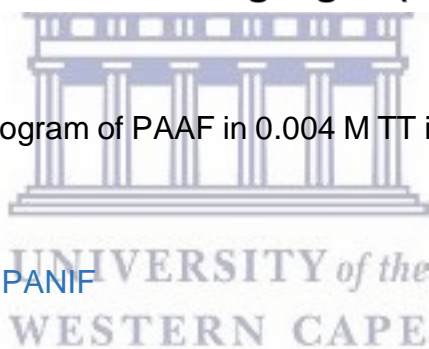


Figure 4.24: Cyclic voltammogram of PAAF in 0.004 M TT in PC at different scan rates (10-100 mV.s⁻¹).



4.5.3 Cyclic voltammetry of PANIF

PANIF showed more noticeable pseudocapacitive nature of the thin film as compared to PAAF. All experiments showed the characteristic pseudocapacitor characteristic voltammogram except the evaluation of specific capacitance using electrolyte TT in water. However, 1 M TT in PC showed the greatest pseudocapacitive characteristic as observed in figure 4.28.

LiClO₄ in PC again resulted in a voltammogram depicting a more capacitive behaviour owing to the voltammograms more rectangular in shape as compared to PANIF in other electrolytes used. This is affirmed with by the specific capacitance value for the system being the greatest at 5,28x10⁻⁰⁷ F.g⁻¹

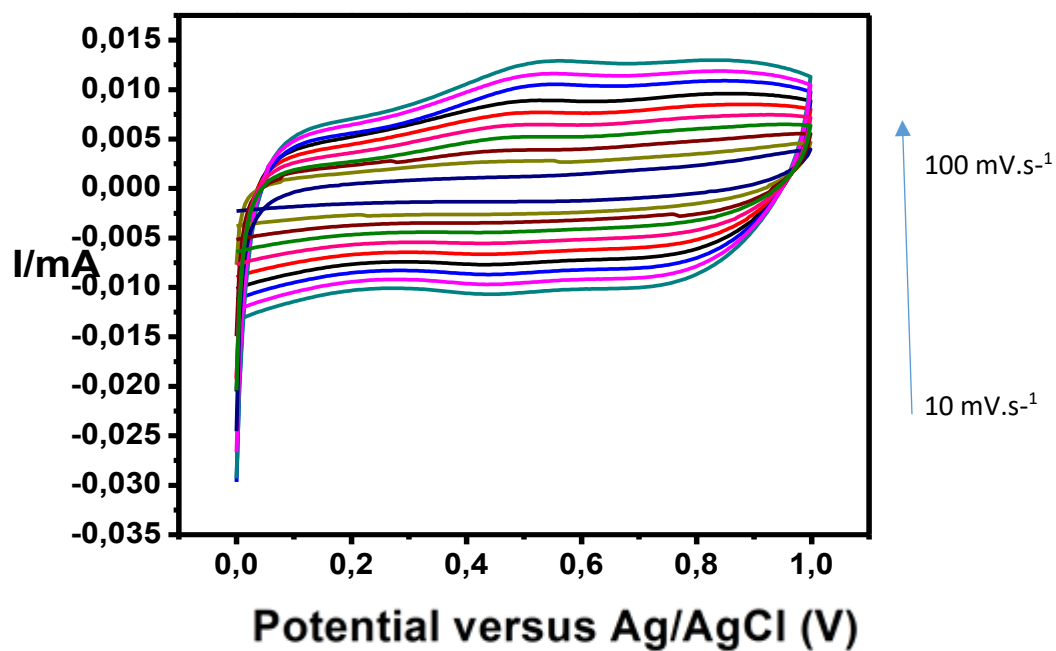


Figure 4.25: Cyclic voltammogram of PANIF in 1 M $LiClO_4$ in PC at different scan rates (10-100 $mV.s^{-1}$).

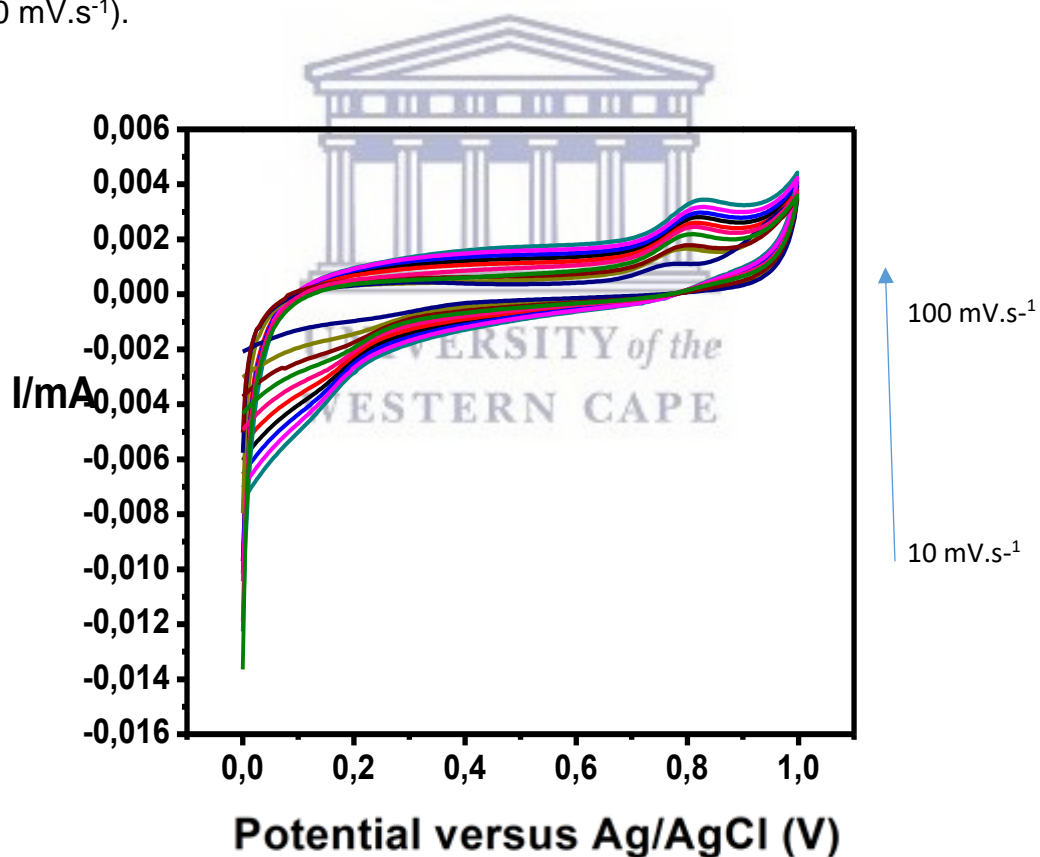


Figure 4.26: Cyclic voltammogram of PANIF in 1 M $LiClO_4$ in water at different scan rates (10-100 $mV.s^{-1}$).

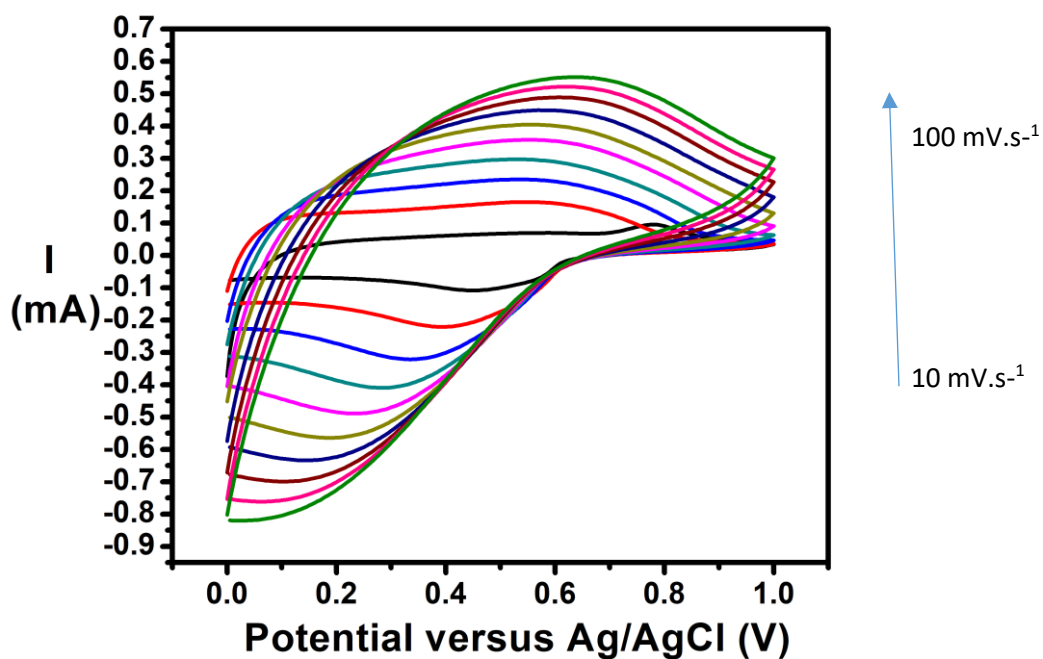


Figure 4.27: Cyclic voltammogram of PANIF in 1 M TT in PC at different scan rates (10-100 $\text{mV}\cdot\text{s}^{-1}$).

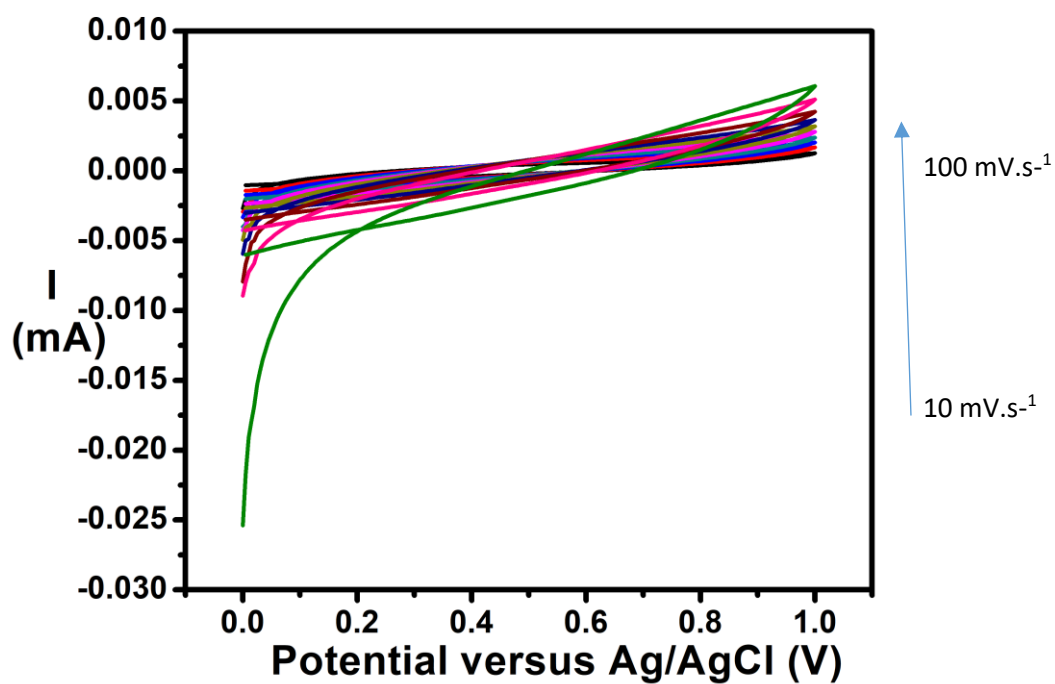


Figure 4.28: Cyclic voltammogram of PANIF in 0.004 M TT in water at different scan rates (10-100 $\text{mV}\cdot\text{s}^{-1}$).

4.5.3 Cyclic voltammetry of PBF

The CV analysis for PBF showed a peak current of 0.005 mA for all analysis. PBF in PBF in TT in PC displayed the most visible pseudocapacitance behaviour. However PBF in 1 M LiClO₄ in PC displayed greater specific capacitance value of 9.9x10⁻⁶ F.g⁻¹ owing to the rectangular shape of its voltammogram .

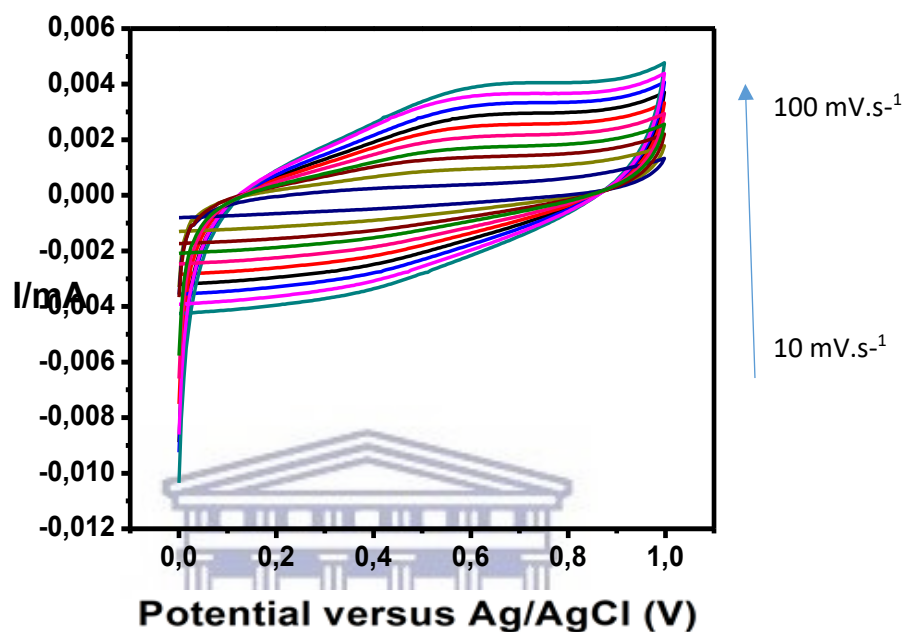


Figure 4.29: Cyclic voltammogram of PBF in 1 M LiClO₄ in PC at different scan rates (10-100 mV.s⁻¹).

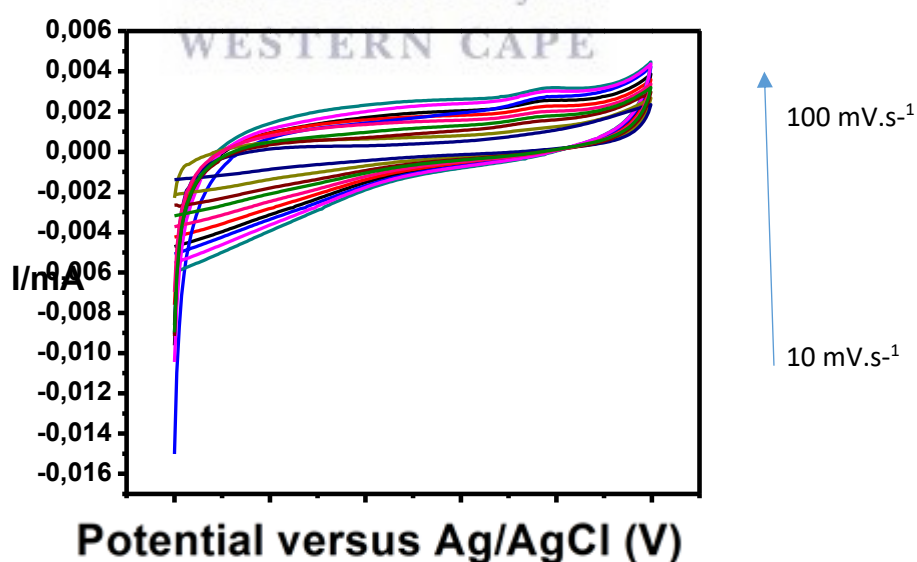


Figure 4.30: Cyclic voltammogram of PBF in 1 M LiClO₄ in water at different scan rates (10-100 mV.s⁻¹).

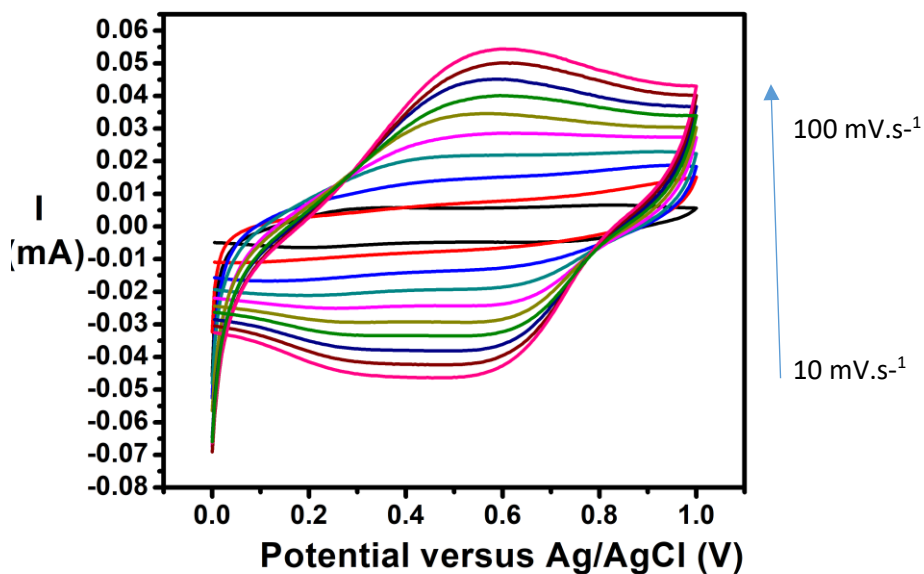


Figure 4.31: Cyclic voltammogram of PBF in 0.1 M TT in PC at different scan rates (10-100 mV.s⁻¹).

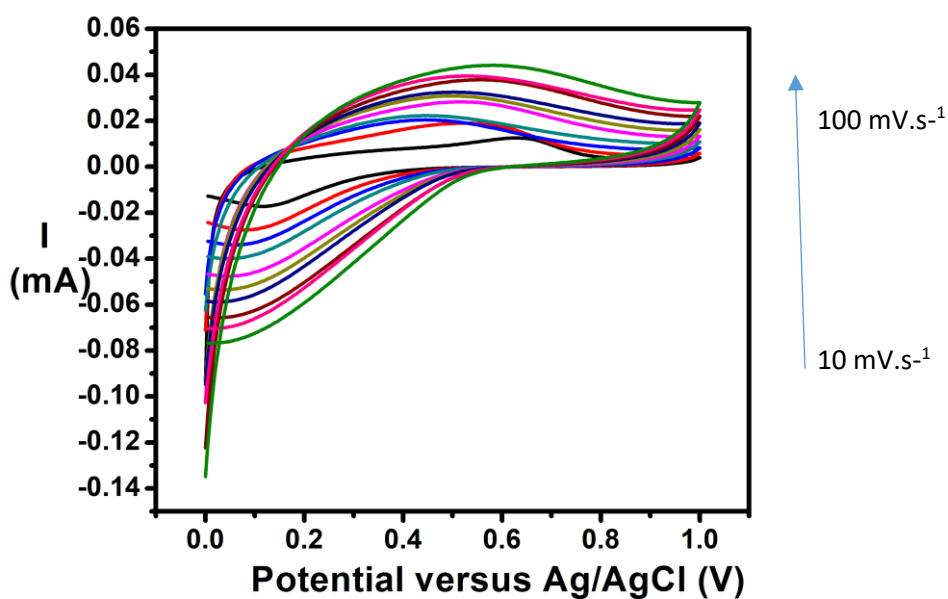


Figure 4.32: Cyclic voltammogram of PBF in 0.004 M TT in water at different scan rates (10-100 mV.s⁻¹).

The specific capacitance can be calculated from CV using the following equations.

$$C_s = \frac{\int I dV}{vm\Delta V}$$

Where:

C_s represents the specific capacitance ($F g^{-1}$),

I is the current (A),

v is the potential scan rate ($V s^{-1}$),

ΔV is the potential window (V) and

m is the mass of the electroactive materials in the electrodes (g).

It should be noted that the degree of polymerization to calculate the mass was taken as 1 for both individual polymers and the polymer blend.

Table 4.8 below shows that the electrolyte 1 M $LiClO_4$ in PC provides a greater specific capacity value as compared to alternative 3 electrolytes used. Further as seen in Figure 4.34 PBF has the highest associated capacitance than the individual polymers.

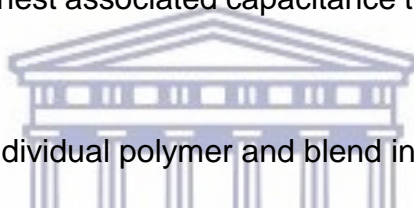


Table 4.9: Capacitance of individual polymer and blend in different electrolytes

	<i>Lithium perchlorate in propylene carbonate</i>	<i>Lithium perchlorate in water</i>	<i>Tetrabutylammonium tetrafluoroborate in propylene Carbonate</i>	<i>Tetrabutylammonium tetrafluoroborate in water</i>
PAAF	$1,07 \times 10^{-08}$	$8,30 \times 10^{-15}$	$1,14 \times 10^{-8}$	$3,60 \times 10^{-16}$
PANIF	$5,28 \times 10^{-07}$	$3,75 \times 10^{-12}$	$1,45 \times 10^{-07}$	$4,47 \times 10^{-14}$
PBF	$9,9 \times 10^{-06}$	$5,20 \times 10^{-11}$	$2,93 \times 10^{-8}$	$2,82 \times 10^{-10}$

4.6 Galvanostatic Charge/Discharge (GCD)

Galvanostatic Charge/Discharge experiments were carried using PalmSens 4.0 electrochemical workstation (Bioanalytical Systems, USA.) Cyclic voltammetry (CV) experiments were carried using PalmSens 3.0 electrochemical workstation (Bioanalytical Systems, USA.). The PAAF, PANIF and PBF modified electrode were further characterized using GCD in 1M lithium perchlorate in propylene carbonate for a constant current density of 1 μA for all thin films. PAAF and PBF time per cycle was seen to be 60 seconds where as PANIF was 500 seconds.

The galvanostatic discharge of the thin films shows different life cycles for the various thin films as seen in Figure 4.37. However, only PBF shows the idea life cycle nature of a supercapacitor material. The IR drop for PAAF was the smallest while PBF was the largest. The capacitance values obtained $8,00 \times 10^{-12} \text{ F.g}^{-1}$, $2,70 \times 10^{-10} \text{ F.g}^{-1}$ and $2,70 \times 10^{-09} \text{ F.g}^{-1}$ for PAA, PANI and PANI/PAA respectful. The PANI/PAA obtained the highest capacitance value.

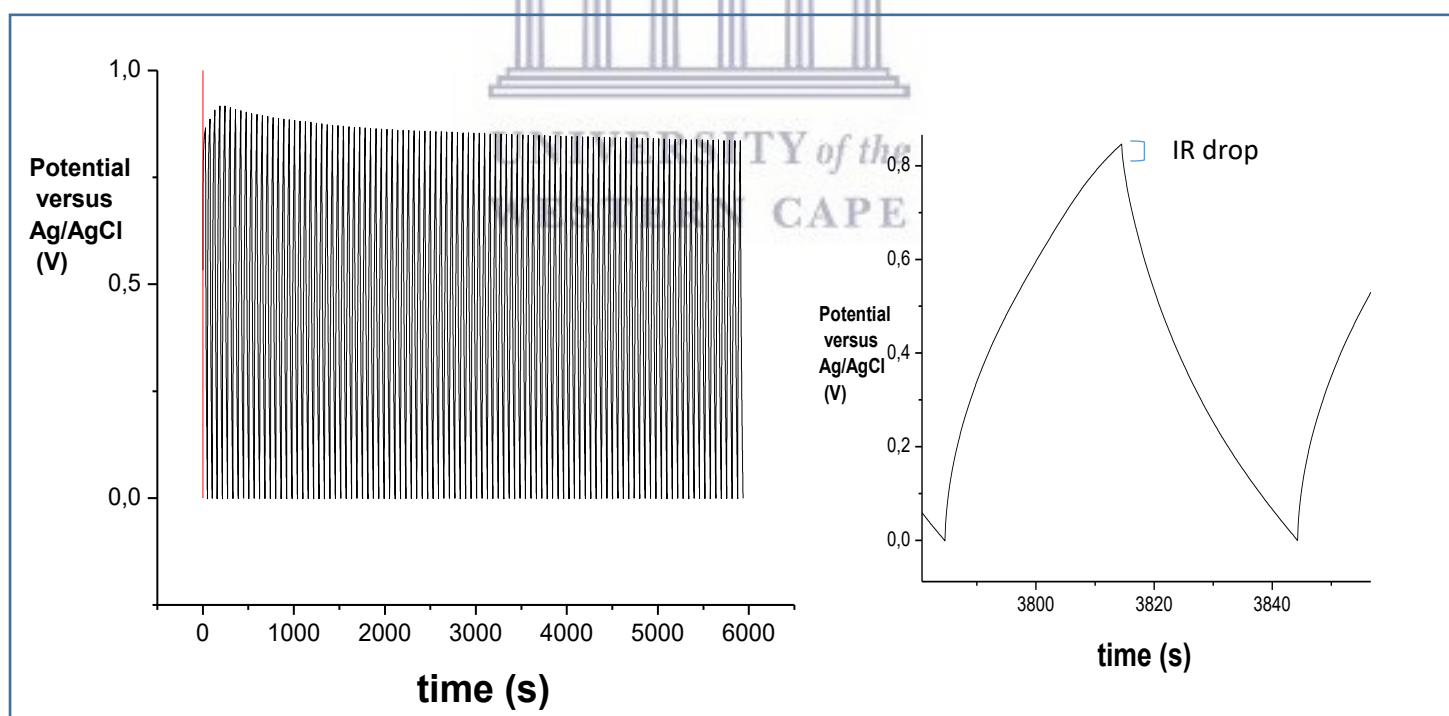


Figure 4.33: Galvanostatic plot of PAAF.

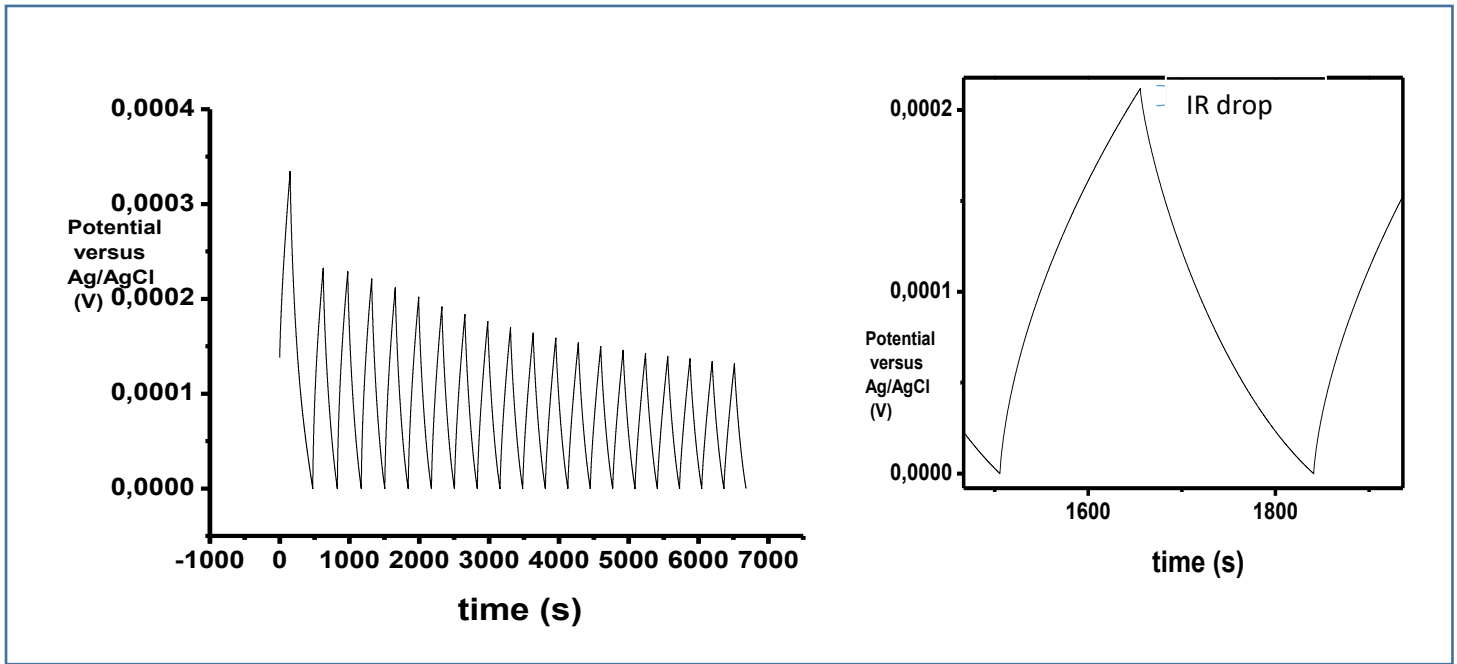


Figure 4.34: Galvanostatic plot of PANIF.

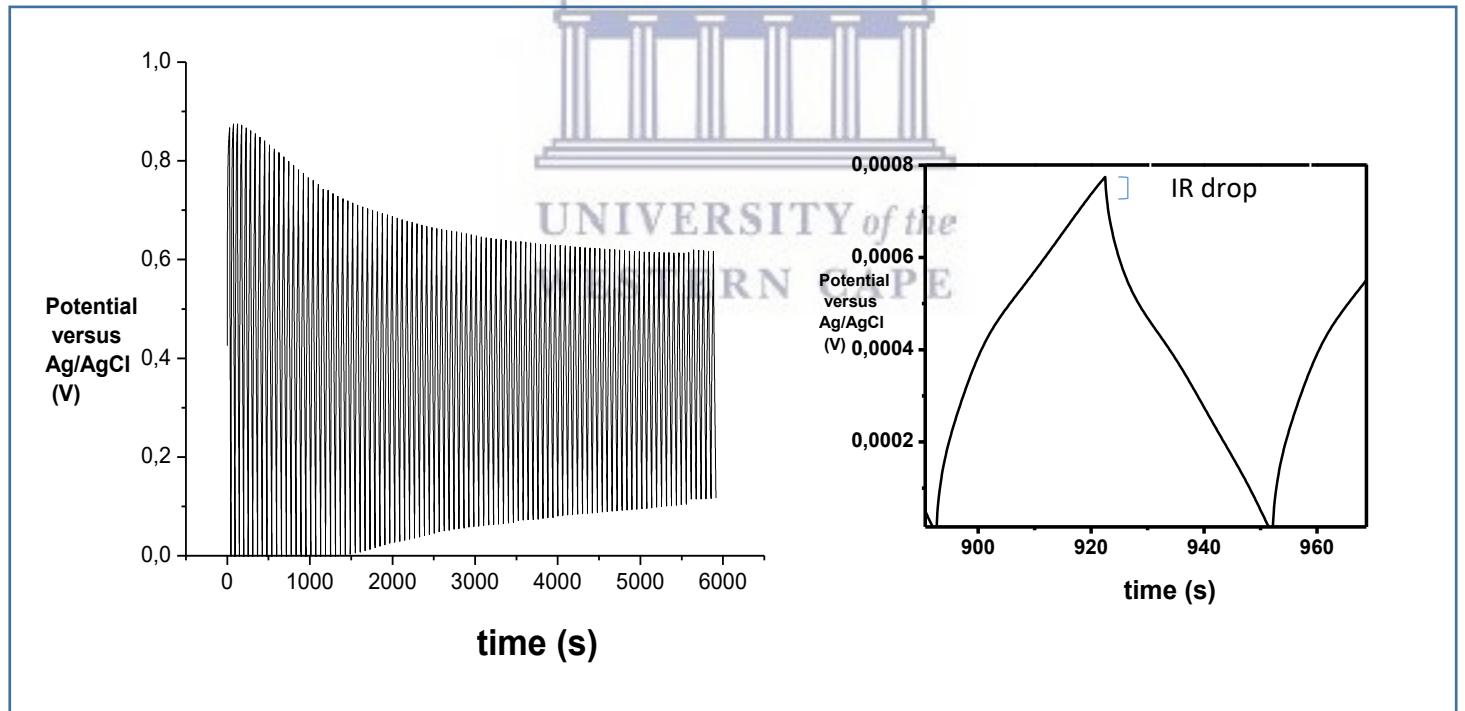


Figure 4.35: Galvanostatic plot of PBF.

The specific capacitance in galvanostatic charge discharge can be calculated by following equation

$$C_s = \frac{4C}{m} = \frac{4I\Delta t}{m\Delta V}$$

Where:

I is the constant current,

Δt is the discharging time,

m is the total mass of the activated material on the electrode surface,

ΔV is the voltage drop during discharging process

Electrochemical results show that the ideal potential for PANI/PAA is 0.5 V, as at this potential the material has superior capacitance properties than the individual polymer material. This capacitance nature observed is seen to be correct as higher capacitance values were seen for PBF as compared to PAAF and PANIF. These capacitance values were calculated using CV and GCD electrochemical techniques. The blend capacitance was seen to be $2,70 \times 10^{-9} \text{ F.g}^{-1}$ by GCD. Capacitance values for PAAF and PANIF at the current density of 1 A/g was $8,00 \times 10^{-12}$ and $2,70 \times 10^{-10}$ respectively.

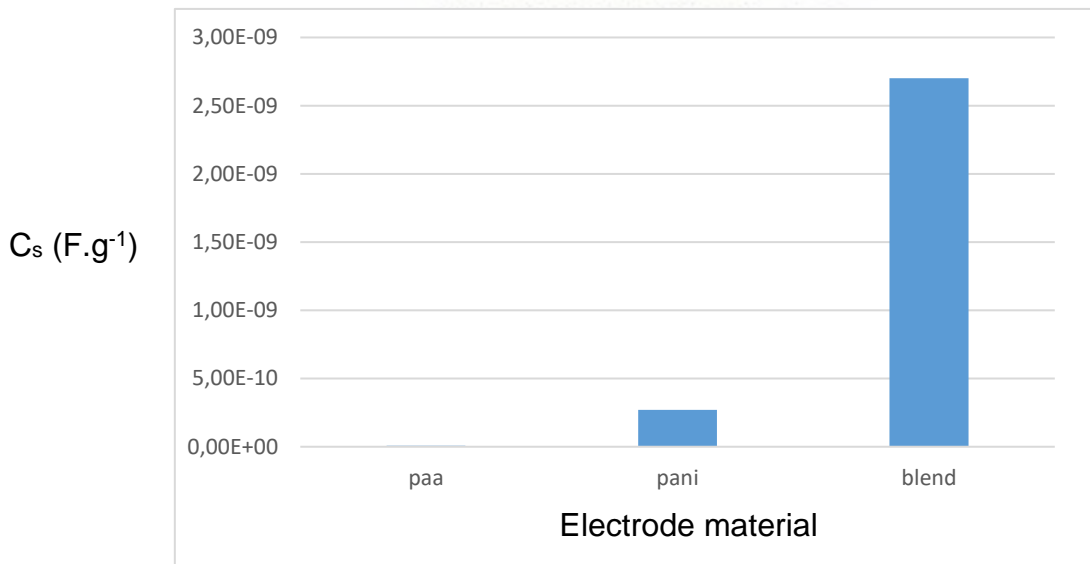


Figure 4.36: Depiction of the capacitance values obtained by PAAF, PANIF and PBF.

4.7 Energy density and power density

The energy densities at the current density was obtained using the following formula:

$$E = \frac{1}{2}(C/m)V^2 = \frac{1}{8}C_s V^2$$

The corresponding power density was calculated according to the equation:

$$P = \frac{E}{\Delta t}$$

A energy low density of $2,8 \times 10^{-10}$ Wh.kg⁻¹ at 1 A.g⁻¹ was achieved with LiClO₄ in PC at room temperature. For comparison, previous reported values of PANI supercapacitor are between 96 - 130 Wh.kg⁻¹ at 1A.g⁻¹, and the energy density of lithium-ion batteries is in the range of 100-160 Wh.kg⁻¹. (Eftekhari, Li and Yang, 2017). In addition, the highest power density of 1.7×10^{-8} W/kg was obtained. These values suggests that the PBF supercapacitor is not suitable for peak-power applications.



Chapter 5

Electron microscopy and force sensing microscopy was used to evaluate the morphology of the polymers and blend. A correlation between electrochemical performance and surface features was inferred.

5.1 Surface characterization of electrode material

PANI, PAA and PANI/PAA was dissolved in 1 M HCl (0.03 g/ml solution) there upon the polymer was then electrochemically deposited onto screen printed carbon electrode (SPCE) using CV at 15 cycles between the potential range of -1000 V and 1000 V and at $50\text{ mV}\cdot\text{s}^{-1}$. The thin film samples were subjected to microscopy analysis.

The SEM analysis was performed on a Hitachi Model X-650 Scanning electron analyser coupled to an Energy Dispersive X-ray analyser. With the aid of conductive glue the sample SPCE were placed on aluminium stubs and coated with a thin layer of gold (Au), for viewing.

5.1.1 Scanning Electron Microscopy of PAA

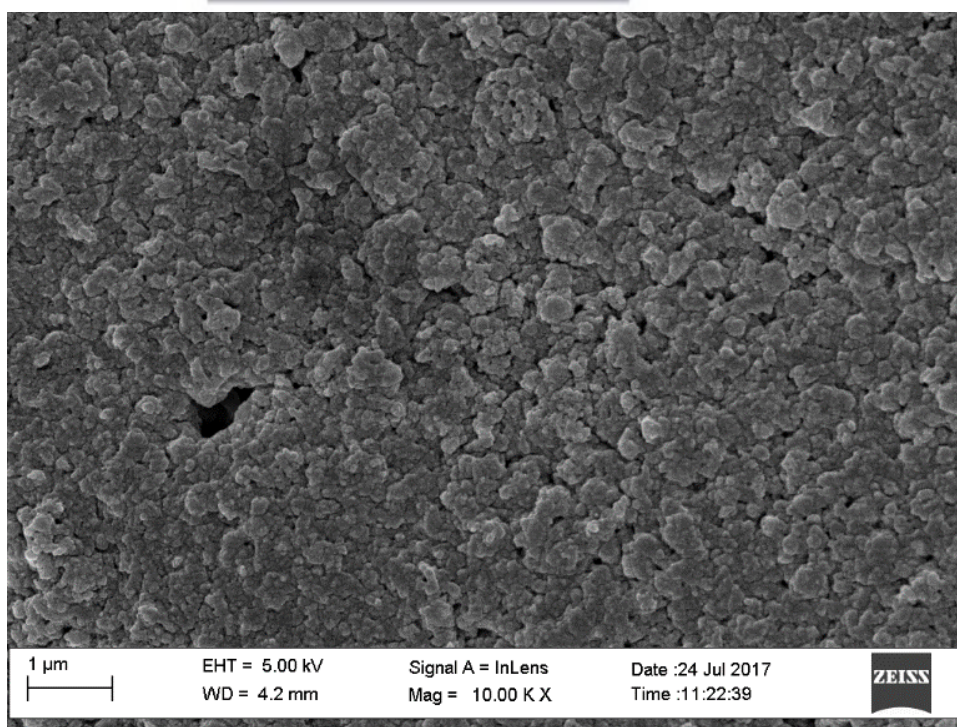


Figure 5.1: SEM image of PAAF.

The HR-SEM image of PAAF shown above indicates a cluster like dense structure of the polymer. The cluster structure is typical of polyamic acid and provides a high surface area for movement of ions as to enhance capacitance properties.

5.1.2 Scanning Electron Microscopy of PANI

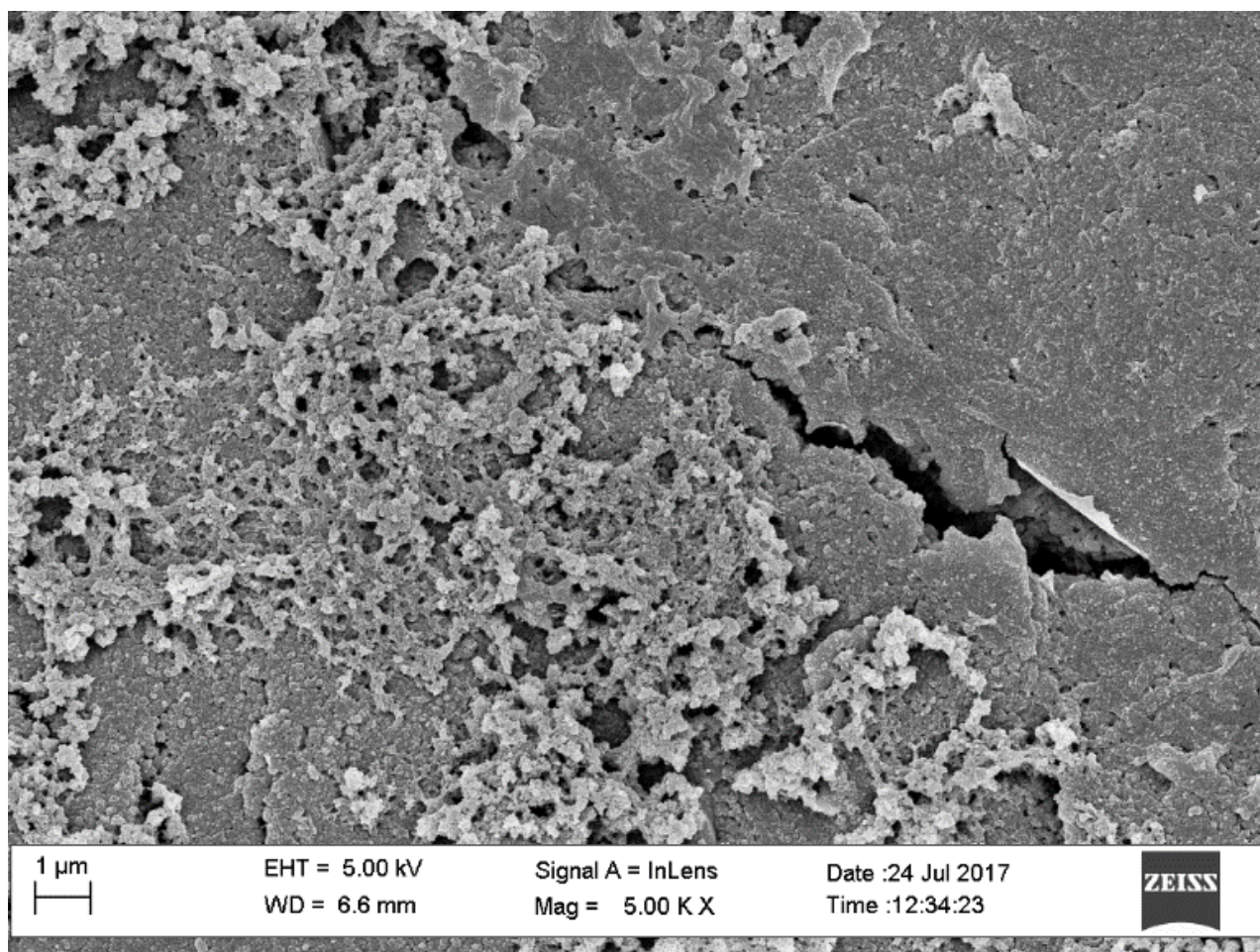


Figure 5.2: SEM image of PANIF.

The HR-SEM image of PANIF shown above indicates a porous network structure of the thin film. This is indication of the successful polymerization of aniline and the

different degrees of polymerization of the polymer. The structure provides a high surface area for movement of ions as to enhance capacitance properties.

5.1.3 Scanning Electron Microscopy of PAA/PANI Blend

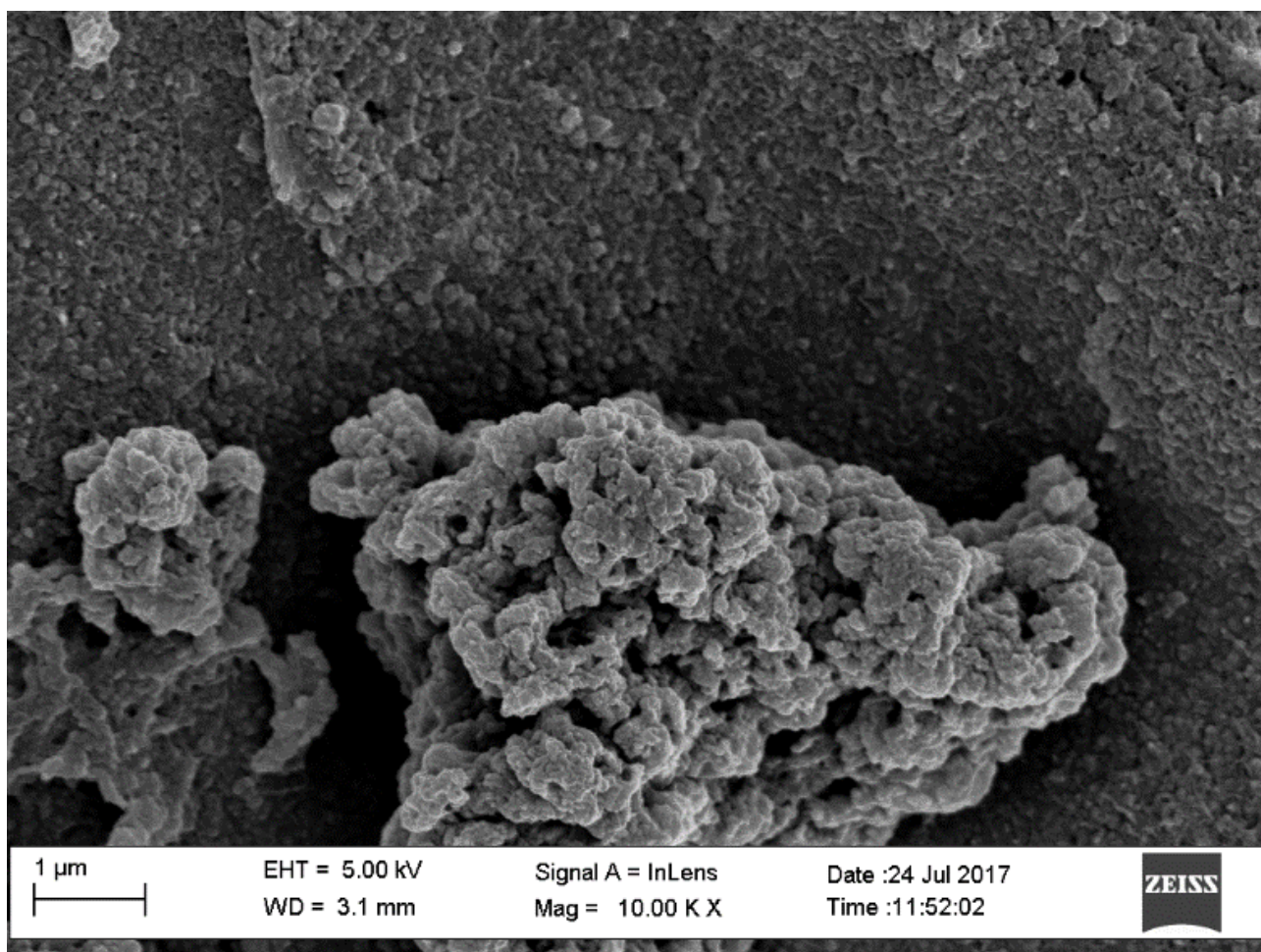


Figure 5.3: SEM image of PBF.

The SEM image above depicts the surface morphology of PBF where PANI and PAA are seen as distinct features (as compared to their individual SEM). The blend does not form a homogenous film as would be expected from chemical interaction between the two polymers. The SEM of the polymer blend indicates that the interaction between the two polymers is due to physical forces and these forces are strong enough to form an intact stable film, for electrochemical evaluation.

The agglomeration of PBF as compared to PANIF resulted in a composite film with electrochemical response of the oxidation process being slower for PBF as seen from the CV behaviour of the electrodeposition of PBF, possibly due to increased thickness in the physisorbed material.

5.1.4 Atomic Force Microscopy

AFM was used to characterise the surface roughness. Surface roughness may be related to reactive surface area for reaction kinetics. A high surface area is an important characteristic for supercapacitor materials. The results obtained showed that PBF had higher surface roughness compared PAAF. It also has an area roughness similar to that of PANI. This is affirmed by the CV data as PANI reaches higher charge.

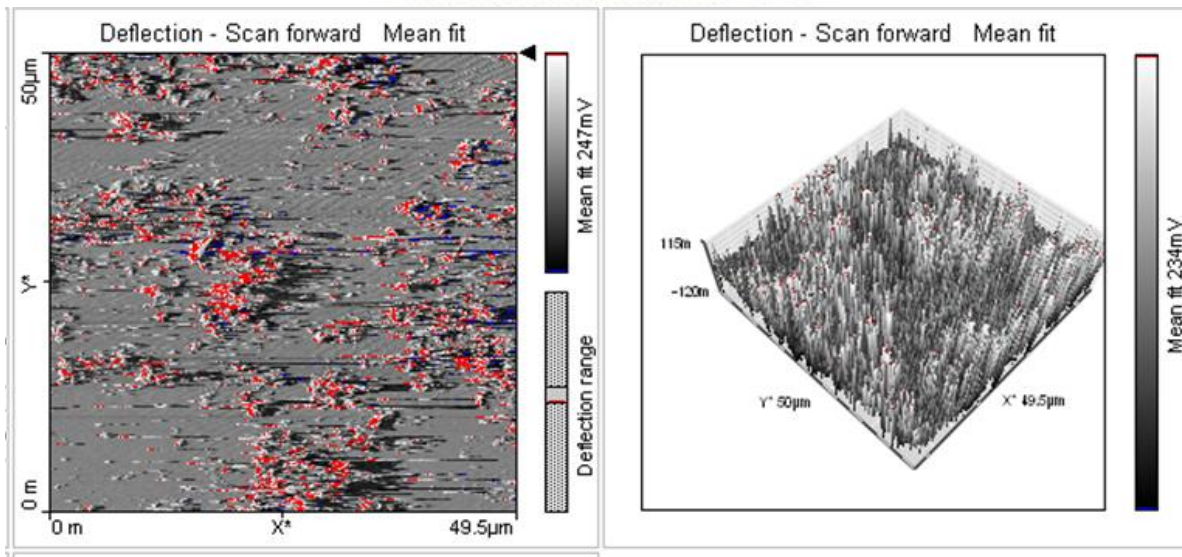
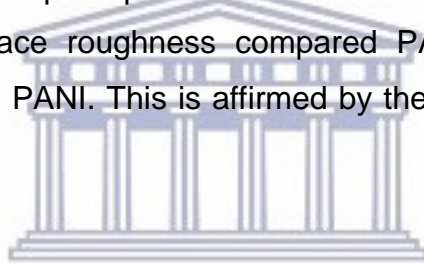


Figure 5.4: AFM image of PAAF.

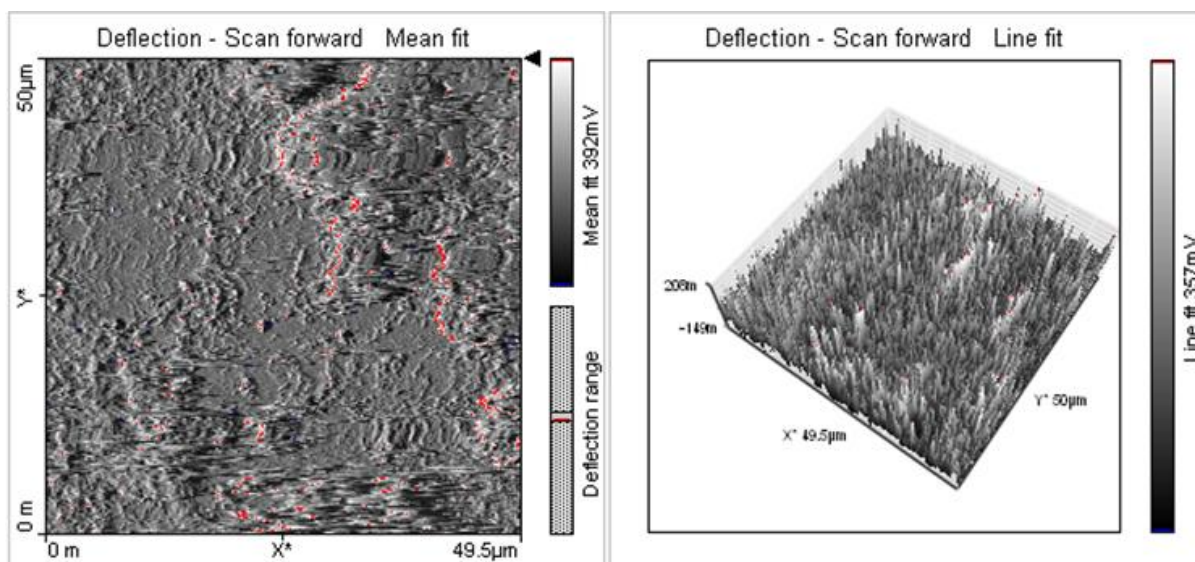


Figure 5.5: AFM image of PANIF.

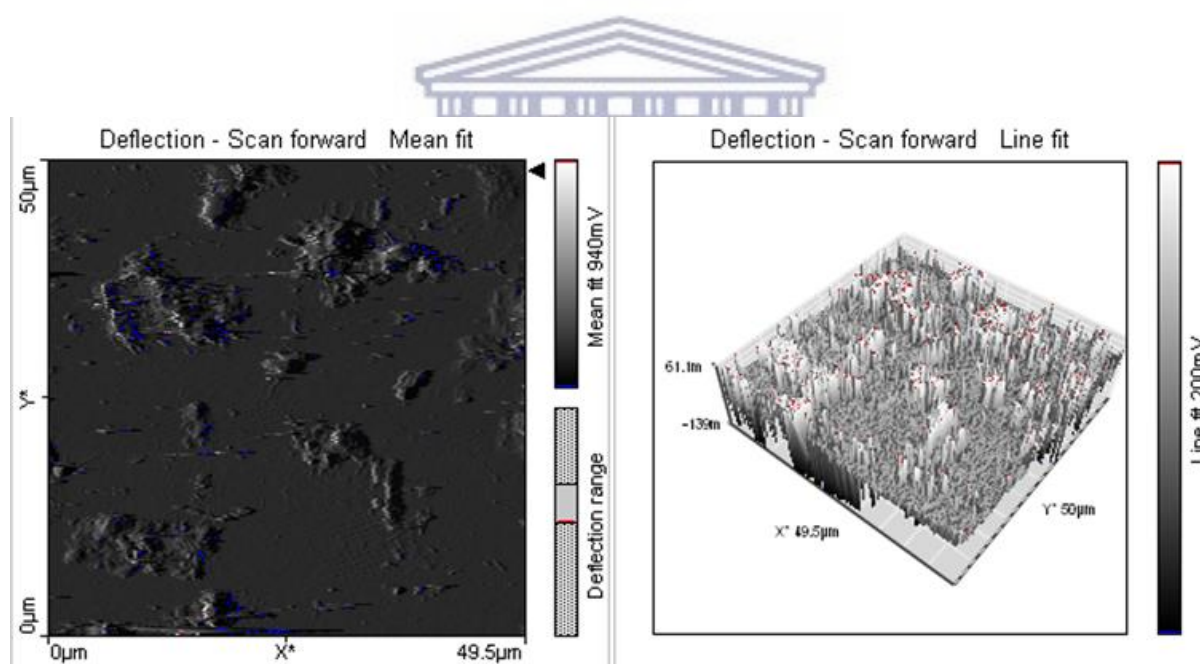


Figure 5.6: AFM image of PBF.

Table 5.1: Roughness assessment by AFM of PAAF, PANIF and PBF.

	Bare GCE	PAA	PANI	Blend
Image Size (μm)	50	50	50	50
Area Roughness S_a (mV)	6.14	38.97	47.649	45.83

The surface roughness calculated by the system software, places the value of roughness obtained for the PBF, in the same range as that of the individual PANI. This confirms that PANI is the dominant polymer in controlling the surface morphology of the blend materials.

Therefore it is interesting to note that even though the electrochemistry of the polymer blend was dominated by PAA, the surface morphology was dominated by PANI. The dominance of PANI in the morphology could be ascribed to the fact that PANI is introduced into the blend as electropolymerised polymer (from monomer) whilst PAA is introduced as a chemically synthesised polymer. This makes the blended polymer suitable for electrochemical applications in two ways i.e. it retains reproducible redox signalling due to the presence of PAA and displays marginally enhanced surface roughness due to the presence of PANI.

Chapter 6

This chapter presents concluding remarks and summarizes the key results obtained as well as some recommendations for the contribution this work can make to future research investigations.

Modern day supercapacitors can be used for applications that require a combination of high power delivery over a short period of time, high cycling stability, short charging time and long shelf life. The way forward in the fabrication of supercapacitors should be focused on the area of improving efficient method of reducing equivalent series resistance and optimization of electrolytes.

In this study PANI/PAA was successfully synthesised by in-situ polymerization techniques. The SEM and AFM results showed the presence of a porous, rough nature of the material, largely due to the surface feature of PANI, introduced as an electropolymerised polymer from its monomer. Electrochemical results show that the ideal potential for PBF is 0.5 V, as at this potential the material has superior capacitance properties than the individual polymer material. The capacitance behaviour was evaluated at this potential and was observed to be higher for the polymer blend film (PBF) as compared to individual polymer films (PAAF and PANIF). The capacitance values were calculated using CV and GCD electrochemical techniques. CV was used to evaluate the effect of electrolyte on the capacitance of the electrodes, LiClO₄ in polypropylene carbonate emerged as the best of three electrolytes evaluated and displayed the highest specific capacitance of $1,37 \times 10^{-12}$ F.g⁻¹ for the blended material. The blend capacitance by GCD was seen to be $2,70 \times 10^{-09}$ F.g⁻¹ with a good cycling stability. A cycling test was conducted at the current density of 1 A.g⁻¹ and a low energy density of $2,8 \times 10^{-10}$ Wh.kg⁻¹ was achieved with LiClO₄ in propylene carbonate at room temperature, as well as the highest power density of 1.7×10^{-8} W/kg. These values suggests that the PBF supercapacitor is not necessarily suitable for peak-power applications. This could be attributed to the strong redox nature of both PAA and PANI, as opposed to inherently capacitive materials. To clarify and verify the relationship between energy and power density, the Ragone plot for PBF is given in below.

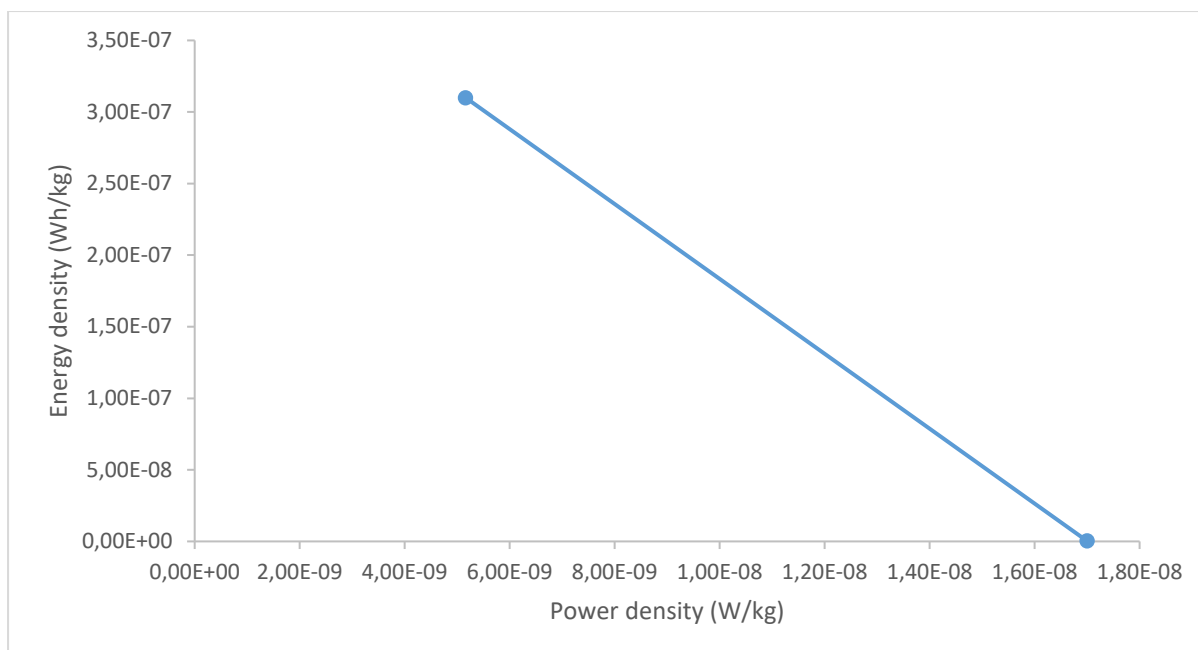


Figure 6.1: Ragone plot of PBF supercapacitor.

To date supercapacitors still have not performed respectably enough to replace batteries. However, with new research it quite possible that it would be introduced into the market in the near future. It will along a new revelation of technological advancement with it. Before this can occur is critical to find the balance point between cost and performance. More research into blended polymer and hybrid polymer blended materials for supercapacitor materials needs to occur. In this work we have demonstrated the simplicity of blending polymer materials in a one pot electrochemical synthesis method and the successful evaluation of key parameters on which to base the evaluation of supercapacitor behaviour. This method can easily be adapted to blend polymers starting from monomers or starting from chemically synthesised polymers, provided the individual polymers have a common solubility in a suitable electrolyte. The method is cost effective, efficient and utilises small quantities for synthesis. However the polymer blends can constructively be admitted or dismissed as suitable candidates for further investigation as supercapacitors or other electrochemical applications.

Much is still desired in terms of supercapacitor research, namely improvements in the electrode preparation, device structure and electrolyte selection require further investigation in order for them to be able to be used in applications needing high energy density.

References

- Al-Mashat, L., Shin, K., Kalantar-zadeh, K., Plessis, J., Han, S., Kojima, R., Kaner, R., Li, D., Gou, X., Ippolito, S. and Wlodarski, W. (2010). Graphene/Polyaniline Nanocomposite for Hydrogen Sensing. *The Journal of Physical Chemistry C*, 114(39), pp.16168-16173.
- Anand, J., Palaniappan, S. and Sathyanarayana, D. (1998). Conducting polyaniline blends and composites. *Progress in Polymer Science*, 23(6), pp.993-1018.
- Andreescu, D., Wanekaya, A. K., Sadik, O. A., & Wang, J. (2005). Nanostructured polyamic acid membranes as novel electrode materials. *Langmuir*, 21(15), pp. 6891-6899.
- Angelopoulos, M. (2001). Conducting polymers in microelectronics. *IBM Journal of Research and Development*, 45(1), pp.57-75.
- Aroon, M., Ismail, A., Montazer-Rahmati, M. and Matsuura, T. (2010). Morphology and permeation properties of polysulfone membranes for gas separation: Effects of non-solvent additives and co-solvent. *Separation and Purification Technology*, 72(2), pp.194-202.
- B. E. Conway, W. G. Pell, "Double-layer and pseudocapacitance types of Electrochemical capacitors and their applications to the development of hybrid Devices" *Journal of Solid State Electrochemistry*, vol. 7, pp. 637-644, 2003.
- B.E.Conway, *Electrochemical Supercapacitors: Scientific Fundamentals and Technological Applications*. New York, N.Y.: Kluwer Academic, 1999.
- Babu, K., Senthilkumar, R., Noel, M. and Kulandainathan, M. (2009). Polypyrrole microstructure deposited by chemical and electrochemical methods on cotton fabrics. *Synthetic Metals*, 159(13), pp.1353-1358.
- Balint, R., Cassidy, N. and Cartmell, S. (2014). Conductive polymers: Towards a smart biomaterial for tissue engineering. *Acta Biomaterialia*, 10(6), pp.2341-2353.
- Berresheim, A., Müller, M. and Müllen, K. (1999). Polyphenylene Nanostructures. *Chemical Reviews*, 99(7), pp.1747-1786.

- Bhadra, S., Chattopadhyay, S., Singha, N. and Khastgir, D. (2008). Improvement of conductivity of electrochemically synthesized polyaniline. *Journal of Applied Polymer Science*, 108(1), pp.57-64.
- Bhadra, S., Khastgir, D., Singha, N. and Lee, J. (2009). Progress in preparation, processing and applications of polyaniline. *Progress in Polymer Science*, 34(8), pp.783-810.
- Bhadra, S., Singha, N. and Khastgir, D. (2006). Polyaniline by new miniemulsion polymerization and the effect of reducing agent on conductivity. *Synthetic Metals*, 156(16-17), pp.1148-1154.
- Bhadra, S., Singha, N. and Khastgir, D. (2006). Polyaniline by new miniemulsion polymerization and the effect of reducing agent on conductivity. *Synthetic Metals*, 156(16-17), pp.1148-1154.
- Bhadra, S., Singha, N. and Khastgir, D. (2008). Effect of aromatic substitution in aniline on the properties of polyaniline. *European Polymer Journal*, 44(6), pp.1763-1770.
- Bil'dyukevich, A., Semenkevich, N., Pratsenko, S. and Zharkevich, I. (2009). The influence of the porofor type on the transport properties of polysulfone membranes. *Theoretical Foundations of Chemical Engineering*, 43(4), pp.517-521.
- Bossi, A., Piletsky, S., Piletska, E., Righetti, P. and Turner, A. (2000). An Assay for Ascorbic Acid Based on Polyaniline-Coated Microplates. *Analytical Chemistry*, 72(18), pp.4296-4300.
- Bubna, P., Advani, S. and Prasad, A. (2012). Integration of batteries with ultracapacitors for a fuel cell hybrid transit bus. *Journal of Power Sources*, 199, pp.360-366.
- Burke, A. "Ultracapacitors: why ,how, and where is the technology", *Journal Of Power Sources* 91, 37-50 (2000).
- Carothers, W. (1931). Polymerization. *Chemical Reviews*, 8(3), pp.353-426.
- Chen, C., Wang, S., Tien, Y., Tsai, W. and Lin, C. (2009). Hybrid manganese oxide films for supercapacitor application prepared by sol-gel technique. *Thin Solid Films*, 518(5), pp.1557-1560.

- Chen, Y., Zou, C., Mastalerz, M., Hu, S., Gasaway, C. and Tao, X. (2015). Applications of Micro-Fourier Transform Infrared Spectroscopy (FTIR) in the Geological Sciences- A Review. *Molecular Sciences*, pp. 30223-30250.
- Chiang, C., Fincher, C., Park, Y., Heeger, A., Shirakawa, H., Louis, E., Gau, S. and MacDiarmid, A. (1977). Electrical Conductivity in Doped Polyacetylene. *Physical Review Letters*, 39(17), pp.1098-1101.
- Cho, M., Park, S., Hwang, J. and Choi, H. (2004). Synthesis and electrical properties of polymer composites with polyaniline nanoparticles. *Materials Science and Engineering: C*, 24(1-2), pp.15-18.
- Conway, B. (1999). *Electrochemical supercapacitors*. New York: Kluwer Academic/Plenum.
- De, R., Albuquerque, D., Cruz, T., Yamaji, F. and Leite, F. (2012). Measurement of the Nanoscale Roughness by Atomic Force Microscopy: Basic Principles and Applications. *Atomic Force Microscopy - Imaging, Measuring and Manipulating Surfaces at the Atomic Scale*.
- Dufresne, M., Bacchin, P., Cerino, G., Remigy, J., Adrianus, G., Aimar, P. and Legallais, C. (2013). Human hepatic cell behavior on polysulfone membrane with double porosity level. *Journal of Membrane Science*, 428, pp.454-461.
- Dupuis, A. (2011). Proton exchange membranes for fuel cells operated at medium temperatures: Materials and experimental techniques. *Progress in Materials Science*, 56(3), pp.289-327.
- Eftekhari, A., Li, L. and Yang, Y. (2017). Polyaniline supercapacitors. *Journal of Power Sources*, 347, pp.86-107.
- El-din, H., El-Naggar, A. and Ali, F. (2003). Miscibility of poly(vinyl alcohol)/polyacrylamide blends before and after gamma irradiation. *Polymer International*, 52(2), pp.225-234.
- Evans, D. H., O'Connell, K., Petersen, R. A., & Kelly, M. J. (1983). Cyclic Voltammetry. *Chemical Education*, pp. 290-293.
- Fan, Z., Wang, Z., Sun, N., Wang, J. and Wang, S. (2008). Performance improvement of polysulfone ultrafiltration membrane by blending with polyaniline nanofibers. *Journal of Membrane Science*, 320(1-2), pp.363-371.

- Fasmin, F., and Srinivasan, R. (2017). Review-Nonlinear electrochemical impedance spectroscopy. *Electrochemical Society*, pp.443-455.
- Frackowiak, E. and Béguin, F. (2001). Carbon materials for the electrochemical storage of energy in capacitors. *Carbon*, 39(6), pp.937-950.
- Frackowiak, E., and Lota, G, J. (2005) Room-temperature phosphonium ionic liquids for Supercapacitor applications, *Applied Physics Letters*,86, pp. 164104.
- Gorey, B., Smyth, M., White, B. and Morrin, A. (2014). Fabrication of homogenous three dimensionally ordered conducting polymer–polystyrene opal structures in microfluidic channels. *J. Mater. Chem. C*, 2(30), pp.6004-6009.
- Guimard, N., Gomez, N. and Schmidt, C. (2007). Conducting polymers in biomedical engineering. *Progress in Polymer Science*, 32(8-9), pp.876-921.
- Gvozdenovic, M., Jugovic, B., Stevanovic, J. and Grgur, B. (2014). Electrochemical synthesis of electroconducting polymers. *Chemical Industry*, 68(6), pp.673-684.
- Henson, W. (2008). Optimal battery/ultracapacitor storage combination. *Journal of Power Sources*, 179(1), pp.417-423.
- Hess, E. H., Waryo, T., Sadik, O. A., Iwuoha, E. I., & Baker, P. G. (2014). Constitution of novel polyamic acid/polypyrrole composite films by in-situ electropolymerization. *Electrochimica Acta*, 128, pp. 439-447.
- Hou, H., Vacandio, F., Vona, M. and Knauth, P. (2012). Electropolymerization of sulfonated phenol by cyclic voltammetry. *Journal of Applied Polymer Science*, 129(3), pp.1151-1156.
- Hu, X., Zhang, Y., Tang, K. and Zou, G. (2005). Hemoglobin-biocatalysts synthesis of a conducting molecular complex of polyaniline and sulfonated polystyrene. *Synthetic Metals*, 150(1), pp.1-7.
- Huang, L., Chen, C. and Wen, T. (2006). Development and characterization of flexible electrochromic devices based on polyaniline and poly(3,4-ethylenedioxythiophene)-poly(styrene sulfonic acid). *Electrochimica Acta*, 51(26), pp.5858-5863.
- Huang, W. and MacDiarmid, A. (1993). Optical properties of polyaniline. *Polymer*, 34(9), pp.1833-1845.

- Inzelt, G., Pineri, M., Schultze, J. and Vorotyntsev, M. (2000). Electron and proton conducting polymers: recent developments and prospects. *Electrochimica Acta*, 45(15-16), pp.2403-2421.
- Iwuoha, E. I.; Saenz de Villaverde, D.; Garcia, N. P.; Smyth, M. R.; Pingarron, J. M.(1997). Reactivities of organic phase biosensors. 2. The amperometric behaviour of horseradish peroxidase immobilised on a platinum electrode modified with an electrosynthetic polyaniline film. *Biosensors and Bioelectronics*, (12), pp. 749-761.
- Jorcin, J., Orazem, M., Pébère, N. and Tribollet, B. (2006). CPE analysis by local electrochemical impedance spectroscopy. *Electrochimica Acta*, 51(8-9), pp.1473-1479.
- Kang, X.M., Zou, Z., Cai, X., and Jinyuan, P.M. (2007). A novel glucose biosensor based on immobilization of glucose oxidase in chitosan on a glassy carbon electrode modified with gold-platinum alloy nanoparticles/multiwall carbon nanotubes. *Analytical Biochemistry*. 369(1), pp. 71-79.
- Karden, E., Buller, S. and De Doncker, R. (2000). A method for measurement and interpretation of impedance spectra for industrial batteries. *Journal of Power Sources*, 85(1), pp.72-78.
- Kim, K., Lee, K., Cho, K. and Park, C. (2002). Surface modification of polysulfone ultrafiltration membrane by oxygen plasma treatment. *Journal of Membrane Science*, 199(1-2), pp.135-145.
- Kötz, R. and Carlen, M. (2000). Principles and applications of electrochemical capacitors. *Electrochimica Acta*, 45(15-16), pp.2483-2498.
- Kumar, D. and Sharma, R. (1998). Advances in conductive polymers. *European Polymer Journal*, 34(8), pp.1053-1060.
- Laforgue, A., Simon, P., Sarrazin, C. and Fauvarque, J. (1999). Polythiophene-based supercapacitors. *Journal of Power Sources*, 80(1-2), pp.142-148.
- Li, R., Xiong, C., Kuang, D., Dong, L., Lei, Y., Yao, J., Jiang, M. and Li, L. (2008). Polyamide 11/Poly(vinylidene fluoride) Blends as Novel Flexible Materials for Capacitors. *Macromolecular Rapid Communications*, 29(17), pp.1449-1454.

- Liberman, V., Malba, V. and Bernhardt, A. (1996). A Study Of Anisotropy Of Spin Cast And Vapor Deposited Polyimide Films Using Internal Reflection Techniques. MRS Proceedings, 443.
- Liu, C., Yu, Z., Neff, D., Zhamu, A. and Jang, B. (2010). Graphene-Based Supercapacitor with an Ultrahigh Energy Density. Nano Letters, 10(12), pp.4863-4868.
- Long, Y., Li, M., Gu, C., Wan, M., Duvail, J., Liu, Z. and Fan, Z. (2011). Recent advances in synthesis, physical properties and applications of conducting polymer nanotubes and nanofibers. Progress in Polymer Science, 36(10), pp.1415-1442.
- Luckachan, G. and Pillai, C. (2011). Biodegradable Polymers- A Review on Recent Trends and Emerging Perspectives. Journal of Polymers and the Environment, 19(3), pp.637-676.
- MacDiarmid, A. (2001). "Synthetic Metals": A Novel Role for Organic Polymers (Nobel Lecture). Angewandte Chemie International Edition, 40(14), pp.2581-2590.
- Macdonald, D. D. (2006). Reflections on the history of electrochemical impedance spectroscopy. Electrochimica Acta, pp.1376-1388.
- Malliaras, G. and Friend, R. (2005). An Organic Electronics Primer. Physics Today, 58(5), pp.53-58.
- Mathakari, N., Jadhav, V., Kanjilal, D., Boraskar, V. and Dhole, S. (2009). Surface and structural changes in polyimide by 100 MeV Ag⁷⁺ ion irradiation. Surface and Coatings Technology, 203(17-18), pp.2620-2624.
- Mayer, S. (1993). The Aerocapacitor: An Electrochemical Double-Layer Energy-Storage Device. Journal of The Electrochemical Society, 140(2), p.446.
- Naarmann, H. (2002). Polymers, Electrically Conducting. Chichester: Wiley, pp.506–572.
- Nalwa, H. (1997). Handbook of organic conductive molecules and polymers. Chichester: Wiley, pp.506–572.
- Nam, K. and Kim, K. (2006). Manganese Oxide Film Electrodes Prepared by Electrostatic Spray Deposition for Electrochemical Capacitors. Journal of The Electrochemical Society, 153(1), p.A81.

- Nambiar, S. and Yeow, J. (2011). Conductive polymer-based sensors for biomedical applications. *Biosensors and Bioelectronics*, 26(5), pp.1825-1832.
- Nekrasov, A., Ivanov, V. and Vannikov, A. (2000). Analysis of the structure of polyaniline absorption spectra based on spectroelectrochemical data. *Journal of Electroanalytical Chemistry*, 482(1), pp.11-17.
- Nenoff, T. M., Spontak, R. J., & Aberg, C. M. (2006). Membranes for hydrogen purification: An important step toward a hydrogen-based economy. *MRS Bulletin*, 31(10), 735–744.doi:10.1557/mrs2006.18616.
- Nguyen, D. and Yoon, H. (2016). Recent Advances in Nanostructured Conducting Polymers: from Synthesis to Practical Applications. *Polymers*, 8(4), p.118.
- Nguyen, D. and Yoon, H. (2016). Recent Advances in Nanostructured Conducting Polymers: from Synthesis to Practical Applications. *Polymers*, 8(4), p.118.
- Nicholson, R. (1965). Theory and Application of cyclic voltammetry for measurements of electrode reaction kinetics. *Analytical Chemistry*, pp. 1351-1355.
- Noah, N. M., Omole, M., Stern, S., Zhang, S., Sadik, O. A., Hess, E. H., ... & Iwuoha, E. I. (2012). Conducting polyamic acid membranes for sensing and site-directed immobilization of proteins. *Analytical biochemistry*, 428(1), pp. 54-63.
- Pan, L., Qiu, H., Dou, C., Li, Y., Pu, L., Xu, J. and Shi, Y. (2010). Conducting Polymer Nanostructures: Template Synthesis and Applications in Energy Storage. *International Journal of Molecular Sciences*, 11(12), pp.2636-2657.
- Park, Y., Choi, S., Song, S. and Miyata, S. (2018). Synthesis of highly conducting nylon-6 composites and their electrical properties.
- Pena-Pereira, F., Costas-Mora, I., Romero, V., Lavilla, I. and Bendicho, C. (2011). Advances in miniaturized UV-Vis spectrometric systems. *Trends in Analytical Chemistry*, pp.1637-1648.
- Peng, C., Zhang, S., Jewell, D. and Chen, G. (2008). Carbon nanotube and conducting polymer composites for supercapacitors. *Progress in Natural Science*, 18(7), pp.777-788.

- Percec, V. (2001). Introduction: Frontiers in Polymer Chemistry. *Chemical Reviews*, 101(12), pp.3579-3580.
- Polyaniline: The Infrared Spectroscopy of Conducting Polymer Nanotubes (IUPAC Technical Report). (2011). *Chemistry International -- Newsmagazine for IUPAC*, 33(5).
- Qiu, S., Wu, L., Pan, X., Zhang, L., Chen, H. and Gao, C. (2009). Preparation and properties of functionalized carbon nanotube/PSF blend ultrafiltration membranes. *Journal of Membrane Science*, 342(1-2), pp.165-172.
- Rafiq, S., Man, Z., Maitra, S., Maulud, A., Ahmad, F. and Muhammad, N. (2011). Preparation of asymmetric polysulfone/polyimide blended membranes for CO₂ separation. *Korean Journal of Chemical Engineering*, 28(10), pp.2050-2056.
- Rao, P., Subrahmanya, S. and Sathyanarayana, D. (2003). Synthesis by inverse emulsion pathway and characterization of conductive polyaniline–poly(ethylene-co-vinyl acetate) blends. *Synthetic Metals*, 139(2), pp.397-404.
- Reid, B., Ruiz-Trevino, F., Musselman, I., Balkus, K. and Ferraris, J. (2001). Gas Permeability Properties of Polysulfone Membranes Containing the Mesoporous Molecular Sieve MCM-41. *Chemistry of Materials*, 13(7), pp.2366-2373.
- Roncali, J. (2002). Conjugated poly(thiophenes): synthesis, functionalization, and applications. *Chemical Reviews*, 92(4), pp.711-738.
- Ryu, K., Wu, X., Lee, Y. and Chang, S. (2003). Electrochemical capacitor composed of doped polyaniline and polymer electrolyte membrane. *Journal of Applied Polymer Science*, 89(5), pp.1300-1304.
- Savage, N. and Diallo, M. (2005). Nanomaterials and Water Purification: Opportunities and Challenges. *Journal of Nanoparticle Research*, 7(4-5), pp.331-342.
- Scally, S., Davison, W. and Zhang, H. (2006). Diffusion coefficients of metals and metal complexes in hydrogels used in diffusive gradients in thin films. *Analytica Chimica Acta*, 558(1-2), pp.222-229.
- Sezer, E., Ustamehmetoğlu, B. and Saraç, A. (1999). Chemical and electrochemical polymerisation of pyrrole in the presence of N-substituted carbazoles. *Synthetic Metals*, 107(1), pp.7-17.

- Shacklette, L., Han, C. and Luly, M. (1993). Polyaniline blends in thermoplastics. *Synthetic Metals*, 57(1), pp.3532-3537.
- Shah, A.-u.-H. A.; Holze, R. (2008). Spectroelectrochemistry of two-layered composites of polyaniline and poly (o-aminophenol). *Electrochimica Acta*, (53), pp. 4642-4653.
- Shinar, R., Shinar, J., Wang, L., Fine, D., Dodabalapur, A., Torsi, L., Cioffi, N., Marinelli, F., Ieva, E., Colaianni, L., Dell'Aquila, A., Suranna, G., Mastroianni, P., Mhaisalkar, S., Buchholt, K., Spetz A. Lloyd., Sabbatini L., Manunza, I., Bonfiglio, A., Stadlober, B., Schon, H., Groten, J., Zirkl, M., Jakopic, G., Cai, Y., Huang, J., DeMello, J., Woggon, T., Punke, M., Stroisch, M., Bruendel, M., Schelb, M., Vannahme, C., Mappes, T., Mohr, J., Lemmer U., Singh, T., Bauer, S., Sariciftci, N., Nilsson, K., Dhand, C., Malhotra, B., Berggren, M. and Richter-Dahlfors, A. (2009). *Organic electronics in sensors and biotechnology*. New York: McGraw-Hill.
- Shirakawa, H. (2001). Die Entdeckung der Polyacetylenfilme - der Beginn des Zeitalters leitfähiger Polymere (Nobel-Aufsatz). *Angewandte Chemie*, 113(14), pp.2642-2648.
- Shirakawa, H., Louis, E., MacDiarmid, A., Chiang, C. and Heeger, A. (1977). Synthesis of electrically conducting organic polymers: halogen derivatives of polyacetylene, (CH)_x. *Journal of the Chemical Society, Chemical Communications*, (16), p.578.
- Skotheim, T. and Reynolds, J. (2007). *Conjugated Polymers*. Boca Raton, Fla.: CRC Press.
- Stephans, L., Myles, A. and Thomas, R. (2000). Kinetics of Alkaline Hydrolysis of a Polyimide Surface. *Langmuir*, 16(10), pp.4706-4710.
- Tóth, P., Samu, G., Endrődi, B. and Visy, C. (2013). Hyphenated in situ conductance and spectroelectrochemical studies of polyaniline films in strongly acidic solutions. *Electrochimica Acta*, 110, pp.446-451.
- Tran, H., Li, D. and Kaner, R. (2009). One-Dimensional Conducting Polymer Nanostructures: Bulk Synthesis and Applications. *Advanced Materials*, 21(14-15), pp.1487-1499.
- Unsworth, J., Lunn, B., Innis, P., Jin, Z., Kaynak, A. and Booth, N. (1992). Technical Review : Conducting Polymer Electronics. *Journal of Intelligent Material Systems and Structures*, 3(3), pp.380-395.

- Vikki, T., Pietilä, L., Österholm, H., Ahjopalo, L., Takala, A., Toivo, A., Levon, K., Passiniemi, P. and Ikkala, O. (1996). Molecular Recognition Solvents for Electrically Conductive Polyaniline. *Macromolecules*, 29(8), pp.2945-2953.
- Wang, Q., Moser, J., & Gratzel, M. (2005). Electrochemical impedance spectroscopic analysis of dye-sensitized solar cells. *Physical Chemistry B*, pp.14945-14953.
- Wang, Y., Li, H. and Xia, Y. (2006). Ordered Whiskerlike Polyaniline Grown on the Surface of Mesoporous Carbon and Its Electrochemical Capacitance Performance. *Advanced Materials*, 18(19), pp.2619-2623.
- Yu, T., Zhu, P., Xiong, Y., Chen, H., Kang, S., Luo, H. and Guan, S. (2016). Synthesis of microspherical polyaniline/graphene composites and their application in supercapacitors. *Electrochimica Acta*, 222, pp.12-19.
- Zamfir, L., Rotariu, L., Marinescu, V., Simelane, X., Baker, P., Iwuoha, E. and Bala, C. (2016). Non-enzymatic polyamic acid sensors for hydrogen peroxide detection. *Sensors and Actuators B: Chemical*, 226, pp.525-533.
- Zhu, H., Peng, S. and Jiang, W. (2013). Electrochemical Properties of PANI as Single Electrode of Electrochemical Capacitors in Acid Electrolytes. *The Scientific World Journal*, 2013, pp.1-8.

